Extracting Electromechanical Signals for Icebreaker Insights

by

Andrew William Moeller

B.S., U.S. Coast Guard Academy (2016)

Submitted to the Department of Mechanical Engineering
in partial fulfillment of the requirements for the degrees of

Master of Science in Mechanical Engineering

and

Master of Science in Naval Architecture and Marine Engineering

at the

MASSACHUSETTS INSTITUTE OF TECHNOLOGY

May 2022

© Massachusetts Institute of Technology 2022. All rights reserved.

Author .....
Department of Mechanical Engineering
May 6, 2022

Certified by .....
Steven B. Leeb
Professor
Thesis Supervisor

Certified by .....
Daisy H. Green
Doctoral Candidate
Thesis Supervisor

Accepted by .....
Nicolas G. Hadjiconstantinou
Chairman, Mechanical Engineering Committee on Graduate Studies

Extracting Electromechanical Signals for Icebreaker Insights

by

Andrew William Moeller

Submitted to the Department of Mechanical Engineering
on May 6, 2022, in partial fulfillment of the
requirements for the degrees of
Master of Science in Mechanical Engineering
and
Master of Science in Naval Architecture and Marine Engineering

Abstract

Nonintrusive load monitoring has a proven track record of providing benefits for equipment operation logging, fault detection and diagnostics, condition-based maintenance, and energy scorekeeping. A nonintrusive load monitor (NILM) can measure the aggregate electrical power at a central utility point and extract individual loads from this power stream. Segregating and identifying these unique electrical signatures from various shipboard machinery components allow a NILM to assess the health of equipment and predict potential failures before they are evident through traditional monitoring methods. NILMs have been installed on multiple US Coast Guard and US Navy vessels over the past several years, collecting vital data that has rapidly accelerated the monitoring capabilities of this technology. This work specifically expands upon the previous successes and applies the same concepts to a 140 ft icebreaking tug, USCGC THUNDER BAY. The NILMs installed on THUNDER BAY are capable of directly monitoring the electric propulsion drive, which coupled with its unique icebreaking mission allow the NILM to gain crucial insights into ship operation that have not been previously available. Additional improvements were developed for the NILM's software and hardware components to incorporate an added wireless capability, allowing the NILM to act as a central processor for a physically securable network of wireless sensing nodes. Testing was conducted in four separate shipboard environments to confirm the feasibility of this network architecture. Specific methods for implementing this sensor network are discussed, and techniques for combining both power and vibration measurements are presented to identify faults that were previously unattainable strictly through power monitoring alone.

Thesis Supervisor: Steven B. Leeb
Title: Professor

Thesis Supervisor: Daisy H. Green
Title: Doctoral Candidate

Acknowledgments

I want to thank everyone who has helped me reach this milestone in my career. I would not be where I am today without the unconditional support from all of my family and friends. To my parents, thank you for encouraging me to push myself beyond what I thought I was capable of, and instilling in me the desire to continue to be a lifelong learner. To Kat and Dave, it's been good to be close to home and every opportunity we've had to hang out over the past two years has been a well needed release from academia. To Sidnie, thank you for always being there to support me. You definitely saw me at my highs and lows, and without your constant support I would not have been able to complete this arduous two years of work. I would like to thank the US Coast Guard for allowing me to continue my academic pursuits, as well as the American Society of Naval Engineers (ASNE), The Grainger Foundation, and the Office of Naval Research NEPTUNE program for their financial assistance. Thank you Professor Leeb for challenging me and pushing me beyond what I thought was possible. I was extremely nervous starting work in this lab due to my lack of electrical knowledge, but you've shown me that with some determination and hard work that anything is possible, and for that I will be forever grateful. Thank you Daisy for all of your guidance and helping lead me down the path of all things NILM. To Devin, I'd say we've done a pretty good job since we've been here, and hopefully we will be able to work together again in the future. Thank you to all of my fellow LEES-GEM students: Joey, Brian, Łukasz, Tommy, Aaron, Isabelle, Mike, Jay, Erik S., Eric P., Dan, David, and Dayo. Thank you to all of the crews of SPENCER, ESCANABA, MARLIN, THUNDER BAY, INDIANAPOLIS, and the Self Defense Test Ship for their support with my research. I want to give special thanks to MKCS John Kovacevich, CWO3 Nate Reese, EMCS Quintrell Simmons, and EMC Rob Kinman for all of your technical shipboard expertise that helped make this project possible.

"A smooth sea never made a skilled sailor" - Franklin D. Roosevelt

THIS PAGE INTENTIONALLY LEFT BLANK

Contents

1 Introduction **23**

1.1 Nonintrusive Load Monitoring 24

1.2 Icebreakers 28

2 Icebreaking Fundamentals **29**

2.1 Ice Formation 30

2.2 Powering Requirements 32

2.3 Icebreaking Techniques 33

2.3.1 Continuous Icebreaking 34

2.3.2 Backing and Ramming 35

2.3.3 Wake Icebreaking 35

3 USCGC THUNDER BAY Equipment Report **37**

3.1 NILM Installation 37

3.2 Monitored Power Panels 40

3.3 Identified Loads on 2-32-1 41

3.3.1 MPDE Crankcase Blower 41

3.3.2 MPDE Pre-Lube Pump 44

3.3.3 MPDE Lube Oil Heater 46

3.3.4 MPDE Lube Oil Circulation Pump 48

3.3.5 MPDE Jacket Water Heater 50

3.3.6 MPDE Jacket Water Circulation Pump 52

3.3.7 SSDG Jacket Water Heater 54

3.3.8 Engine Room Supply Fan . . . 56
3.3.9 Gray Water Pump . . . 59
3.3.10 Submersible Pump Receptacle . . . 60
3.4 Identified Loads on 1-66-1 . . . 60
3.4.1 Main Motor Cooling Pump . . . 61
3.4.2 Main Motor/Main Propulsion Generator Exciters . . . 63
3.5 Sample Identification of Faults - MPDE Jacket Water Heater . . . 64
3.5.1 #1 MPDE Jacket Water Heater . . . 64
3.5.2 #2 MPDE Jacket Water Heater . . . 67
3.5.3 NILM Insight . . . 67

4 THUNDER BAY Electric Propulsion 73
4.1 Propulsion System Design . . . 73
4.2 Propulsion System Monitoring . . . 77
4.3 Advanced Insights . . . 80
4.3.1 Experimental Setup . . . 80
4.3.2 Icebreaking Observations . . . 85

5 Sensor Upgrades 87
5.1 Sensing Platforms . . . 87
5.1.1 "All-In-One" Box Modifications . . . 88
5.1.2 Wireless Sensing Platform . . . 89
5.2 Physically Securable Network . . . 90
5.2.1 Wireless Platform Evaluation . . . 90
5.2.2 Data Transmission and Synthesis . . . 94
5.2.3 Security . . . 95
5.3 Sensor Demonstration . . . 97
5.3.1 Bilge and Fire Pump . . . 97
5.3.2 Air Conditioning Plant . . . 99
5.3.3 Crankcase Blower . . . 102
5.3.4 Sewage Vacuum Pumps . . . 106

5.4 Implementation 111

6 Conclusions and Future Work **113**

A USCGC THUNDER BAY NILM Documentation **115**

A.1 MIT NILM Research Proposal for USCGC THUNDER BAY (WTGB 108) 116

A.1.1 Introduction 116

A.1.1.1 Research Focus 116

A.1.1.2 Background 117

A.1.1.3 NILM Technology 118

A.1.1.4 Past NILM Installations 119

A.1.2 Installation Requirements 121

A.1.2.1 All-in-One (AIO) NILM Box 121

A.1.2.2 Other Installation Hardware 122

A.1.3 Proposed Installation & Mounting 124

A.1.3.1 Hardware Mounting Location 124

A.1.4 Conclusion 126

A.2 MIT NILM Installation Proposal for USCGC THUNDER BAY (WTGB 108) 127

A.2.1 Proposed Mounting 127

A.2.1.1 Mounting Hardware Details 127

A.2.1.2 Mounting Brackets 127

A.2.1.3 Cable Runs 130

A.2.2 Installation on Panel 133

A.2.2.1 Cable Entry into Panel 133

A.2.2.2 Panel 1S-4P-(1-66-2) (Engineering Control Center) . 134

A.2.2.3 Panel 1S-4P-(2-32-1) (Engine Room) 135

A.2.3 Inside the Panel 136

A.2.3.1 Current Transducer Installation 136

A.2.3.2 Voltage Lead Installation 137

A.3 Equipment Testing 139
A.4 Equipment Removal 139
A.4.1 Electrical 139
A.4.1.1 Current Transducer Removal 139
A.4.1.2 Voltage Lead Removal 140
A.4.1.3 Cable Holes 140
A.4.2 Hardware 140
A.5 Cybersecurity 141
A.5.1 Conclusion 141

B AIO Box Version 3.0 Technical Specifications 143
B.1 Assembly Instructions 144
B.2 Selected Technical Drawings 170

List of Figures

1-1 Schematic overview of a NILM monitoring an electrical subpanel. . . 24
1-2 Example turn-on power transient acquired by a NILM. 25
1-3 NILM installation on USCGC ESCANABA. 26
1-4 NILM Dashboard installation on USCGC SPENCER. 26
1-5 Installation of three NILMs on USS INDIANAPOLIS. 27
1-6 Installation of two NILMs on USCGC MARLIN. 27
1-7 USCGC THUNDER BAY in ice on the Penobscot River, ME. 28

2-1 Frazil ice with snow coverage as seen from THUNDER BAY. 31
2-2 Varying forms of brash ice as seen from THUNDER BAY. 31
2-3 Varying forms of fast ice as seen from THUNDER BAY. 31
2-4 SHP testing from level plate and brash ice testing on USCGC KATMAI BAY [11]. 33
2-5 Two primary methods of ice failure [7]. 34
2-6 Example of radial cracking of an ice sheet on THUNDER BAY. . . . 35

3-1 AIO installation on power panel 2-32-1 in THUNDER BAY Engine Room. 38
3-2 AIO installation on power panel 1-66-2 in THUNDER BAY ECC. . . 39
3-3 Current sensors and voltage taps for USCGC THUNDER BAY power panels. 39
3-4 USCGC THUNDER BAY primary load tree 40
3-5 Load tree for power panel 1-66-2 40
3-6 Load tree for power panel 2-32-1 41

3-7 USCGC THUNDER BAY MPDE Crankcase Blower 42
3-8 #1 MPDE Crankcase Blower on/off transient. 42
3-9 #2 MPDE Crankcase Blower on/off transient. 43
3-10 USCGC THUNDER BAY MPDE Pre-Lube Pump 44
3-11 #1 MPDE Pre-Lube Pump on/off transient. 45
3-12 #2 MPDE Pre-Lube Pump on/off transient. 45
3-13 USCGC THUNDER BAY MPDE Lube Oil Heater 46
3-14 #1 MPDE Lube Oil Heater on/off transient. 47
3-15 #2 MPDE Lube Oil Heater on/off transient. 47
3-16 USCGC THUNDER BAY MPDE Lube Oil Circulation Pump 48
3-17 #1 MPDE Lube Oil Circulation Pump on/off transient. 49
3-18 #2 MPDE Lube Oil Circulation Pump on/off transient. 49
3-19 USCGC THUNDER BAY MPDE Jacket Water Heater 50
3-20 #1 MPDE Jacket Water Heater on/off transient. 51
3-21 #2 MPDE Jacket Water Heater on/off transient. 51
3-22 USCGC THUNDER BAY MPDE Jacket Water Circulation Pump . . 52
3-23 #1 MPDE Jacket Water Circulation Pump on/off transient. 53
3-24 #2 MPDE Jacket Water Circulation Pump on/off transient. 53
3-25 USCGC THUNDER BAY SSDG Jacket Water Heater 54
3-26 #1 SSDG Jacket Water Heater on/off transient. 55
3-27 #2 SSDG Jacket Water Heater on/off transient. 55
3-28 USCGC THUNDER BAY Engine Room Supply Fan (Starboard) . . 56
3-29 USCGC THUNDER BAY Engine Room Supply Fan Controllers . . . 57
3-30 Engine Room Supply Fan on/off transient (LOW setting). 57
3-31 Engine Room Supply Fan on/off transient (HIGH setting). 58
3-32 USCGC THUNDER BAY Gray Water Pump 59
3-33 USCGC THUNDER BAY Submersible Pump Receptacle 60
3-34 Main motor cooling pumps. 61
3-35 #1 Main Motor Cooling Pump on/off transient. 62
3-36 #2 Main Motor Cooling Pump on/off transient. 62

3-37 Sample of exciters located within the main switchboard cabinet. . . . 63
3-38 Exciter transformer breaker on transient. 64
3-39 Initial #1 MPDE Jacket Water Heater Transient (10 February 2021). 65
3-40 Visible corrosion on #1 jacket water heater wiring. 66
3-41 #1 Jacket Water Heater Power Transient After Re-Wiring (21 June 2021) 66
3-42 #2 MPDE Jacket Water Heater Transient (21 June 2021) 67
3-43 Delta-connected heater under both healthy (a) and fault conditions (b-e). 70
3-44 Per-phase real power for scenarios (a)-(d). 71
3-45 Total real power for scenarios (a)-(d). 72

4-1 Conceptual diesel-electric propulsion system. 74
4-2 THUNDER BAY propulsion system schematic. 74
4-3 Comparison of motor field current to throttle position input. 76
4-4 Comparison of diesel engine rpm to throttle position input. 76
4-5 Comparison of generator armature voltage to throttle position input. 77
4-6 Sample power stream of THUNDER BAY getting underway. 78
4-7 Multiple day measurement of panel 1-66-2 (underway periods highlighted). 78
4-8 Time plot of THUNDER BAY commencing underway operations and breaking ice. 79
4-9 Time plot of THUNDER BAY commencing underway operations and breaking ice with enhanced view of icebreaking timeframe. 79
4-10 Multiple single day views of panel 1-66-2 power stream. 80
4-11 Line diagram of the modified Gulf Coast accelerometer. 81
4-12 Source code used to program X16-1C accelerometers. 82
4-13 Gulf Coast X16-1C accelerometer installations onboard CGC THUNDER BAY. 84
4-14 Potential icebreaking operations from NILM power stream. 86

4-15 Sample of verified continuous icebreaking from USCGC THUNDER BAY. 86

5-1 Upgraded AIO box with internal wireless capabilities 88

5-2 Wireless sensor platform used for integration with the wireless enabled NILM. 89

5-3 USCGC MARLIN Station Mode Testing 92

5-4 USCGC THUNDER BAY Station Mode Testing 92

5-5 USCGC SPENCER Station Mode Testing (Upper Engine Room) . . 93

5-6 USCGC SPENCER Station Mode Testing (Lower Engine Room) . . . 93

5-7 US Navy Self Defense Test Ship 94

5-8 Power and vibration data streams, captured synchronously with multiple sensors. 96

5-9 Estimated power and shaft angular velocity for different operating pressures of the MARLIN bilge and fire pump. 98

5-10 A/C compressor and unloader arrangement onboard SPENCER. . . . 100

5-11 SPENCER A/C compressor power stream. 100

5-12 SPENCER A/C compressor accelerometer time-domain plots of varying loading states. Impulsive events due to activated pistons are labeled.101

5-13 THUNDER BAY MPDE crankcase blower. 103

5-14 Cantilever mounting arrangements. 104

5-15 Crankcase blower time-domain comparison. 105

5-16 Crankcase blower frequency-domain comparison. 105

5-17 Vacuum pump time domain comparison (pre-repair). 107

5-18 Vacuum pump MES comparison. 108

5-19 Deteriorated vacuum relief valve. 109

5-20 Vacuum pump time-domain comparison (post-repair). 110

5-21 Wi-Fi enabled NILM with wireless sensing platform installed in a laboratory setup. 111

A-1 Schematic overview of a typical installation of a NILM at the feeder to a power panel on a ship. The NILM Meter provides sensing for waveform measurement. The NILM Software runs on a Linux-based personal computer, laptop, or similar platform. 119
A-2 The NILM Dashboard display on USCGC SPENCER (WMEC 905). 120
A-3 AIO NILM Box install. 122
A-4 Current and voltage sensor installation on USCGC SPENCER (WMEC 905). 123
A-5 USCGC THUNDER BAY (WTGB 108) electrical diagram with NILM sensor installation points identified (black boxes). 124
A-6 Proposed installation location for AIO box on Power Panel 1S-4P-(1-66-2) located in the Engineering Control Center (1-58-0-C). 125
A-7 Proposed installation location for AIO box on Power Panel 1S-4P-(2-32-1) located in the Engine Room. 125
A-8 Proposed mounting location for AIO box in ECC. 128
A-9 Proposed mounting location for AIO box in the Engine Room. 128
A-10 Layout of bracket mounting configuration for Engine Room and ECC. 129
A-11 Struts and holes with bolt inferences. 130
A-12 View of the double cable run in the vicinity of the mounting location in the Engine Room. 130
A-13 Location of power receptacle for Panel 1S-4P-(1-66-2) 131
A-14 Location of power receptacle for Panel 1S-4P-(2-32-1) 132
A-15 Example of bootshrink and cord grip fittings feeding into power panel (from US Navy panel). 134
A-16 Example of voltage leads (in conduit) and Conxall cables exiting from power panel. 134
A-17 Cables entries into the bottom of 1S-4P-(1-66-2). 135
A-18 Cables entries into the bottom of 1S-4P-(2-32-1). 135
A-19 Current transducers and Conxall cables installed on power cables feeding an electrical panel on USCGC SPENCER (WMEC 905). 136

A-20 USCGC THUNDER BAY (WTGB 108) Power Panels 137
A-21 Interior panel view on USCGC SPENCER (WMEC 905) showing voltage leads wired into a spare breaker as well as current transducers installed on power feed cables. 138

B-1 Original AIO Box (Kane Box). 144
B-2 Original AIO Box (Kane Box) with side plates removed. 144
B-3 1/4" holes drilled into side plate #2 145
B-4 AIO box with new side plates (expanded view). 145
B-5 AIO box with new side plates. 145
B-6 Grommets installed on squirrel cage. 146
B-7 Installation of watertight cord grip and Conxall receptacles. 146
B-8 Braided Conxall receptacle wires. 147
B-9 Conxall cable prior to connection with Nanomizer cable. 147
B-10 Conxall cables attached to side plate #2. 148
B-11 Installation of USB-A panel mounts and IEC panel mount. 148
B-12 UPS power cable wiring. 149
B-13 Example UPS power cable configuration. 149
B-14 Cooling fan wiring configuration. 150
B-15 Cooling fan installation (internal & external views). 150
B-16 WiFi antenna cabel installation. 151
B-17 Wi-Fi router with associated wiring connections. 151
B-18 Right angle USB cables connected to USB-A mounts. 152
B-19 NEMO box installation. 152
B-20 Ethernet cable connected to NEMO box. 153
B-21 Secured squirrel cage with appropriate cables exiting from the top opening. 153
B-22 GK41 computer prior to installation. 154
B-23 GK41 with up/down USB adapters connected. 154
B-24 Power cable configuration for AIO box. 155

B-25 GK41 in place next to the NEMO box. 155
B-26 GK41 bracket with gasket. 156
B-27 GK41 mounted with bracket. 156
B-28 GK41 mounted with holder. 157
B-29 Rocker switch with soldered wires. 157
B-30 Rocker switch adaptor. 158
B-31 Rocker switch installed on front plate with flip cover. 158
B-32 Faceplate with appropriate gasket. 159
B-33 Touch screen crossbar with appropriate gasket. 159
B-34 WIMAXIT touch screen installed on face plate with cross bar. 160
B-35 Installed flip cover for external hard drive holder. 160
B-36 WIMAXIT touch screen cable connection points. 161
B-37 Final AIO box design. 161

THIS PAGE INTENTIONALLY LEFT BLANK

List of Tables

3.1 MPDE Crankcase Blower Information. 43
3.2 MPDE Pre-Lube Pump Information. 45
3.3 MPDE Lube Oil Heater Information. 47
3.4 MPDE Lube Oil Circulation Pump Information. 49
3.5 MPDE Jacket Water Heater Information. 51
3.6 MPDE Jacket Water Circulation Pump Information. 53
3.7 SSDG Jacket Water Heater Information. 55
3.8 #1 Engine Room Supply Fan Information (LOW Setting). 58
3.9 #1 Engine Room Supply Fan Information (HIGH Setting). 58
3.10 Gray Water Pump Information. 59
3.11 Main Motor Cooling Pump Information. 62
3.12 #1 Jacket Water Heater Initial Steady State Power Data - 10 February 2021 65
3.13 #1 Jacket Water Heater Steady State Power Data (Post Repair) - 22 June 2021 66
3.14 #2 Jacket Water Heater Steady State Power Data - 21 June 2021 . . 67
3.15 23 March 2021 - Pre Repair of #1 Jacket Water Heater Wiring 68
3.16 22 June 2021 - Post Repair of #1 Jacket Water Heater Wiring 68
3.17 Impedance and Power Relationships 69

5.1 A/C power factor and shaft frequency for loading conditions. 102
5.2 Centrifugal fan power and vibration comparison. 103

B.1 Current conversion factors 167

B.2 AIO Box v3.0 bill of materials 169

Acronyms

AIO "All-In-One".

COMDTINST Commandant Instruction.

DAQ Data Acquisition Unit.

DCMS Deputy Commandant for Mission Support.

DFT Discrete Fourier Transform.

ECC Engineering Control Center.

ESD Engineering Services Division.

FDD Fault Detection & Diagnostics.

GUI Graphical User Interface.

IEPE Integrated Electronics Piezoelectric.

IoT Internet of Things.

MES Mean Envelope Spectrum.

MPDE Main Propulsion Diesel Engine.

MPG Main Propulsion Generator.

NILM Nonintrusive Load Monitor.

PSD Power Spectral Density.

SF Ship's Force.

SFLC Surface Forces Logistics Center.

SHP Shaft Horsepower.

SSDG Ship Service Diesel Generator.

TCP Transmission Control Protocol.

UDP User Datagram Protocol.

USCGC United States Coast Guard Cutter.

WPA2 Wi-Fi Protected Access II.

Chapter 1

Introduction

The maritime industry is unique in the fact that complex engineering infrastructures exist and operate in environments with little to no outside support. Failure of critical equipment can be catastrophic as well as costly for a ship. Operators of both military and commercial vessels are limited to storing a finite number of replacement parts onboard their ships, and without enhanced insights into machinery operating characteristics it can become increasingly difficult to predict when particular components are going to fail. As members of the maritime fleet have been searching for methods to decrease operating costs and improve maintenance efforts, increased investments in automation and monitoring systems have become potential solutions [1] [2]. While these new advancements in technology can provide benefits to crews, it becomes important that the data being collected is properly managed and targeted for maximal insights as opposed to a simple mass collection of shipboard information. Nonintrusive load monitoring is one technology that can provide both answers and benefits for those in the maritime industry seeking a low cost and effective tool for equipment operation logging, fault detection and diagnostics, condition-based maintenance, and energy scorekeeping. This work will leverage the strengths and capabilities of NILM and apply them specifically to a US Coast Guard icebreaking tug to gain insights not previously studied within the NILM research community.

1.1 Nonintrusive Load Monitoring

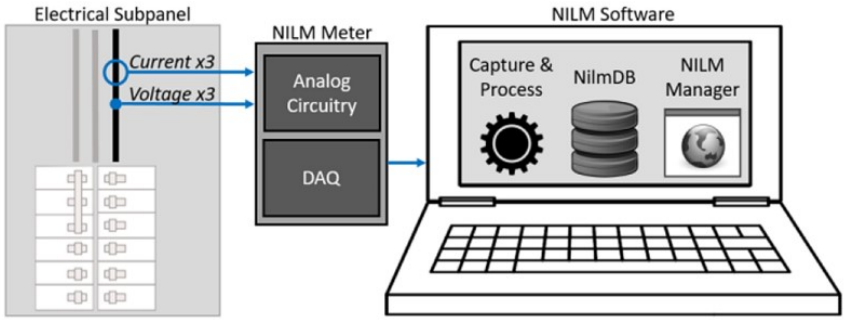

Figure 1-1: Schematic overview of a NILM monitoring an electrical subpanel.

Nonintrusive load monitoring is one method that can be utilized to provide vital insights to load operation on a marine micro-grid. While other shipboard monitoring systems typically require individual sensors for different loads and simply observe the on/off equipment events, a nonintrusive load monitor (NILM) can provide further diagnostic information with less sensors. A NILM can be placed at the utility panel of a micro-grid and segregate individual loads from the aggregate power stream. Once individual loads are identified through their unique features, diagnostics can be performed to assess their individual health, and monitor for potential "soft faults" that could eventually result in catastrophic failure [3]. A sample schematic overview of the NILM can be seen in Figure 1-1 and a typical load transient visible on the NILM power stream can be seen in Figure 1-2. Individual features such as inrush peak, steady-state power consumption, and transient duration can all be used to help identify a particular load within the aggregate stream. NILMs are able to easily and nonintrusively integrate within existing machinery infrastructure, and can analyze data in real-time to provide actionable information for crews.

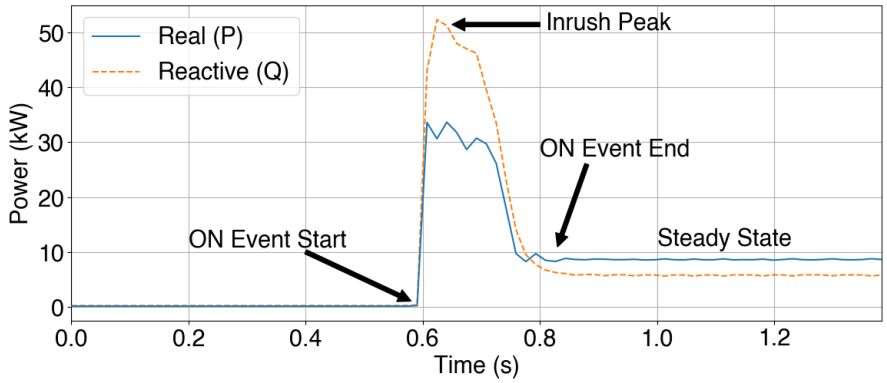

Figure 1-2: Example turn-on power transient acquired by a NILM.

Nonintrusive load monitoring has a proven track record of providing crucial data and insights within shipboard environments [4] and have recently been installed on several US Coast Guard and US Navy vessels, including USS INDIANAPOLIS, USCGC SPENCER, USCGC ESCANABA, USCGC MARLIN, and USCGC THUNDER BAY. The original shipboard NILM installation on the 270 ft WMEC involved the mounting of separate hardware boxes for the NILM meter and the NILM computer, as seen in the USCGC ESCANABA installation of Figure 1-3. The only way to view the information provided by the NILM was to download and copy the data from the computer after the ship returned from a patrol. While still able to provide valuable insights to the crew, this variation of NILM lacked the ability to provide real-time feedback for the end user. Later adaptations of the NILM infrastructure involved the creation of a "Dashboard", which included a separate graphical user interface (GUI) that was capable of providing the desired real-time diagnostic information for crew utilization [5]. This upgrade can be seen in the USCGC SPENCER installation of Figure 1-4. Upgraded "All-In-One" (AIO) boxes were later developed and installed on USS INDIANAPOLIS (Figure 1-5) and USCGC MARLIN (Figure 1-6) that integrated the NILM meter, computer, and touchscreen into one compact unit, providing all the benefits of Dashboard in a single and easy to access location. The latest AIO installation was completed on USCGC THUNDER BAY (Feb 2021) and will be the focus of this work, highlighting the advancements of fault detection technology with the NILM.

(a) NILM installed on power panel 3-117-2.

(b) NILM installed on power panel 3-117-1.

Figure 1-3: NILM installation on USCGC ESCANABA.

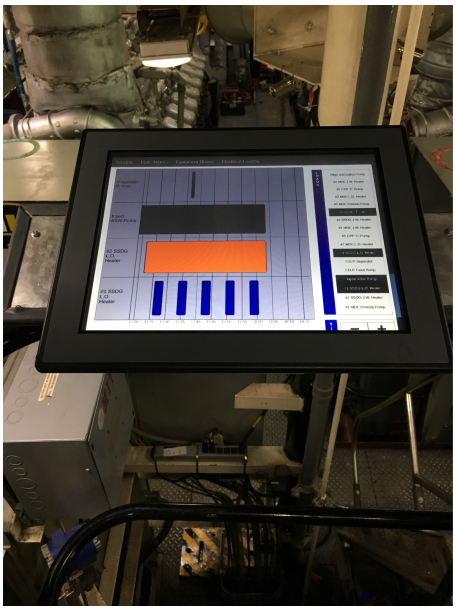

Figure 1-4: NILM Dashboard installation on USCGC SPENCER.

Figure 1-5: Installation of three NILMs on USS INDIANAPOLIS.

Figure 1-6: Installation of two NILMs on USCGC MARLIN.

1.2 Icebreakers

Icebreakers are ships that are designed for a specific subset of maritime operations. Specifically, US domestic icebreakers operate yearly to conduct a variety of mission critical operations to facilitate the demands of commerce in ice laden waters, complete flood control sorties on rivers, and respond to vessels beset in ice [6]. These types of ships possess specific characteristics to assist with the completion of these jobs, such as increased hull plating thickness, specially designed hullforms, and propulsion systems capable of providing increased horsepower [7]. While there are different variations of propulsion configurations that can meet the increased demands of icebreaking, an electric propulsion drive is very attractive, and can be found on many different icebreakers across the globe [8]. This particular characteristic of icebreakers provides a unique opportunity for a NILM to directly monitor the operation of a ship's propulsion system. This is not possible on the typical diesel engine configurations of previous installations, where ship operation has to be inferred from the status of equipment related to the propulsion system. The most recent NILM installation on USCGC THUNDER BAY, the ship seen in Figure 1-7, is capable of providing these unique insights.

Figure 1-7: USCGC THUNDER BAY in ice on the Penobscot River, ME.

Chapter 2

Icebreaking Fundamentals

While this work will reference the electrical monitoring results of previous shipboard NILM installations, the main focus will be the newly acquired data and insights gained from USCGC THUNDER BAY, a US Coast Guard bay class icebreaking tug. This ship is specifically designed to break ice, a unique mission set not conducted by many other vessels. Electrically monitoring this type of vessel allows for the opportunity to obtain insights in a field of nonintrusive monitoring not commonly studied. Before further analyzing the data obtained from this ship it is important to first have a more comprehensive understanding regarding the fundamentals of icebreaking and icebreaker design. While the methods discussed in this chapter can be applied to various types of icebreaking and icebreakers, one should be aware that differences exist in ice formation and icebreaking tactics dependent upon geographic location. For example, the multi-year ice that develops within the polar regions has vastly different characteristics than those of the seasonal river ice encountered by THUNDER BAY. This work will focus on discussing ice types and icebreaking tactics specific to THUNDER BAY within the rivers of New England waterways.

2.1 Ice Formation

The formation of ice can be a complex process, and is driven by numerous environmental factors. Two of the most critical factors that can impact the formation of ice are temperature and turbulence of water. Intuitively, when surface water cools to sub-freezing temperatures, ice will begin to form. If the surface water is calm, that is with little turbulence, then a continuous sheet of ice will form. With continued sub-freezing temperatures, the extent of these continuous sheets can spread rapidly within the narrow rivers of which THUNDER BAY operates. These continuous sheets of ice are mostly uniform in crystalline structure, and can be referred to either as plate ice, or in the case of rivers will typically be referred to as fast ice once it stretches the entire width of the river [9]. Left untouched this sheet of ice will continue to thicken as heat is transferred from the ice into the surrounding air. If sub-freezing temperatures exist and there is more turbulence presence in the water, then the potential for frazil ice exists. Frazil ice forms when ice crystallizes within turbulent flow, and can form smaller ice particles of diameters 1 mm or less. As frazil particles interact with each other they can form a variety of shapes and structures, including slush, "pancake" ice, and other various types of floes [10]. While frazil ice itself does not pose an issue for icebreakers like THUNDER BAY, if left unattended it can form larger pieces of ice and restrict critical waterways. One final type of ice encountered by THUNDER BAY is brash ice. Brash ice can either be formed by the accumulation of smaller pieces of ice (such as frazil) or by being dislodged from a continuous sheet. Pieces of brash ice can vary in size and thickness, but are generally recognized as having diameters of less than 6 ft. Brash ice will typically cause less challenges for icebreakers when compared to thicker plate ice, however if multiple pieces of brash ice freeze together then this can require increased demand in power from the icebreaker. Examples of these types of ice can be seen in Figure 2-1 through Figure 2-3. All photos were taken on the Penobscot and Kennebec rivers from the 2019 and 2020 icebreaking seasons.

Figure 2-1: Frazil ice with snow coverage as seen from THUNDER BAY.

(a) Multiple sizes and shapes of brash ice.

(b) Refrozen brash ice with snow coverage.

Figure 2-2: Varying forms of brash ice as seen from THUNDER BAY.

(a) Level plate ice (bank to bank coverage), also referred to as fast ice.

(b) Fast ice.

Figure 2-3: Varying forms of fast ice as seen from THUNDER BAY.

2.2 Powering Requirements

Due to the inherent nature of icebreaking operations, installed propulsion systems need to be extremely responsive to rapid maneuvering, and need to be able to withstand repeated high levels of torque on the shaft from impacts with ice [7]. These requirements make an electric propulsion system an attractive solution for this particular application, and for that reason many icebreakers of the world today can be found operating with some form of electric propulsion. The specifics of THUNDER BAY's electric propulsion system will be discussed in further detail in Chapter 4.

A study published in 1980 by the Cold Regions Research and Engineering Laboratory of the US Army Corps of Engineers [11] analyzed the icebreaking performance of the USCGC KATMAI BAY, the first in class of US Coast Guard bay class icebreaking tugs. While this study analyzed various ship characteristics, particular consideration was taken to observe the performance of the ship and its propulsion system while interacting with ice. Testing was conducted in both level plate ice as well as brash ice within Whitefish Bay and the St. Mary's River in the Great Lakes. Specifically, this testing analyzed ship resistance levels and required shaft horsepower (SHP) in varying ice thicknesses to help develop an operational profile for this class of icebreakers. Testing for level plate ice was conducted for ice thicknesses of 12, 14, and 16 inches. In each of these tests there was approximately 3-5 inches of snow cover on top of the ice. Additional testing was conducted in brash ice with thicknesses ranging from 18-22 inches. A summary of this testing comparing required SHP to maintain a particular speed at the measured ice thicknesses can be seen in Figure 2-4. This testing shows that for an icebreaker, and in particular the bay class icebreaking tugs, as the level of ice thickness increases, the SHP required to maintain a constant velocity increases. Additionally, even though the brash ice thickness was thicker than any of the level plate ice testing, it still required less SHP to maintain the same velocity. This is due to the inherent differences in the makeup of the internal ice structure, and will be discussed further in Chapter 4.

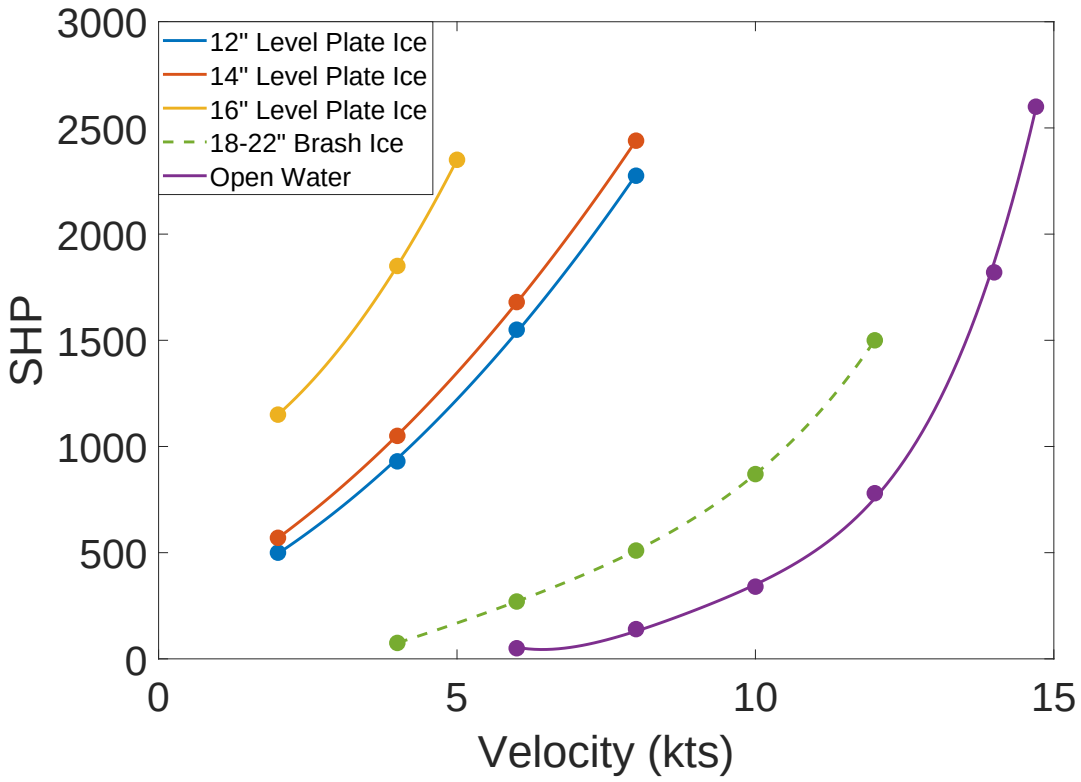

Figure 2-4: SHP testing from level plate and brash ice testing on USCGC KATMAI BAY [11].

2.3 Icebreaking Techniques

While there are many different types of icebreaking techniques, the methods discussed in this work will focus on those primarily used by the US Coast Guard bay class icebreaking tugs. These include, but are not limited to, continuous icebreaking, backing and ramming, and wake icebreaking. Each of these techniques will vary based on the specific ice conditions, environmental conditions, and even the operating tendencies of the ship driver. Two major ways in which an ice sheet can undergo failure can be seen in Figure 2-5. These include both bending failures and splitting failures. A bending failure occurs when the weight of the ship exceeds the structural strength of the ice sheet. The splitting failures, also referred to as radial cracking, occur upon initial

impact between the icebreaker and the ice edge. In addition to these two larger scale ice fracture events, localized failures within the ice structure will also occur based on ice structure and pressure regions within the ice formation.

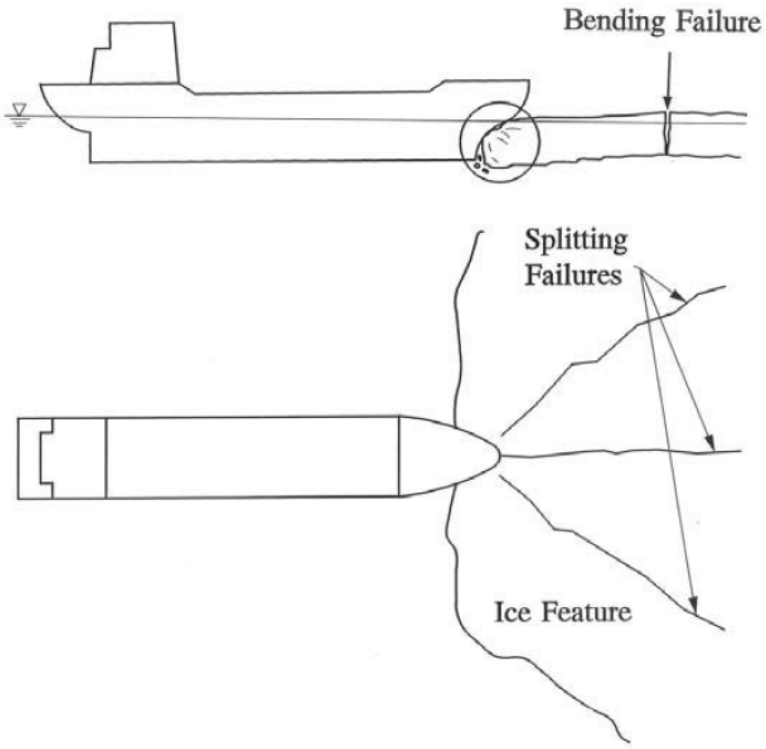

Figure 2-5: Two primary methods of ice failure [7].

2.3.1 Continuous Icebreaking

Continuous icebreaking occurs when the combination of ship's horsepower, ice thickness, and environmental conditions allow the ship to continuously break through the ice formation. As the ship rides up onto the ice edge, the bending failure demonstrated in Figure 2-5 will occur, and the ship will continue to drive forward into the remaining ice sheet. This process will continue as long as the available power and thickness of the ice permit. When conducting continuous icebreaking operations, the operator will typically remain at a single throttle position and will only adjust this if there is a need for additional power to break the ice.

2.3.2 Backing and Ramming

If the ship does not possess enough power, the ice is too thick, or the environmental conditions are unsatisfactory, then continuous icebreaking cannot occur. In this instance the ship will have to commence a method referred to as backing and ramming to continue breaking through the ice sheet. The ship will back down several ship's lengths from the ice edge and then increase speed as it rams into the previous locations where icebreaking ceased. This will give the ship momentum to break through more ice, and once there is not enough reserved power to operate continuously then the backing and ramming operation will be repeated. The sudden impact of the ramming will cause the splitting failures and radial cracking seen in Figure 2-5 and Figure 2-6. In this particular method there will be frequent handle position changes as the ship has to repeatedly ram into the ice edge in order to affect its operation.

Figure 2-6: Example of radial cracking of an ice sheet on THUNDER BAY.

2.3.3 Wake Icebreaking

One final method that icebreakers like THUNDER BAY will use to break ice is referred to as wake icebreaking. While not a direct icebreaking method it can still

be an effective tool. The hullform of the bay class cutters allows a strong wake to be formed when the vessel is transiting at high enough speeds. Typically when transiting down a river THUNDER BAY will take advantage of this wake in an attempt to break up larger pieces of ice closer to shore that are not reachable by the ship.

Chapter 3

USCGC THUNDER BAY Equipment Report

3.1 NILM Installation

This chapter describes the NILM configuration monitoring USCGC THUNDER BAY and details the specific electrical signatures of all observed equipment. THUNDER BAY is a 140 ft bay class icebreaking tug homeported in Rockland, ME. While the primary mission of this ship is to break ice, it also performs other Coast Guard missions such as law enforcement and search and rescue in near-coastal waterways. Underway trips typically only last for a few days, with some extended icebreaking missions lasting up to several weeks away from homeport. The shortness of these deployments are preferential for monitoring the performance of the NILM installation as well as providing timely feedback on the status of shipboard equipment to the crew. In contrast with previous NILM installations, external hard drives are included to facilitate the rapid transfer of data from the ship to the lab for analysis. Two NILM AIO boxes were installed on THUNDER BAY on 10 February 2021. The first box is located in the Engine Room, as seen below in Figure 3-1, with voltage taps and current sensors located on panel 2-32-1 . The second box is located in the Engineering Control Center (ECC), as seen below in Figure 3-2, with voltage taps and current sensors located on panel 1-66-2.

(a) Prior to NILM installation.

(b) Post NILM installation.

Figure 3-1: AIO installation on power panel 2-32-1 in THUNDER BAY Engine Room.

Consistent with prior NILM installations, the meters record current and voltage at a sampling frequency of 8 kHz. These high sampling rates are necessary for capturing transient shapes as loads change state as well as the higher harmonic content of nonlinear loads. To reduce data volume while maintaining the relevant information, these measurements are pre-processed in an onboard data acquisition unit into harmonic power envelopes. This process compresses the high-rate current and voltage data into real, reactive, and harmonic power streams at the system line frequency (60 Hz). The processed data is streamed to an onboard computer via ethernet cable and stored in a high-speed time-series database named NilmDB, from which the data can be viewed and analyzed in a web-based interface. The installed current sensors and voltage taps for each of the monitored power panels can be seen in Figure 3-3. Additional details concerning the approval and installation process for these two AIO boxes can be found in Appendix A.

(a) Prior to NILM installation.

(b) Post NILM installation.

Figure 3-2: AIO installation on power panel 1-66-2 in THUNDER BAY ECC.

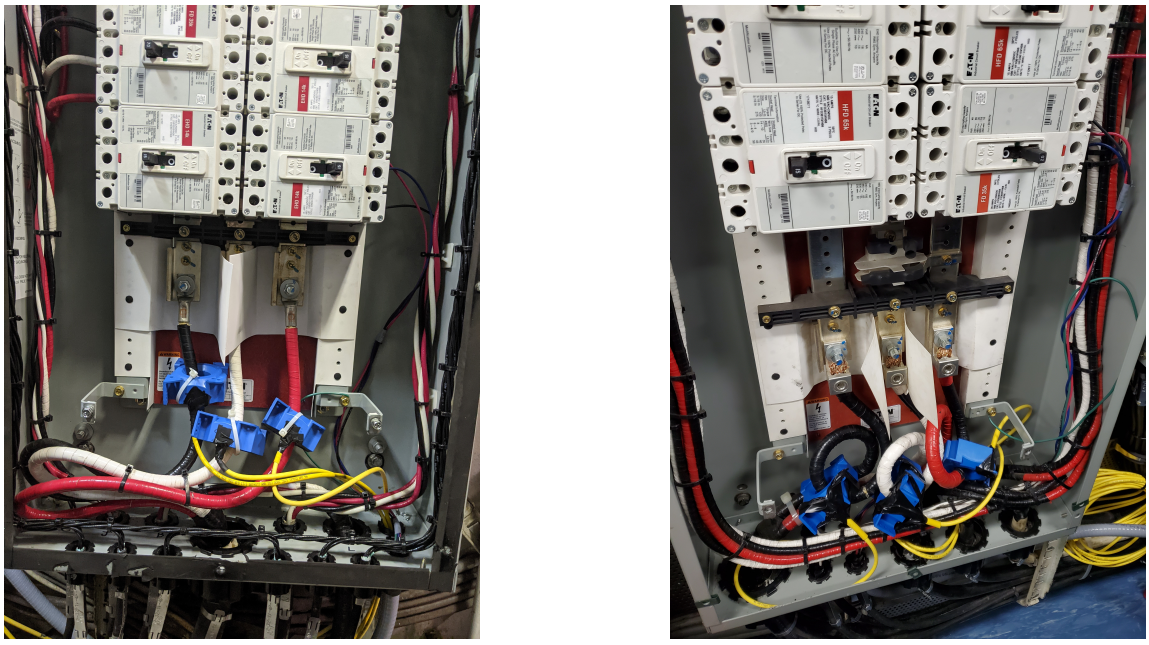

(a) Panel 2-32-1.

(b) Panel 1-66-2.

Figure 3-3: Current sensors and voltage taps for USCGC THUNDER BAY power panels.

3.2 Monitored Power Panels

As previously mentioned, two AIO NILM boxes were installed on THUNDER BAY on power panels 2-32-1 (Engine Room) and 1-66-2 (ECC). Each of these panels provide their own unique insights into different aspects of shipboard equipment. Figures 3-4 through 3-6 show the load trees for each of the panels. After the NILMs were installed each of the individual loads were energized and their respective electrical transients were recorded.

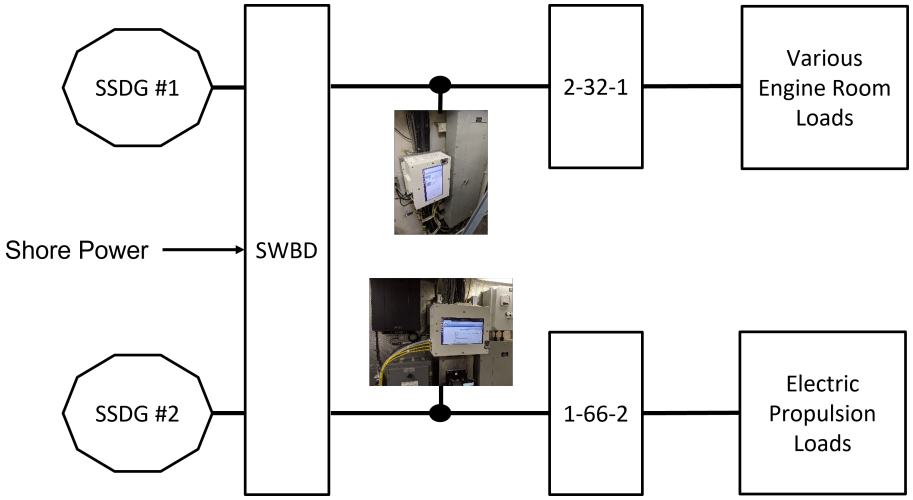

Figure 3-4: USCGC THUNDER BAY primary load tree

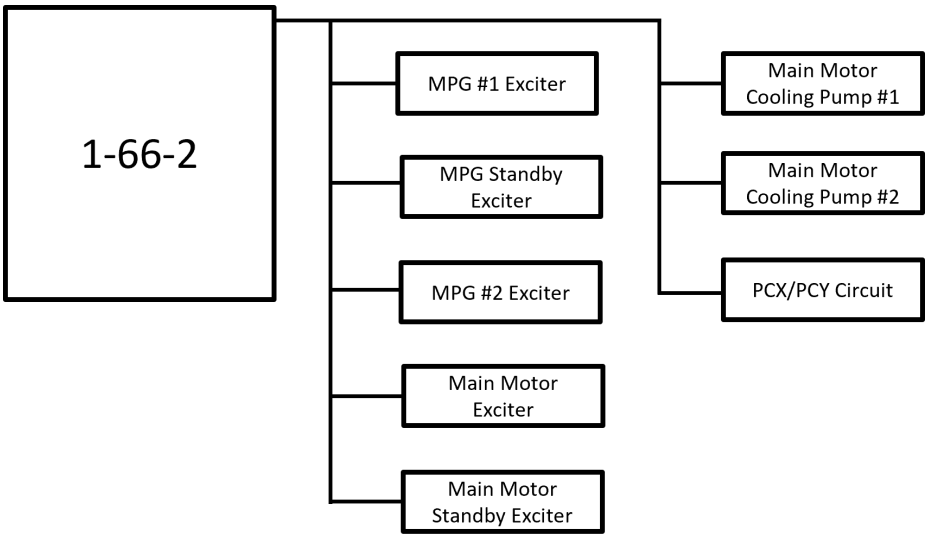

Figure 3-5: Load tree for power panel 1-66-2

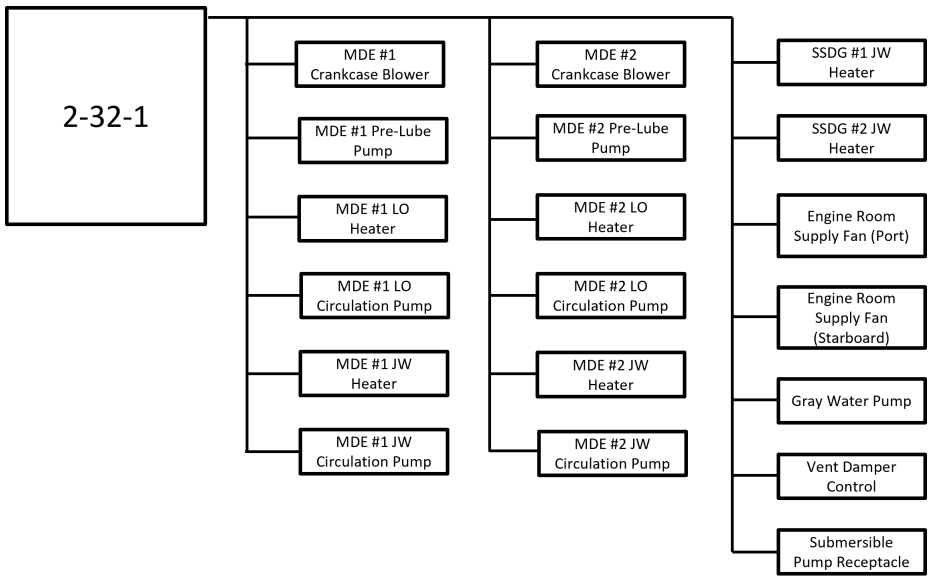

Figure 3-6: Load tree for power panel 2-32-1

3.3 Identified Loads on 2-32-1

Panel 2-32-1 primarily monitors loads related to the two main propulsion diesel engines and associated auxiliary equipment. All of the values presented for these loads are based on the current state of the equipment at the time of the NILM installation. Therefore, some of the loads do not match their rated power consumption and are not consistent across their matching piece of equipment (e.g. #1 and #2 jacket water heaters). All identified discrepancies will be discussed in further detail.

3.3.1 MPDE Crankcase Blower

The Main Propulsion Diesel Engine (MPDE) crankcase blower, as shown in Figure 3-7, consists of a 1hp (0.75kW) induction motor that drives a centrifugal fan to exhaust combustion gases from the engine's crankcase. The centrifugal fan contains a 3-blade radial impeller that maintains a vacuum within the crankcase, exhausts combustion gases, and removes oil mist from the exhaust stream. Combustion gases can build up within the crankcase due to piston blowby, which is expected on a small scale but can drastically increase due to worn or damaged piston seals. The crankcase

blower prevents the buildup of combustion gases within the crankcase which can cause catastrophic engine damage [12]. The crankcase blower is designed to run upon the startup of a MPDE and will remain operating until the MPDE is secured. The steady-state on/off transients for the #1 and #2 blowers can be seen in Figure 3-8 and Figure 3-9.

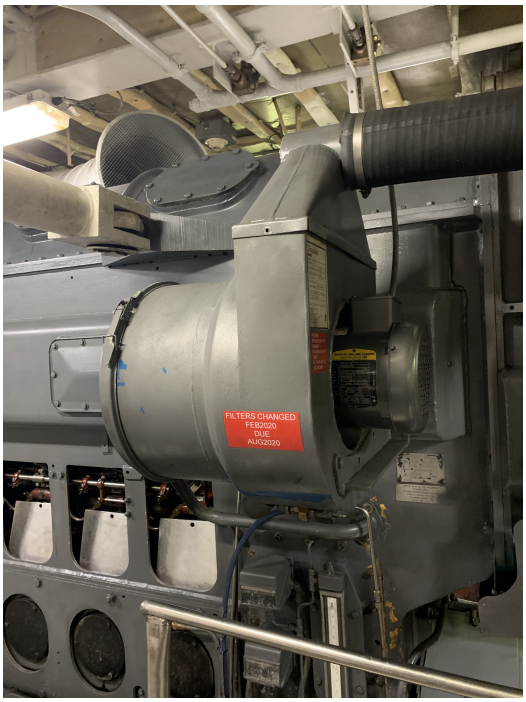

Figure 3-7: USCGC THUNDER BAY MPDE Crankcase Blower

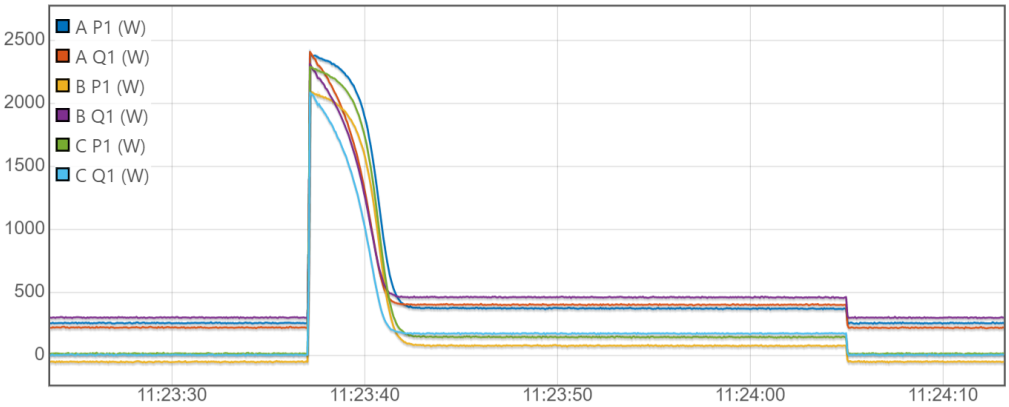

Figure 3-8: #1 MPDE Crankcase Blower on/off transient.

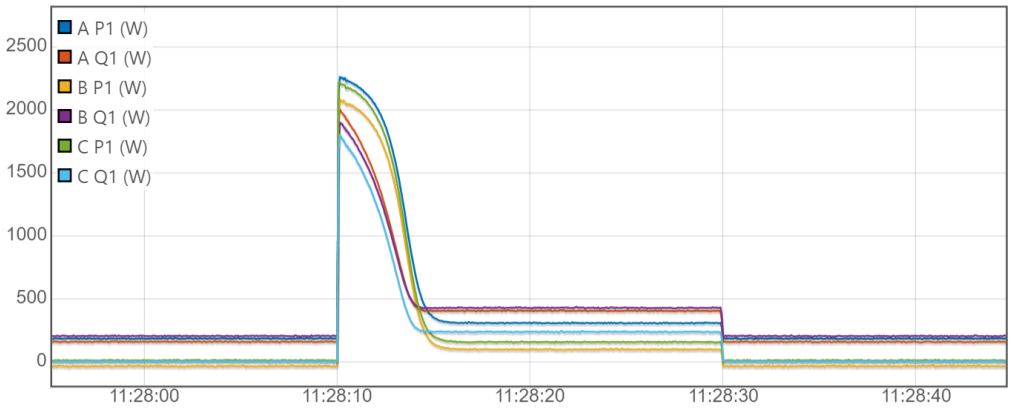

Figure 3-9: #2 MPDE Crankcase Blower on/off transient.

As seen in Table 3.1 there were slight differences noted between the #1 and #2 MPDE crankcase blowers, where the #2 blower is drawing approximately 20% more power at steady-state than the #1 blower. Without more extensive knowledge of the equipment operational history it is difficult to diagnose the exact cause for this difference.

Table 3.1: MPDE Crankcase Blower Information.

Panel	2-32-1	
Power Type	3-phase	
Control Type	Automatic	
Rated Power (W)	750	
Equipment #	#1	#2
Steady-State Real Power (W)	375	400
Steady-State Reactive Power (VAR)	512	703
Steady-State Apparent Power (VA)	635	810

3.3.2 MPDE Pre-Lube Pump

Figure 3-10: USCGC THUNDER BAY MPDE Pre-Lube Pump

The MPDE Pre-Lube Pump, shown in Figure 3-10, is driven by a 5 hp (3.75 kW) induction motor that is automatically actuated when starting a MPDE. When the engine is started, the pre-lube pump is activated and will operate for two minutes before shutting down [13]. The motor operates at a rated speed of 1,140 rpm, and the pump can process 8.2 gpm of lube oil at an operating pressure of 15 psi [14]. This is designed to ensure that the engine has enough lubricant to function and operate properly upon engine startup. The steady-state on/off transients for the #1 and #2 pumps can be seen in Figure 3-11 and Figure 3-12, with associated power information available in Table 3.2.

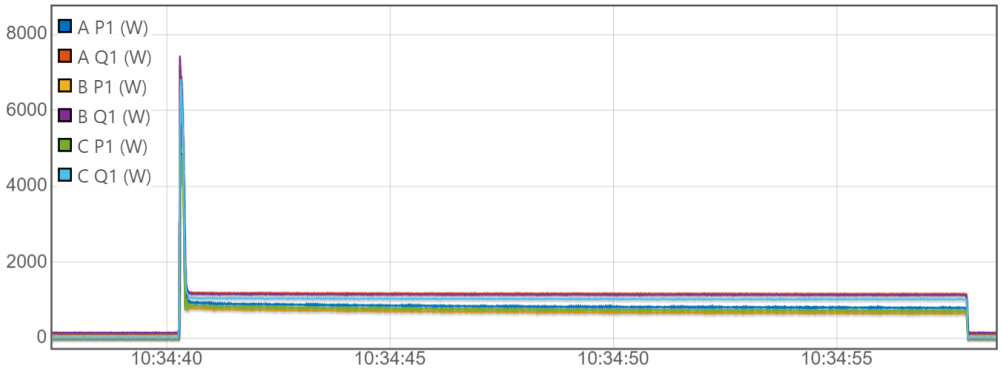

Figure 3-11: #1 MPDE Pre-Lube Pump on/off transient.

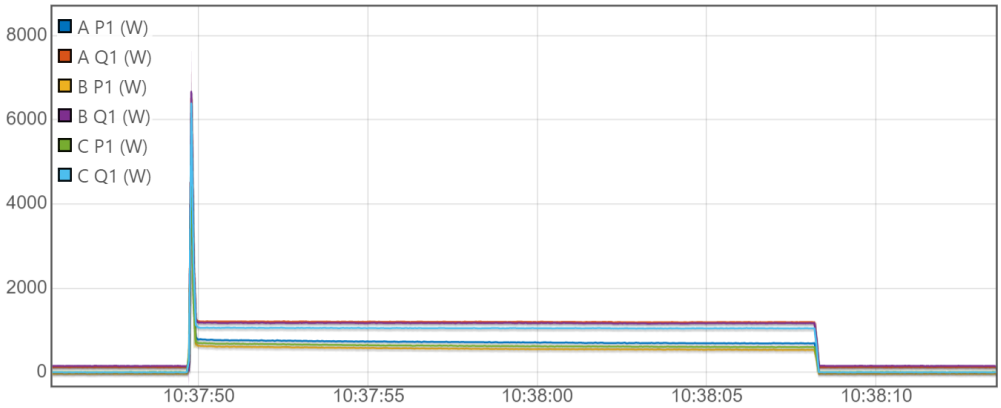

Figure 3-12: #2 MPDE Pre-Lube Pump on/off transient.

Table 3.2: MPDE Pre-Lube Pump Information.

Panel	2-32-1	
Power Type	3-phase	
Control Type	Automatic	
Rated Power (kW)	3.75	
Equipment #	#1	#2
Steady-State Real Power (kW)	2.15	1.80
Steady-State Reactive Power (kVAR)	3.08	3.14
Steady-State Apparent Power (kVA)	3.76	3.61

3.3.3 MPDE Lube Oil Heater

Figure 3-13: USCGC THUNDER BAY MPDE Lube Oil Heater

The MPDE Lube Oil Heater, shown in Figure 3-13, is a 3-phase 6 kW immersion heater that works alongside the MPDE Lube Oil Circulation Pump to maintain the MPDE lube oil system temperatures between 90 and 120 degrees Fahrenheit when the engines are not operating [15]. The steady state on/off transients for both the #1 and #2 heater can be seen below in Figure 3-14 and Figure 3-15, with associated power information available in Table 3.3.

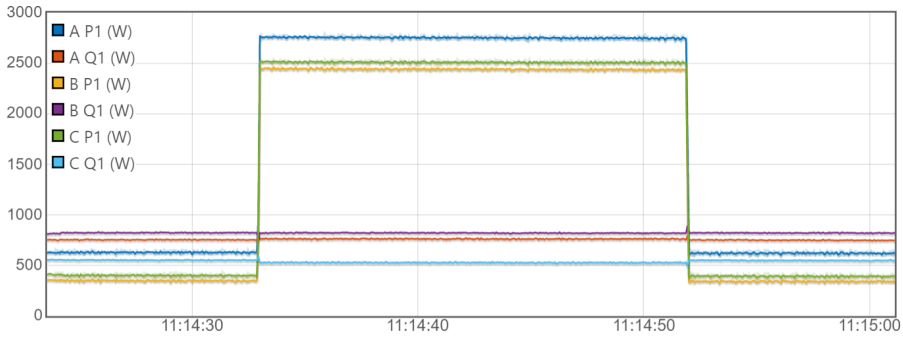

Figure 3-14: #1 MPDE Lube Oil Heater on/off transient.

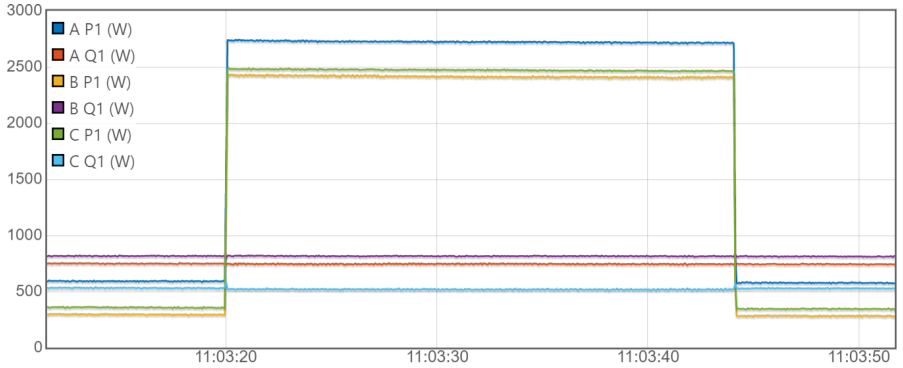

Figure 3-15: #2 MPDE Lube Oil Heater on/off transient.

Table 3.3: MPDE Lube Oil Heater Information.

Panel	2-32-1	
Power Type	3-Phase	
Control Type	Automatic	
Rated Power (kW)	6	
Equipment #	#1	#2
Steady-State Real Power (kW)	6.31	6.36
Steady-State Reactive Power (kVAR)	0.00	0.00

3.3.4 MPDE Lube Oil Circulation Pump

Figure 3-16: USCGC THUNDER BAY MPDE Lube Oil Circulation Pump

Lube oil circulating pumps, as shown in Figure 3-16, are responsible for drawing oil from the sumps of an engine and redistributing it throughout the lubricating oil system after passing through a series of filters and heating elements. The MPDE Lube Oil Circulation Pump installed on THUNDER BAY is driven by a 2 hp (1.5 kW) induction motor that ensures the proper amount of lube oil is circulated through the MPDE system. This pump is set to automatically circulate lube oil when the associated MPDE is not running, and works in concert with the previously mentioned MPDE Lube Oil Heater. The steady-state on/off transients for the #1 and #2 pumps can be seen below in Figure 3-17 and Figure 3-18, with associated power information available in Table 3.4.

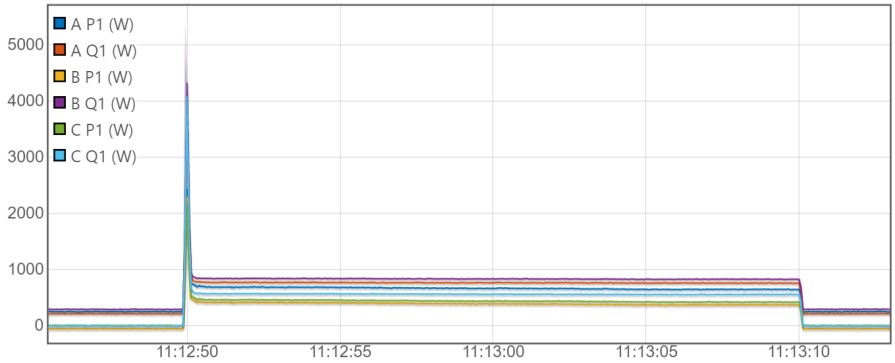

Figure 3-17: #1 MPDE Lube Oil Circulation Pump on/off transient.

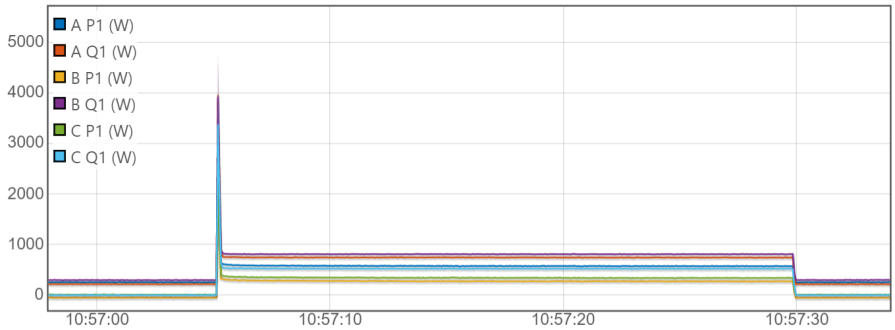

Figure 3-18: #2 MPDE Lube Oil Circulation Pump on/off transient.

Table 3.4: MPDE Lube Oil Circulation Pump Information.

Panel	2-32-1	
Power Type	3-Phase	
Control Type	Automatic	
Rated Power (kW)	1.5	
Equipment #	#1	#2
Steady-State Real Power (kW)	1.29	0.98
Steady-State Reactive Power (kVAR)	1.66	1.56
Steady-State Apparent Power (kVA)	2.10	1.84

3.3.5 MPDE Jacket Water Heater

Figure 3-19: USCGC THUNDER BAY MPDE Jacket Water Heater

The MPDE Jacket Water Heater, shown in Figure 3-19, is responsible for maintaining the temperature of the jacket water system at a temperature of approximately 90 degrees Farenheit [13]. The MPDE Jacket Water Heaters on THUNDER BAY are 3-phase immersion heaters rated at 12 kW. The heaters work with their associated Jacket Water Circulation Pump when the MPDE is not running. The steady state on/off transients for both the #1 and #2 heaters at the time of the NILM installation can be seen in Figure 3-20 and Figure 3-21, with associated power information available in Table 3.5. Note that neither of the jacket water heaters exhibited the anticipated characteristics of a 3-phase 12 kW heater. The #1 heater appears to be a 2 kW single phase line-line load and the #2 heater appears to be a single phase

phase line-line 6 kW load. These anomalies will be discussed further in Section 3.5.

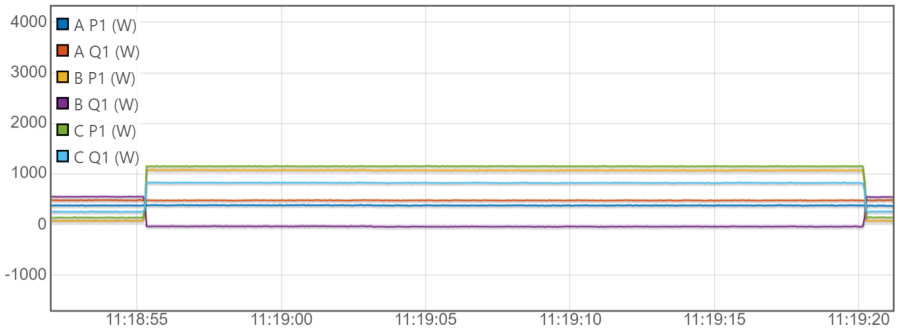

Figure 3-20: #1 MPDE Jacket Water Heater on/off transient.

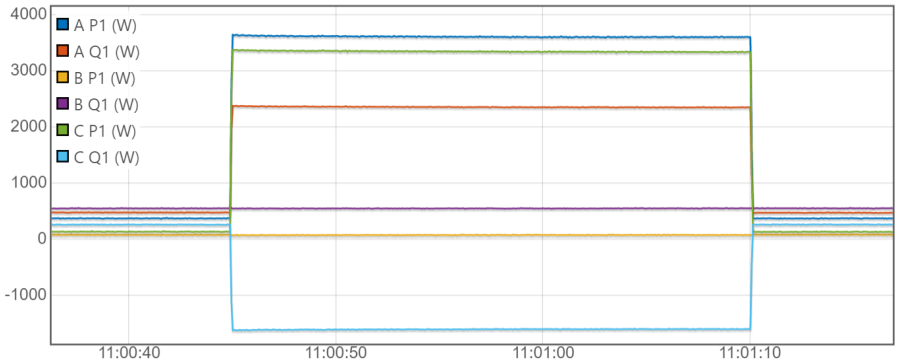

Figure 3-21: #2 MPDE Jacket Water Heater on/off transient.

Table 3.5: MPDE Jacket Water Heater Information.

Panel	2-32-1	
Power Type	3-Phase	
Control Type	Automatic	
Rated Power (kW)	12	
Equipment #	#1	#2
Steady-State Real Power (kW)	2.02	6.44
Steady-State Reactive Power (kVAR)	0.00	0.00

3.3.6 MPDE Jacket Water Circulation Pump

Figure 3-22: USCGC THUNDER BAY MPDE Jacket Water Circulation Pump

Jacket water circulation pumps are responsible for circulating jacket water, water used to maintain a running engine at a desired temperature, throughout the system when the associated engine is not running. The MPDE Jacket Water Circulation Pumps on THUNDER BAY, shown in Figure 3-22, are driven by 1 hp (0.75 kW) induction motors that are rated to operate at 1750 rpm [16]. The steady-state on/off transients for the #1 and #2 pumps can be seen in Figure 3-23 and Figure 3-24, with associated power information available in Table 3.6.

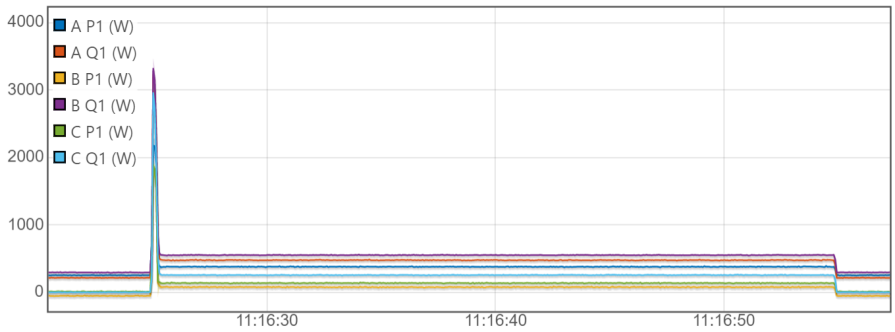

Figure 3-23: #1 MPDE Jacket Water Circulation Pump on/off transient.

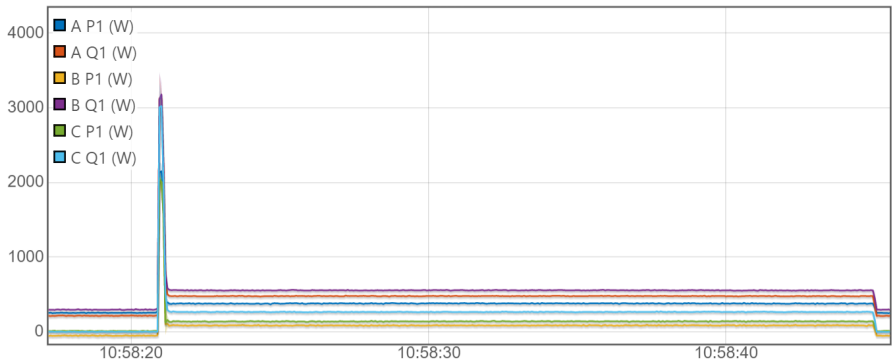

Figure 3-24: #2 MPDE Jacket Water Circulation Pump on/off transient.

Table 3.6: MPDE Jacket Water Circulation Pump Information.

Panel	2-32-1	
Power Type	3-Phase	
Control Type	Automatic	
Rated Power (W)	750	
Equipment #	#1	#2
Steady-State Real Power (W)	383	393
Steady-State Reactive Power (VAR)	776	789
Steady-State Apparent Power (VA)	865	881

3.3.7 SSDG Jacket Water Heater

Figure 3-25: USCGC THUNDER BAY SSDG Jacket Water Heater

The Ship Service Diesel Generator (SSDG) Jacket Water Heaters serve the same purpose and operate in the same manner as the MPDE Jacket Water Heaters described in Section 3.3.5 [17]. These heaters are single phase line-line loads rated at 6 kW. They operate when the generators are not online, and are the only loads for the SSDGs that the NILM observes. Steady-state on/off transients for the #1 and #2 heaters can be seen in Figure 3-26 and Figure 3-27, with associated power information available in Table 3.7.

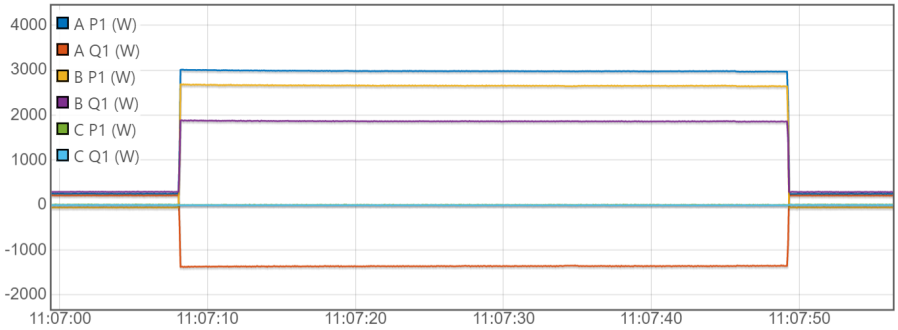

Figure 3-26: #1 SSDG Jacket Water Heater on/off transient.

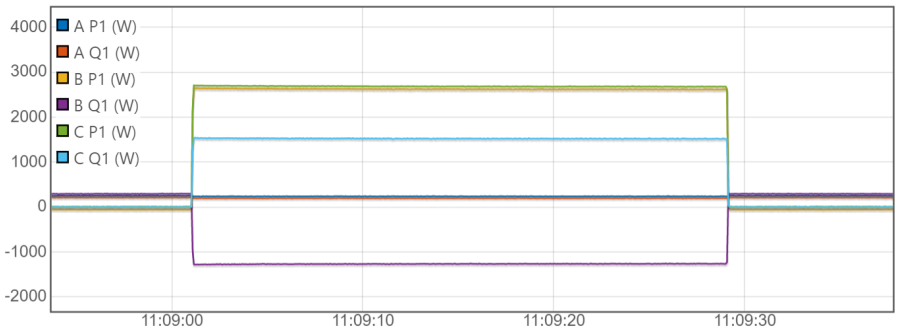

Figure 3-27: #2 SSDG Jacket Water Heater on/off transient.

Table 3.7: SSDG Jacket Water Heater Information.

Panel	2-32-1	
Power Type	Single Phase L-L	
Control Type	Automatic	
Rated Power (kW)	6	
Equipment #	#1	#2
Steady-State Real Power (kW)	5.43	5.34
Steady-State Reactive Power (kVAR)	0.00	0.00

3.3.8 Engine Room Supply Fan

THUNDER BAY's engine room ventilation is supplied by two vane-axial fans with one located on each side of the space. An image of the starboard supply fan can be seen in Figure 3-28, with the associated control panel seen in Figure 3-29. These fans are controllable through both local and remote operation and have a LOW and a HIGH setting, depending on the amount of airflow needed for the space. The rated steady state power consumption for these fans are 5 hp (3.75 kW) at the HIGH setting and 1.2 hp (0.9 kW) at the LOW setting. Sample transients for the #1 supply fan at both LOW and HIGH settings can be seen in Figure 3-30 and Figure 3-31, with associated power information available in Table 3.8 and Table 3.9. While both fans exhibit similar characteristics while at the LOW setting, the #2 supply fan draws less total power at the HIGH setting. Access to the fan is limited, and without further inspection of the system the exact causation for this difference is unknown.

Figure 3-28: USCGC THUNDER BAY Engine Room Supply Fan (Starboard)

Figure 3-29: USCGC THUNDER BAY Engine Room Supply Fan Controllers

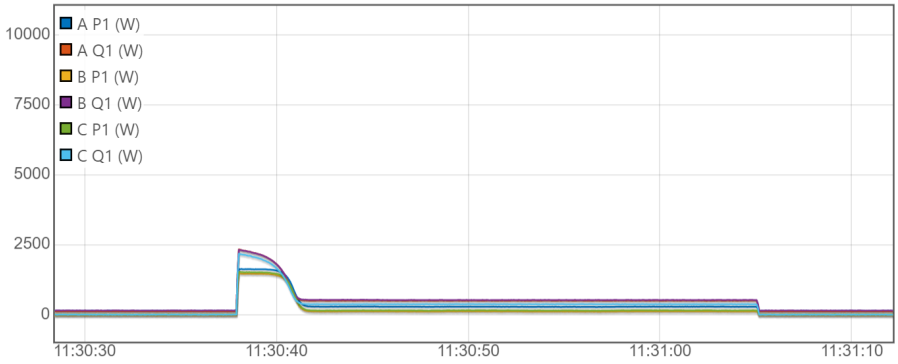

Figure 3-30: Engine Room Supply Fan on/off transient (LOW setting).

Table 3.8: #1 Engine Room Supply Fan Information (LOW Setting).

Panel	2-32-1	
Power Type	3-Phase	
Control Type	Automatic/Manual	
Rated Power (kW)	0.9	
Equipment #	#1	#2
Steady-State Real Power (LOW) (kW)	0.44	0.41
Steady-State Reactive Power (LOW) (kVAR)	1.14	1.24
Steady-State Apparent Power (LOW) (kVA)	1.22	1.30
Power Factor	0.36	0.32

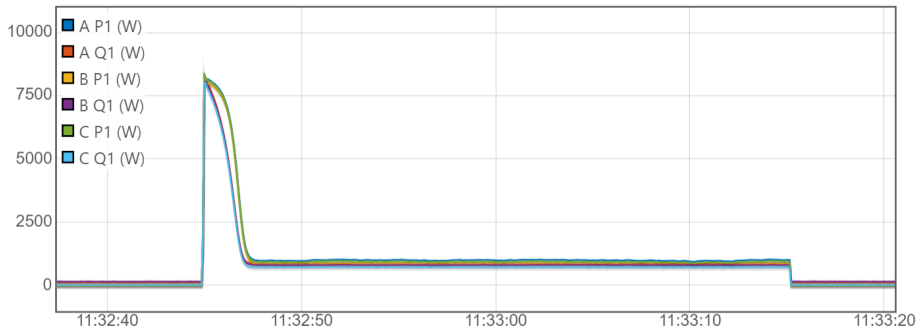

Figure 3-31: Engine Room Supply Fan on/off transient (HIGH setting).

Table 3.9: #1 Engine Room Supply Fan Information (HIGH Setting).

Panel	2-32-1	
Power Type	3-Phase	
Control Type	Automatic/Manual	
Rated Power (kW)	3.75	
Equipment #	#1	#2
Steady-State Real Power (HIGH) (kW)	2.65	2.15
Steady-State Reactive Power (HIGH) (kVAR)	2.10	0.95
Steady-State Apparent Power (HIGH) (kVA)	3.38	2.35
Power Factor	0.78	0.91

3.3.9 Gray Water Pump

Figure 3-32: USCGC THUNDER BAY Gray Water Pump

THUNDER BAY has a single gray water pump, shown in Figure 3-32, that is used to pump "gray" water either overboard or to a shore connection from the ship's gravity fed holding tank. "Gray" water is water that has been contaminated to a lesser extent than sewage or "black" water, and comes from sources such deck drains, shower drains, and sink drains. In order for gray water to be pumped overboard into the sea, a vessel needs to be far enough offshore, and since THUNDER BAY typically operates in a near shore environment, this pump is normally energized when moored and connected to a shoreside receptacle. The rated steady state power consumption for this pump is 5 hp (3.75 kW).

Table 3.10: Gray Water Pump Information.

Panel	2-32-1
Power Type	3-Phase
Control Type	Manual
Rated Power (kW)	3.75

3.3.10 Submersible Pump Receptacle

Figure 3-33: USCGC THUNDER BAY Submersible Pump Receptacle

The submersible pump receptacle is a 450V, 3-phase receptacle located on the forward section (foc'sle) of the Cutter. Its primary purpose is to power an electrical pump that can be used in damage control scenarios, however any other equipment requiring 450V power can be plugged into the receptacle. Although this is not often utilized, the AIO box on panel 2-32-1 is capable of monitoring any equipment that draws power from this receptacle.

3.4 Identified Loads on 1-66-1

Panel 1-66-2 primarily monitors loads related to the electric propulsion system on THUNDER BAY. In particular, all five propulsion exciters as well as the Main Motor cooling pumps are monitored and are explained in further detail in this section.

3.4.1 Main Motor Cooling Pump

Figure 3-34: Main motor cooling pumps.

The Main Motor cooling pumps, shown in Figure 3-34, are centrifugal pumps driven by 3 hp (2.25 kW) motors. There are two separate pumps that are used to provide cooling for the Main Motor. The pumps are controlled by variable pulse width modulation, and the pump speed is varied based upon the propulsion throttle input command [18]. As can be seen in the transient for each of these pumps in Figure 3-35 and Figure 3-36 as well as the power factors identified in Table 3.11, there is minimal reactive power change when the pump is turned on. While most US Coast Guard cooling pumps are not controlled in this particular manner, these pumps are configured with additional power electronics due to the sensitive and expensive nature of the equipment needed to operate the Main Porpulsion Motor.

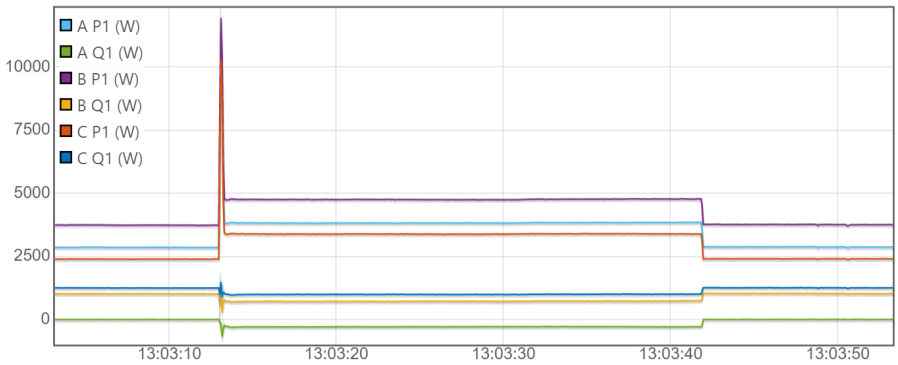

Figure 3-35: #1 Main Motor Cooling Pump on/off transient.

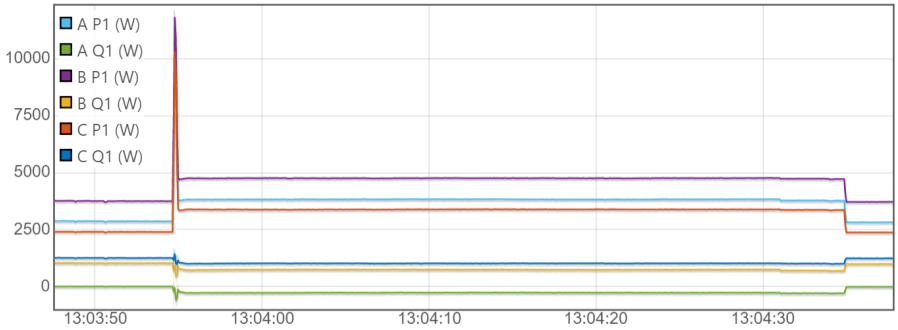

Figure 3-36: #2 Main Motor Cooling Pump on/off transient.

Table 3.11: Main Motor Cooling Pump Information.

Panel	1-66-2	
Power Type	3-Phase	
Control Type	Automatic	
Rated Power (kW)	2.25	
Equipment #	#1	#2
Steady-State Real Power (kW)	2.98	2.95
Steady-State Reactive Power (kVAR)	-0.83	-0.80
Steady State Apparent Power (kVA)	3.10	3.05
Power Factor	0.97	0.97

3.4.2 Main Motor/Main Propulsion Generator Exciters

There are a total of five exciters on THUNDER BAY, all monitored by the NILM. Two of these exciters are designated for the main motor, of which the power electronics can be seen in Figure 3-37, and three are designated for the two main propulsion generators (MPG). Only one of the main motor exciters is required to provide excitation and regulation to the motor field, while the other remains in standby. Of the three exciters available for the main propulsion generators, one is designated for the #1 MPDE, one is designated for the #2 MPDE, and the third is designated as a standby exciter. While the exciters themselves will vary in power draw depending on the propulsion mode setting and throttle position input, a sample on transient of one of the exciter transformer breakers can be seen in Figure 3-38. The monitoring of these particular loads are able to provide critical insights into ship operation and will be further examined in Chapter 4.

Figure 3-37: Sample of exciters located within the main switchboard cabinet.

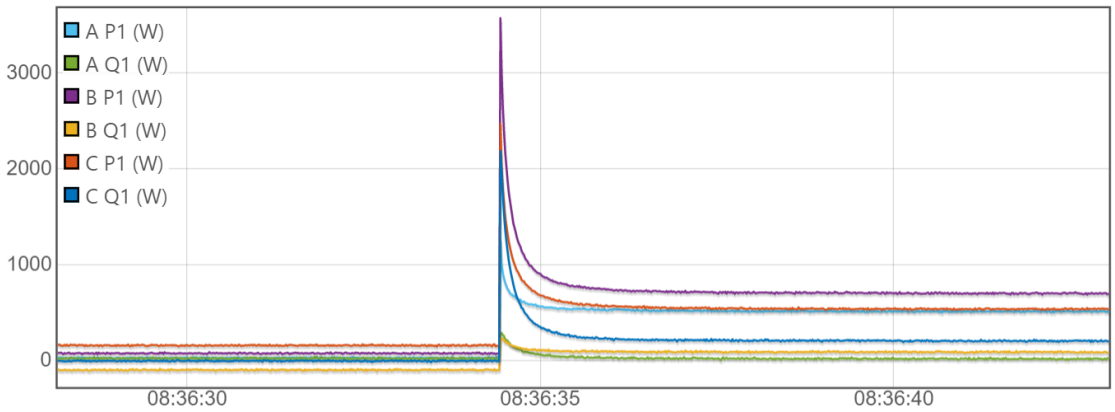

Figure 3-38: Exciter transformer breaker on transient.

3.5 Sample Identification of Faults - MPDE Jacket Water Heater

While several pieces of identical equipment displayed some slight differences in power stream data, the most noticeable of these discrepancies were the MPDE Jacket Water Heaters described in Section 3.3.5. These faults will be described in further detail to illustrate the strengths of the NILM's fault detection capabilities.

3.5.1 #1 MPDE Jacket Water Heater

As previously mentioned, the MPDE Jacket Water Heaters are each 3-phase, 12 kW heaters that are powered through electrical panel 2-32-1. Upon initial inspection of power stream data it was evident that neither heater exhibited their anticipated characteristics. An initial power transient measured for the #1 MPDE jacket water heater can be seen below in Figure 3-39. It displays the characteristics of a 2 kW single phase line-line heater, which does not correspond with the expected 3-phase, 12 kW heater characteristics. The steady state power data is shown in Table 3.12.

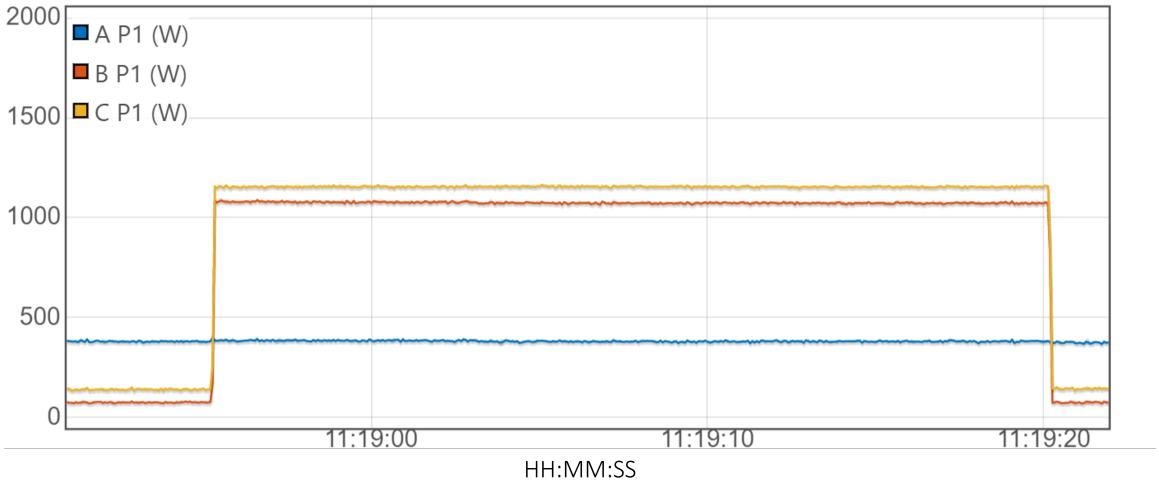

Figure 3-39: Initial #1 MPDE Jacket Water Heater Transient (10 February 2021).

Table 3.12: #1 Jacket Water Heater Initial Steady State Power Data - 10 February 2021

Phase	**Real Power (kW)**
A	0
B	1.0
C	1.0
Total	**2.0**

After determining that there was an issue with the #1 heater, the crew was alerted and examined the element wiring. One phase was found to be disconnected, with visible corrosion on the wiring identified, as shown in Figure 3-40. The heater was re-wired, with the corroded section removed and insulated wire was reattached to the proper phase. A new power transient was measured for the heater, as shown below in Figure 3-41. This new transient displayed the characteristics consistent with those of a 3-phase, 12 kW heater with a degraded coil, drawing approximately 4 kW on one phase and only 2 kW on each of the other two phases (approximately 8 kW total power draw), as shown in Table 3.13.

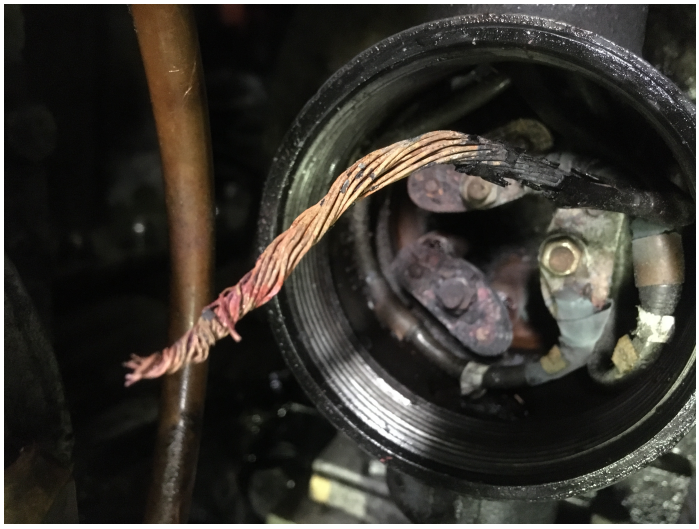

Figure 3-40: Visible corrosion on #1 jacket water heater wiring.

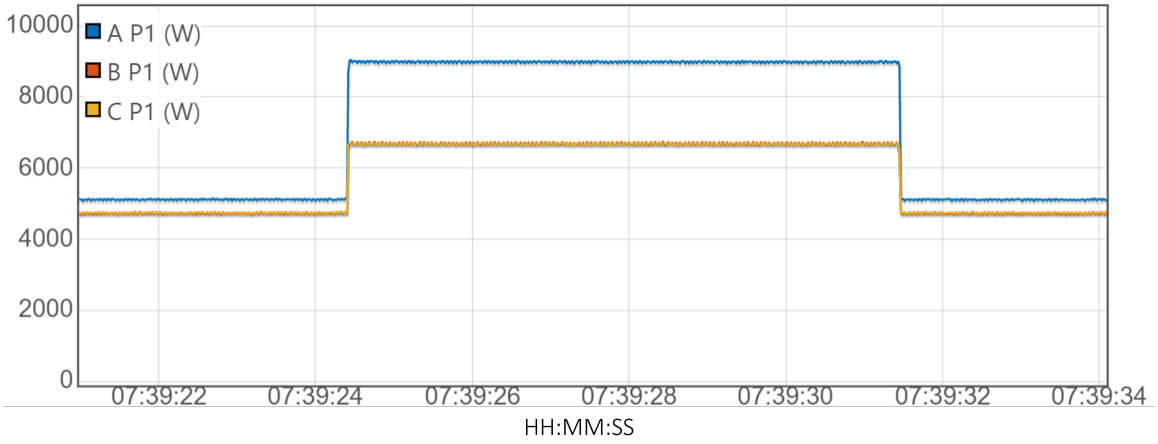

Figure 3-41: #1 Jacket Water Heater Power Transient After Re-Wiring (21 June 2021)

Table 3.13: #1 Jacket Water Heater Steady State Power Data (Post Repair) - 22 June 2021

Phase	**Real Power (kW)**
A	3.87
B	1.96
C	1.94
Total	**7.77**

3.5.2 #2 MPDE Jacket Water Heater

The power transient measured for the #2 MPDE jacket water heater can be seen below in Figure 3-42, with steady-state power data available in Table 3.14. The characteristics observed were those of a 6.2 kW single phase line-line heater, which does not correspond with the expected power demand. This can be verified with further examination of the heating elements.

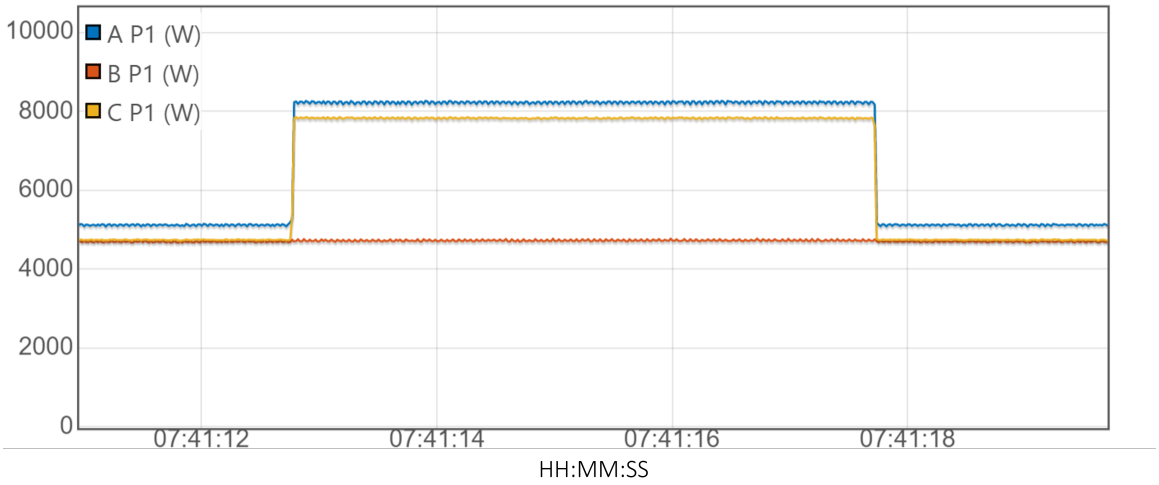

Figure 3-42: #2 MPDE Jacket Water Heater Transient (21 June 2021)

Table 3.14: #2 Jacket Water Heater Steady State Power Data - 21 June 2021

Phase	**Real Power (kW)**
A	3.1
B	0
C	3.1
Total	**6.2**

3.5.3 NILM Insight

Monitoring the power consumption is an effective way to gain insight into the operating conditions of the MPDE jacket water heaters. Without the NILM, the easiest way for a member of the crew to monitor the performance of the heaters would be to observe the temperature gauge on the outlet side of the jacket water system. A sample

of the outlet temperatures on the jacket water system were taken on 23 March 2021, as seen in Table 3.15, prior to the wiring on the #1 heater being repaired. Although this is just a snapshot of one particular moment in time, it is very noticeable that the #2 heater is able to achieve an output temperature that is 20 degrees greater than the #1 heater. After the correction of the #1 jacket water heater wiring, the new outlet temperatures on the system were recorded and are presented in Table 3.16. Looking solely at these temperature gauge readings, a watch stander may be inclined to think that the issue has been corrected; however, it isn't until the power stream data is analyzed that the potential faults can be identified.

Table 3.15: 23 March 2021 - Pre Repair of #1 Jacket Water Heater Wiring

Equipment	**Outlet Temp (°F)**
#1 MPDE Jacket Water Heater - Pre Repair	115.6
#2 MPDE Jacket Water Heater	135.7

Table 3.16: 22 June 2021 - Post Repair of #1 Jacket Water Heater Wiring

Equipment	**Outlet Temp (°F)**
#1 MPDE Jacket Water Heater - Post Repair	138.4
#2 MPDE Jacket Water Heater	135.0

By inspecting the power streams, it is apparent that neither MPDE jacket water heater is operating as expected. Two different fault conditions have been observed with the MPDE jacket water heater: a degraded heating coil and a missing voltage connection to the heater (i.e., the phase a, b, or c voltage). The MPDE jacket water heater consists of three heating elements connected line-line. Thus, when a heating element open-circuits, it manifests as a reduction in two of the line currents. With a missing voltage connection, the heater acts as a single phase line-line heater. Figure 3-43 shows different scenarios for a delta-connected heater, including healthy (Figure 3-43a) and under different fault conditions (Figure 3-43b-Figure 3-43e). The scenarios are:

(a) Balanced delta-connected heater

(b) Delta-connected heater with a missing voltage connection

(c) Delta-connected heater with a open-circuited heating element

(d/e) Delta-connected heater with both a missing voltage connection and an open-circuited heating element

Table 3.17: Impedance and Power Relationships

Scenario	Impedances	Real Power		
a	$Z_{ab} = R$ $Z_{bc} = R$ $Z_{ca} = R$	$P_{ab} = 3\frac{V^2}{R}$ $P_{bc} = 3\frac{V^2}{R}$ $P_{ca} = 3\frac{V^2}{R}$	$P_a = 3\frac{V^2}{R}$ $P_b = 3\frac{V^2}{R}$ $P_c = 3\frac{V^2}{R}$	$P_T = 9\frac{V^2}{R} = P_{rated}$
b	$Z_{bc} = \frac{2}{3}R$	$P_{bc} = \frac{9}{2}\frac{V^2}{R}$	$P_b = \frac{9}{4}\frac{V^2}{R}$ $P_c = \frac{9}{4}\frac{V^2}{R}$	$P_T = \frac{9}{2}\frac{V^2}{R} = \frac{1}{2}P_{rated}$
c	$Z_{ab} = R$ $Z_{bc} = \infty$ $Z_{ca} = R$	$P_{ab} = 3\frac{V^2}{R}$ $P_{bc} = 0$ $P_{ca} = 3\frac{V^2}{R}$	$P_a = 3\frac{V^2}{R}$ $P_b = \frac{3}{2}\frac{V^2}{R}$ $P_c = \frac{3}{2}\frac{V^2}{R}$	$P_T = 6\frac{V^2}{R} = \frac{2}{3}P_{rated}$
d	$Z_{bc} = 2R$	$P_{bc} = \frac{3}{2}\frac{V^2}{R}$	$P_b = \frac{3}{4}\frac{V^2}{R}$ $P_c = \frac{3}{4}\frac{V^2}{R}$	$P_T = \frac{3}{2}\frac{V^2}{R} = \frac{1}{6}P_{rated}$
e	$Z_{ac} = R$	$P_{ac} = 3\frac{V^2}{R}$	$P_a = \frac{3}{2}\frac{V^2}{R}$ $P_c = \frac{3}{2}\frac{V^2}{R}$	$P_T = 3\frac{V^2}{R} = \frac{1}{3}P_{rated}$

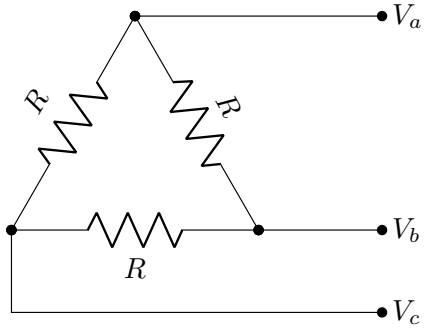

(a) Balanced delta-connected heater.

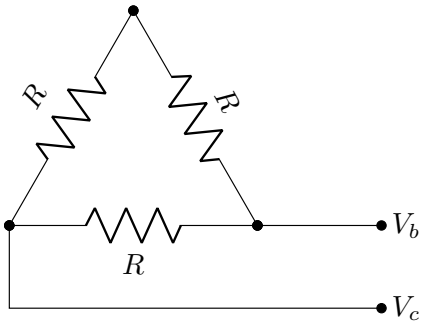

(b) Delta-connected heater with missing voltage connection.

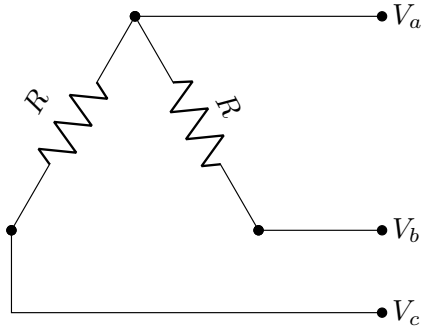

(c) Delta-connected heater with open-circuited heating element.

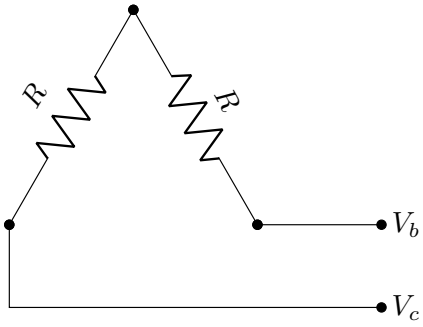

(d) Delta-connected heater with both a missing voltage connection and open-circuited heating element.

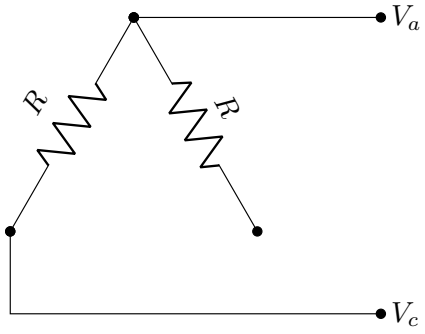

(e) Delta-connected heater with both a missing voltage connection and open-circuited heating element.

Figure 3-43: Delta-connected heater under both healthy (a) and fault conditions (b-e).

Table 3.17 shows the impedances and resulting power for these scenarios. Here, $V = 259.8$ V and P_T is the total power. A missing voltage connection results in the heater drawing only one-half of its rated power. A degraded heating coil results in the heater drawing two-thirds of its rated power. These two faults combined, depending on which voltage is missing and which coil is degraded, results in the heater drawing either one-sixth or one-third of its rated power.

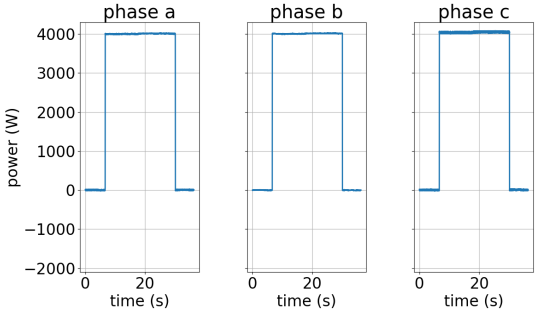

(a) SPENCER MPDE lube oil heater demonstrating a balanced delta heater.

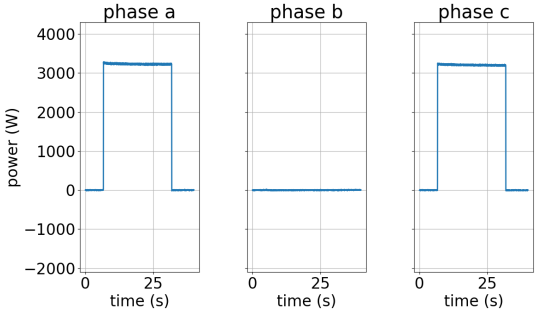

(b) #2 MPDE jacket water heater potentially demonstrating a missing voltage connection.

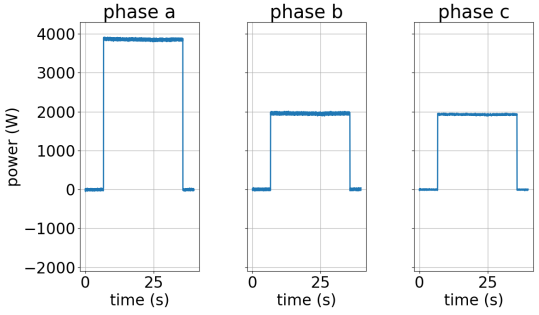

(c) #1 MPDE jacket water heater demonstrating a single open-circuited heating element.

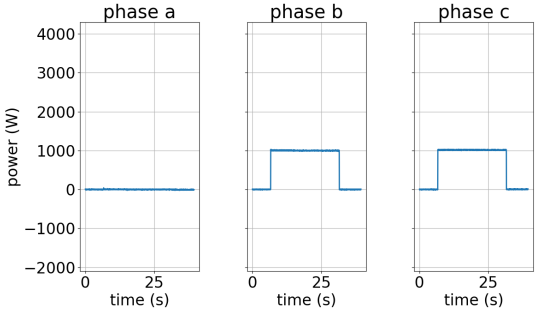

(d) #1 MPDE jacket water heater demonstrating an open-circuited heating element and a missing voltage connection.

Figure 3-44: Per-phase real power for scenarios (a)-(d).

The per-phase real power streams for scenarios (a)-(d) are shown in Figure 3-44. The healthy example in Figure 3-44a is from the MPDE lube oil heater on USCGC SPENCER, which is a 12 kW delta-connected heater, understood to be similar to the MPDE jacket water heater on THUNDER BAY. As shown, the phases are balanced, drawing 4 kW per phase. The remaining three examples are from the MPDE jacket water heaters on THUNDER BAY, presented as plausible explanations

for the observed power streams. The #2 MPDE jacket water heater in Figure 3-44b potentially demonstrates a missing voltage connection. In this case, there would be no phase b voltage connection, resulting in the heater drawing approximately 6 kW. The #1 MPDE jacket water heater in Figure 3-44c shows the behavior of a single open-circuited heating element (possibly corrosion in the heating element between phases b and c), resulting in the heater drawing approximately 8 kW. This was the state of the heater after the wiring was fixed, with the correct voltages. Prior to the wiring fix, the phase a voltage had no connection. Combined with the open-circuited heating element fault, the heater was only drawing 2 kW, as shown in Figure 3-44d. The total power for each of the scenarios is shown in Figure 3-45. These power signatures match the expected values from Table 3.17.

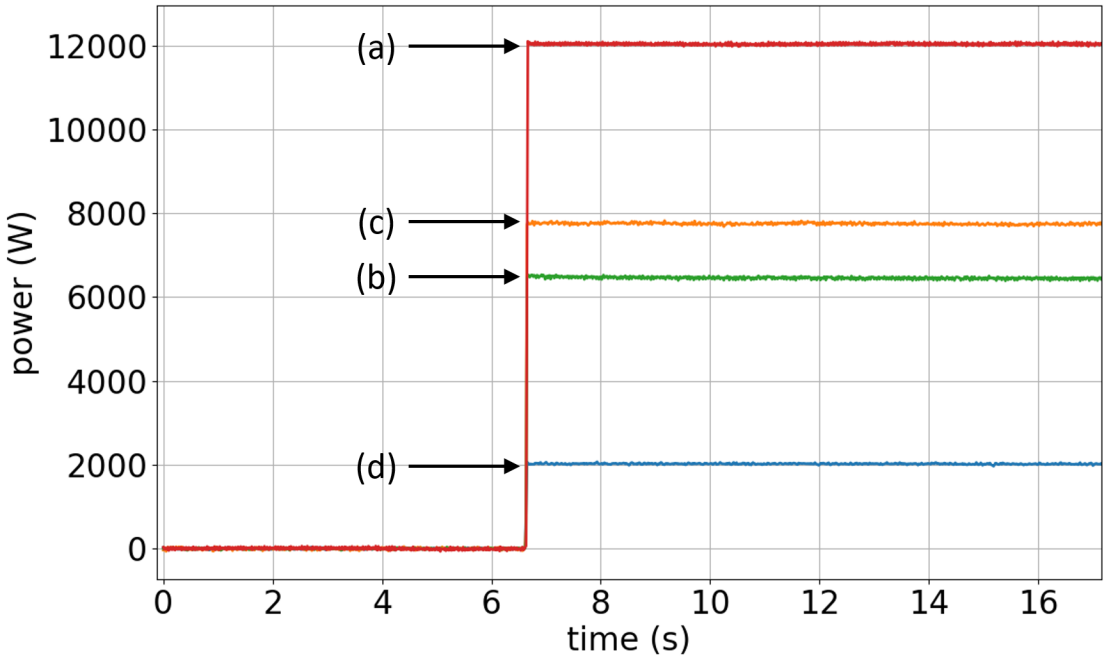

Figure 3-45: Total real power for scenarios (a)-(d).

Chapter 4

THUNDER BAY Electric Propulsion

As previously mentioned, THUNDER BAY is equipped with a diesel-electric propulsion system that drives a single shaft with a fixed pitched propeller. This type of propulsion system design provides benefits to an icebreaker by allowing for the use of more than one prime mover to power a single shaft and meet the varying torque requirements needed for icebreaking operations [19]. Since there is only one propulsion shaft, the architectural design and selection of this system is critical for the safe operation of the ship. With the NILM installed on panel 1-66-2 directly monitoring the exciters for the main propulsion generators and motor, this provides the unique opportunity to directly observe the changes in operation of the propulsion system, and classify these as specific shipboard "mission sets". Portions of this section were written in coordination with LT Devin Quinn, US Coast Guard, as part of a joint thesis presentation.

4.1 Propulsion System Design

The propulsion system on THUNDER BAY consists of two Fairbanks-Morse 38D8-1/8 blower-scavenged diesel engines. Each of the propulsion diesel engines are coupled to a 1,000 kW DC generator set (rated at 900 V and 850 rpm). Each of these generators then provides power to the 2,500 hp Westinghouse electric propulsion motor that drives the single propulsion shaft. The propulsion motor is a DC, shunt-wound,

separately-excited, compensated machine. A conceptual schematic of this type of system can be seen in Figure 4-1, with a more detailed view seen in Figure 4-2. The orange lines in Figure 4-2 represent the electrical power supplying panel 1-66-2, which can originate from either shore power or the SSDGs. The blue lines represent the power leaving panel 1-66-2 that energizes the exciters for both the main propulsion generators and main propulsion motor. The thin black lines represent the power delivered from the main propulsion generators to the main motor. The thicker black lines between the MPDEs and MPGs as well as the thick line between the main motor and the propeller represent physically connected shafts.

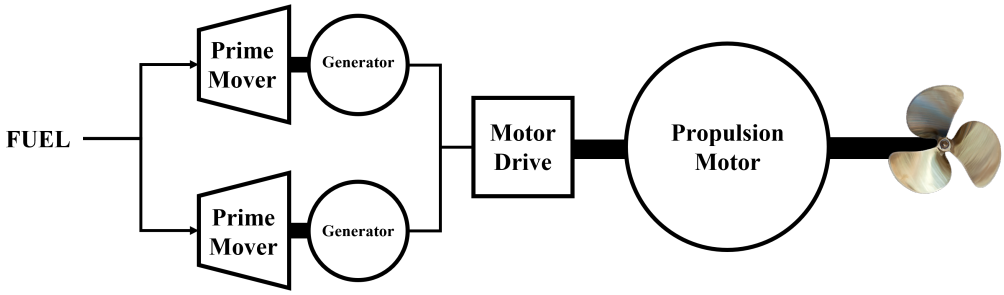

Figure 4-1: Conceptual diesel-electric propulsion system.

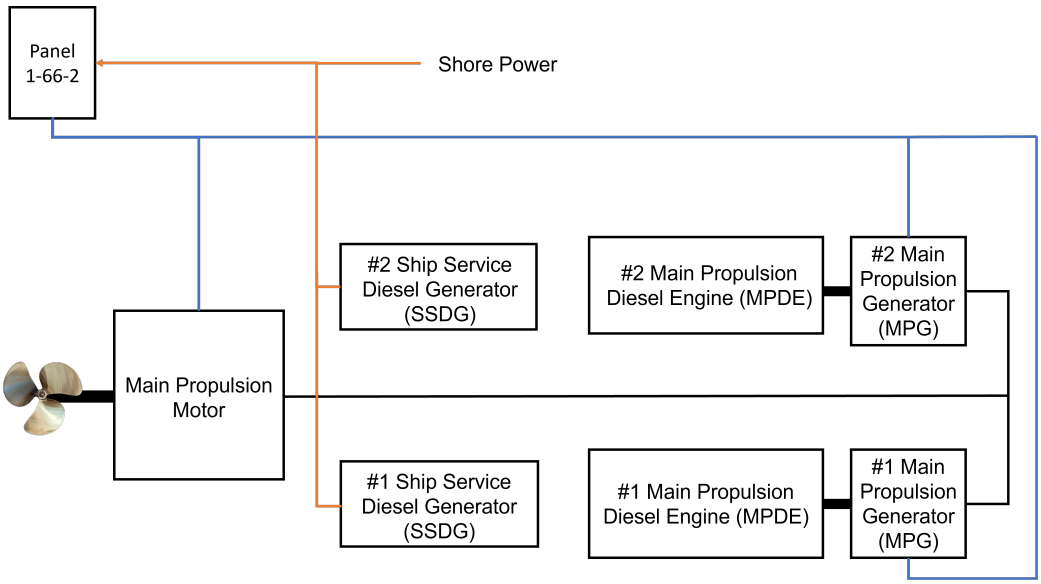

Figure 4-2: THUNDER BAY propulsion system schematic.

The architecture of this system is very similar to that of a Ward-Leonard system. The Ward-Leonard system is an example of an armature voltage control, which was

originally implemented on ships to allow for the operation of DC driven motor winches within a ship's AC supply system [19]. Three rotating machines are required to form this system. A motor-generator set (3-phase induction motor coupled to a DC generator), also commonly referred to as an M-G set, provides a variable DC voltage to the armature of a DC motor, in this case the main propulsion motor.

There are four settings that dictate the operation of the THUNDER BAY propulsion system. The first and most prominently used of these is the Automatic Control Mode. In this mode the operator will input the desired throttle position, and the speed of the propulsion motor shaft is controlled by a combination of automatically adjusting the speed of the diesel engines, DC generator shunt fields, and the DC motor shunt field [20]. This is accomplished through the variation of polarity and voltage of the main propulsion generators, accompanied with the speed variation and excitation changes at the generator. There is an installed "load-control program" that regulates the motor field excitation so that constant horsepower with be absorbed for a given control lever setting with the motor speed being proportionate to the propeller torque increase. When a throttle position input is set by the navigator of the vessel, the main diesel engines will run at a desired speed and load. The control system will then regulate the motor field excitation to draw the regulated line current from the main propulsion generators. Relationships between throttle position input and motor field current, diesel engine rpm, and generator armature voltage can be seen in Figure 4-3 through 4-5.

The second method of propulsion control is Manual Control Mode, where the diesel engine speed, generator field current, and motor field current are set manually. This is typically only used when warming up a diesel engine or for emergency purposes. The third method of propulsion control is the "Auto Gen-Man Motor" Mode, where the diesel engine speed and generator field current are automatically controlled via the throttle input command and the motor field current is manually adjusted. The final propulsion control method is referred to as "Auto Max 10", which is similar to the Automatic Control Mode where the generator and motor field currents are automatically adjusted based on the throttle input, however the diesel engine speed

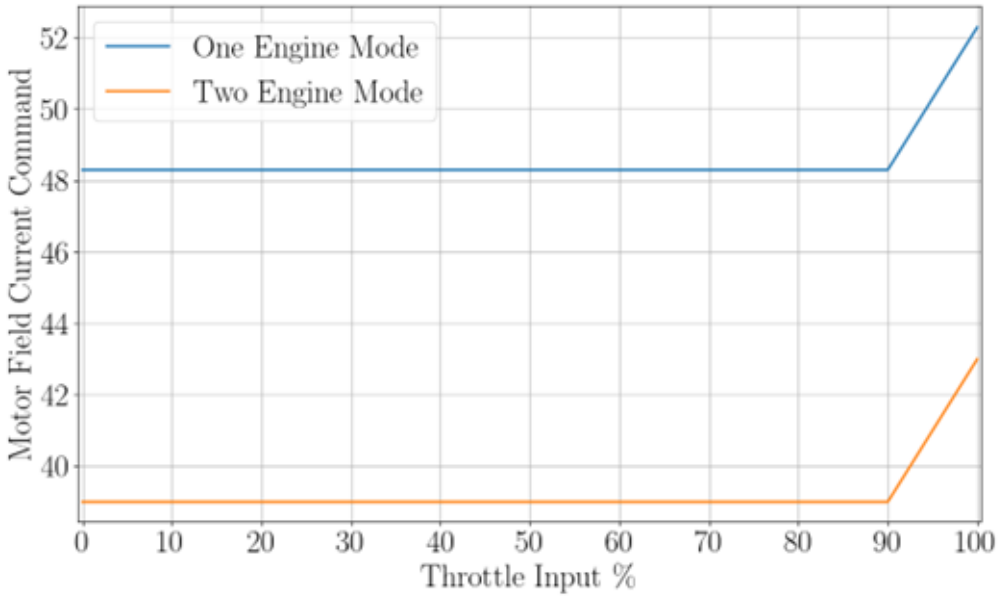

Figure 4-3: Comparison of motor field current to throttle position input.

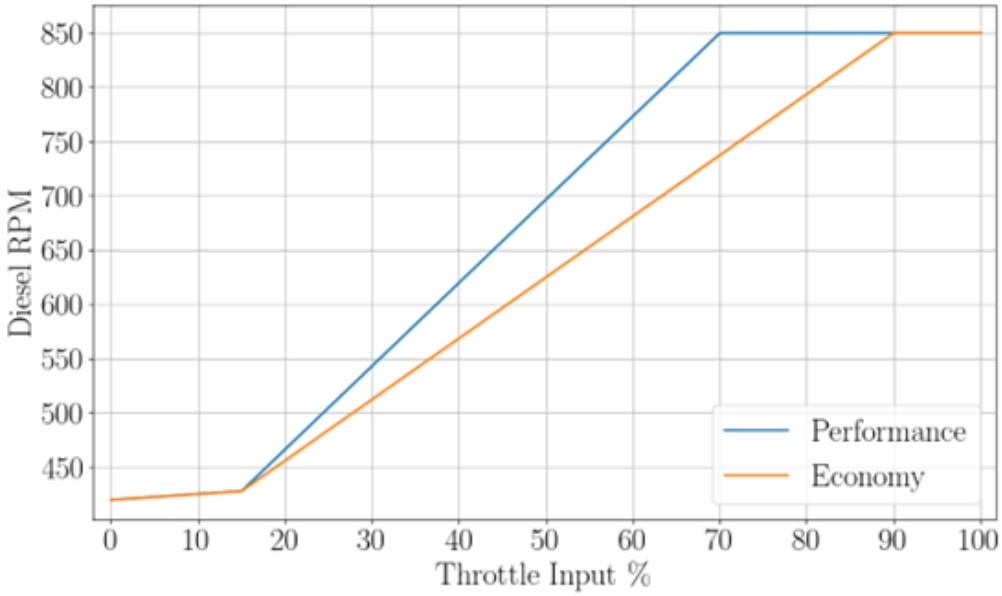

Figure 4-4: Comparison of diesel engine rpm to throttle position input.

is manually adjusted. The "Auto Max 10" control method is typically utilized when THUNDER BAY is engaged with heavy icebreaking and can add an added layer of protection for the diesel engines as heavy torque is applied on the propulsion shaft [21].

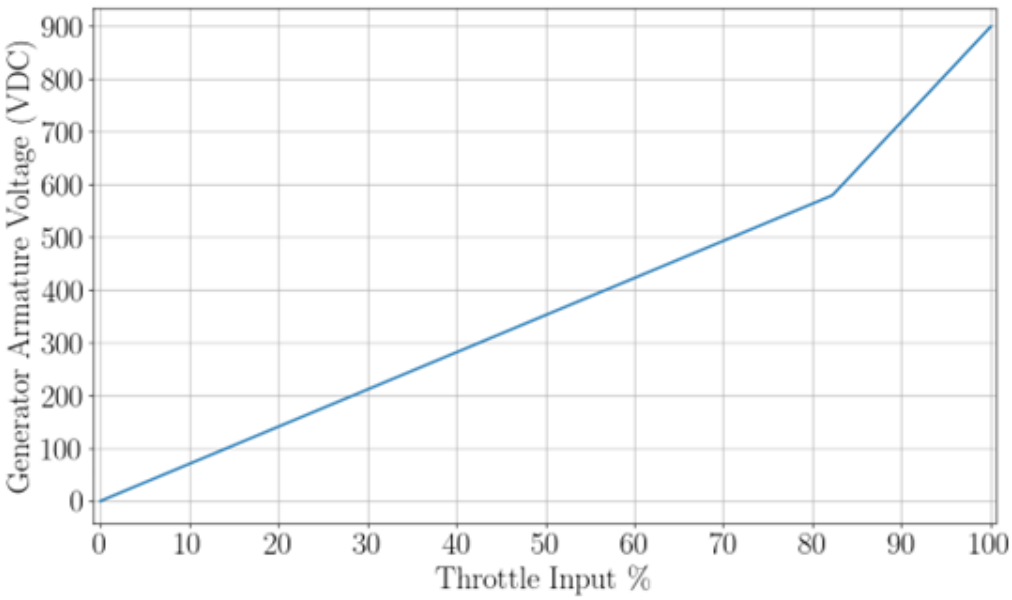

Figure 4-5: Comparison of generator armature voltage to throttle position input.

4.2 Propulsion System Monitoring

Simple insights can be gained by observing the power stream of panel 1-66-2. As discussed in Section 4.1, operator adjustments of the throttle position input will directly impact the excitation of the propulsion generator and motor fields. The NILM monitoring these exciters can thus gain impactful insight and correlate these power fluctuations to the operational status of the ship. Figure 4-6 demonstrates a sample observation of the aggregate power stream of the THUNDER BAY's exciters while getting underway. As seen at approximately 08:51, larger fluctuations of power can be noticed, which indicate the handle positions used by the operator when getting underway from a pier. This trend can be used across a multiple day period to identify specific time frames when THUNDER BAY is underway, as seen in Figure 4-7. While this information can be derived from other equipment monitoring, such as that described in [22], the direct monitoring of the propulsion system can give a more complete picture of operations and contribute to the NILM's ability for automatic log keeping.

In addition to viewing trends across multiple days, additional insights can be

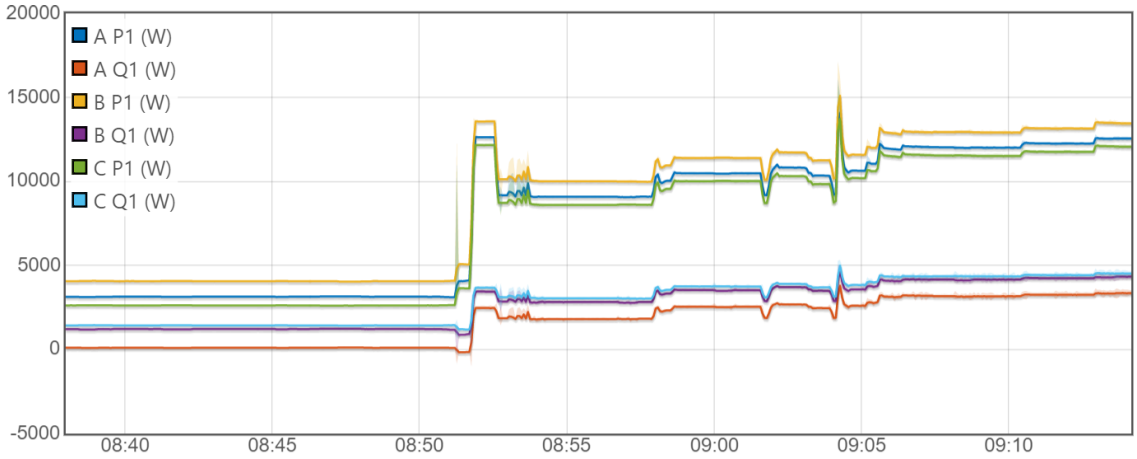

Figure 4-6: Sample power stream of THUNDER BAY getting underway.

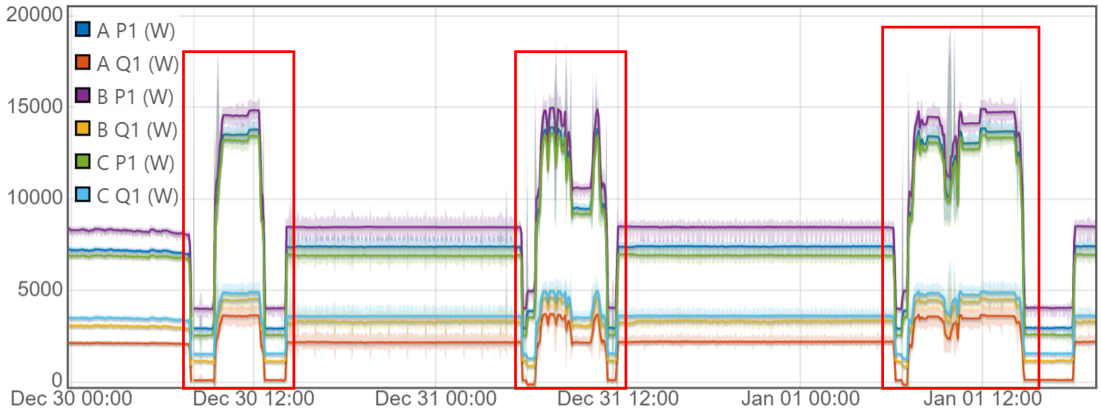

Figure 4-7: Multiple day measurement of panel 1-66-2 (underway periods highlighted).

gained into underway operations with a basic knowledge of THUNDER BAY's standard operating procedures. For example, Figure 4-8 shows a plot from 14 February 2021 when THUNDER BAY commenced an underway trip from homeport, broke ice on the Penobscot River, and then began a transit south for the remainder of the day. The power stream was first identified with the NILM and the schedule was verified with position and log data provided by the crew. A zoomed-in plot of the icebreaking operations can be seen in Figure 4-9. The numerous fluctuations in measured power over a short period of time is indicative of the frequent throttle position changes required for the backing and ramming icebreaking operations discussed in Section 2.3.2.

While this data is extremely useful for identifying underway trends for the ship,

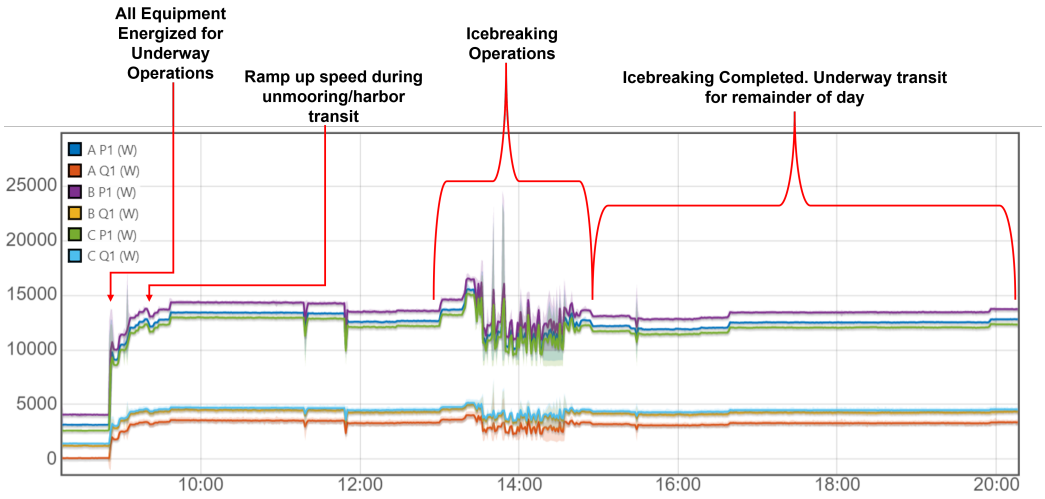

Figure 4-8: Time plot of THUNDER BAY commencing underway operations and breaking ice.

Figure 4-9: Time plot of THUNDER BAY commencing underway operations and breaking ice with enhanced view of icebreaking timeframe.

without the additional verification from the crew it would be difficult to prove that the highlighted section was indeed an icebreaking operation. This difficulty is demonstrated in Figure 4-10 which displays three separate power streams from panel 1-66-2. While they may look nearly identical to the common observer, and could all be mistaken for icebreaking operations, only one is an example of icebreaking. Note that this example of continous icebreaking is consistent with the description provided in

Section 2.3.1, where minimal throttle position changes are needed to break the ice. This difficulty in identification is compounded by the fact that the act of icebreaking is not a discrete event, and each icebreaking sortie will look different from the previous.

(a) Underway proceeding to anchorage (no ice present).

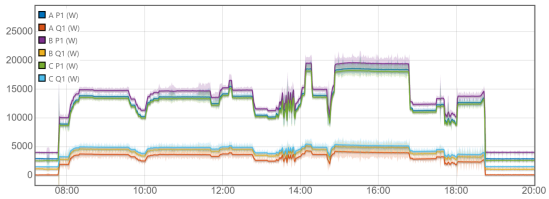

(b) Underway gunnery exercise (no ice present).

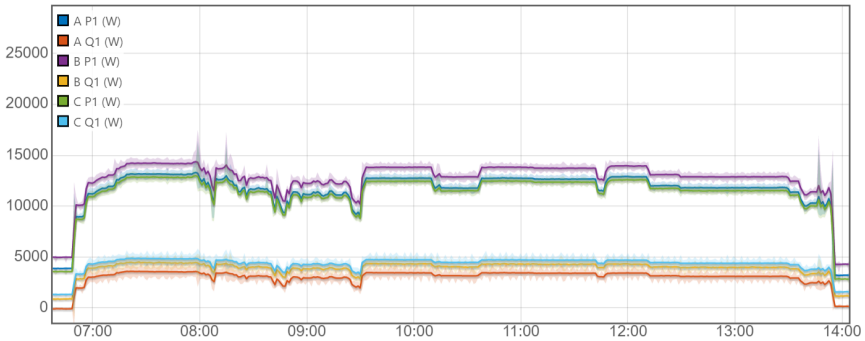

(c) Continuous icebreaking operations on the Hudson River.

Figure 4-10: Multiple single day views of panel 1-66-2 power stream.

4.3 Advanced Insights

While the NILM is capable of giving unique insights into ship operation, further details can be extrapolated with additional nonintrusive sensor verification. For comprehensive testing and verification during icebreaking operations, three single axis accelerometers were strategically mounted on the hull of THUNDER BAY to complement the power stream data provided by the NILM on panel 1-66-2.

4.3.1 Experimental Setup

In addition to the installed NILMs, the Gulf Coast Data Concepts' model X16-1C accelerometer was utilized for the acquisition of low sensitivity vibration data during

icebreaking operations. This device is a compact, battery powered, programmable, 3-axis acceleration sensing device. Measurements acquired by this accelerometer can be compared across time domains to determine periods of low and high activity. The device has programmable settings for sensitivity, sampling rate, and sleep modes, which are set via USB connection. Measurements are saved to an onboard SD card and can be retrieved and viewed via a Java application [23]. Overall, this is a very versatile device but is greatly limited by battery longevity, especially at sampling frequency rates greater than 50 Hz. To extend battery longevity to measure hull vibration of a U.S. Coast Guard icebreaking tug for weeks, the device was modified for use with an auxiliary battery pack. The accelerometer was designed to be powered by a single 1.5 VDC AA battery. Modifications to the device involved jumping the internal battery terminals to an audio jack which would serve as the power input from an auxiliary battery pack of 1.5 VDC D-cell batteries wired in parallel. Note, to avoid batteries discharging into one another, careful attention must be given to ensure batteries are of the same potential when placing in parallel. A line diagram of this modification and the auxiliary battery pack is shown in Figure 4-11.

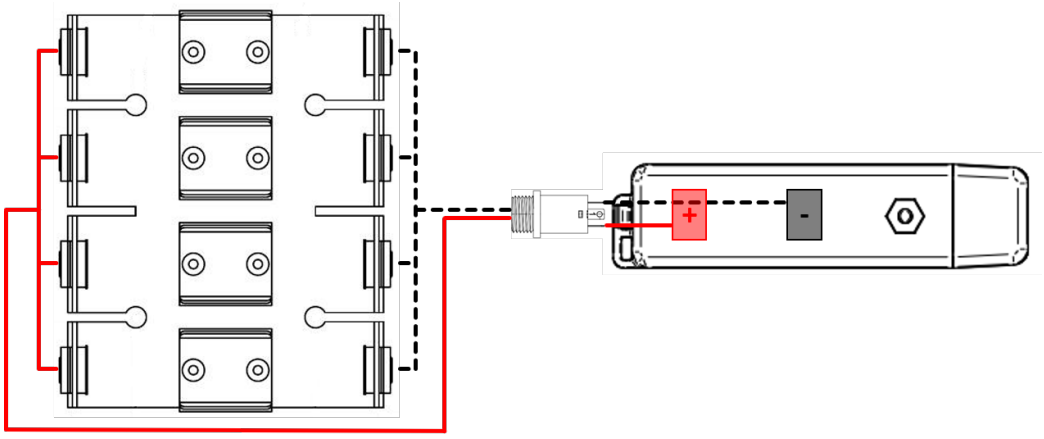

Figure 4-11: Line diagram of the modified Gulf Coast accelerometer.

To further extend the battery life the device was programmed with the following configuration (Figure 4-12):

```
1  ; PRODUCT_ID = X16-1C
2  gain = high
3  deadband = 35
4  deadbandtimeout = 5
5  samplesperfile = 100000
6  statusindicators = Off
7  sampleRate = 50
8  rebootOnDisconnect
```

Figure 4-12: Source code used to program X16-1C accelerometers.

- Line 1 contains the device's product ID and is commented out.
- Line 2 sets gain sensitivity to "high", which defines the sensor's scale. A gain of "high" sets the measurement scale to $+/-2$ g's, which is divided into 65,536 discreet counts, i.e., 16,384 counts are equivalent to 1 g. A gain setting of "low" corresponds to a scale of $+/-4$ g's. The deadband threshold can be set to any integer of 0 to 16,384 counts.
- Line 3 sets the deadband value to 35 counts.
- Line 4 sets the deadband timeout function to 5 sec, which triggers recording a sample every 5 sec regardless of whether or not the deadband threshold is exceeded.
- Line 5 sets the number of measures recorded per data file, until automatically generating a new data file. Based on trial and error, data files greater than 100,000 measurements become cumbersome to retrieve from the SD card and view in the Java viewing application.
- Line 6 secures the LED indicator lights that provide visible indication that the device powered on and recording measurements.

- Line 7 sets the sampling rate to 50 Hz. Note, sampling rate can only be set to 12, 25, 50, 100, 200, or 400 Hz.

- Line 8 sets the device to automatically reboot upon disconnection from USB and begin capturing measurements. Additional programming options can be found in the device's user manual [23].

Using the modified X16-1C accelerometers, hull vibration measurements were measured at three separate locations on THUNDER BAY. These locations included the forward bulkhead (frame 08) and aft bulkhead (frame 19) in the Anchor Handling & Misc. Storage Room (2-8-0-Q) as well as the overhead of Fan Space (01-19-0-Q) at frame 26. These locations were selected based on available mounting locations, proximity to areas prone to vibration during icebreaking, and distance from the vessel's center of gravity. Selecting locations furthest from the vessel's center of gravity maximized vessel movement from rolling, pitching, and yawing. Images of the devices installed in these locations are shown in Figure 4-13.

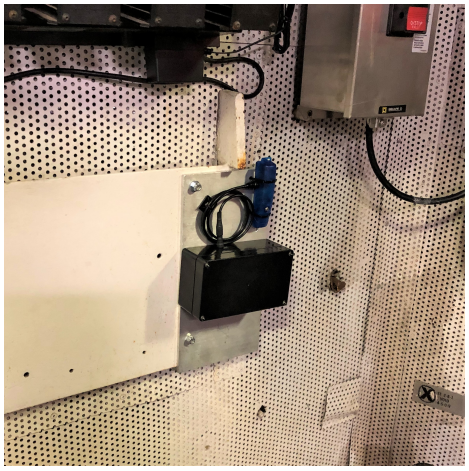

(a) Anchor Handling & Misc. Storage Room 2-8-0-Q (Frame 08)

(b) Anchor Handling & Misc. Storage Room 2-8-0-Q (Frame 19)

(c) Fan Space 01-19-0-Q (Frame 26)

Figure 4-13: Gulf Coast X16-1C accelerometer installations onboard CGC THUNDER BAY.

4.3.2 Icebreaking Observations

After the installation of the hull mounted accelerometers, the NILM continued to record underway data for THUNDER BAY's icebreaking trips. One sample day of operations can be seen in Figure 4-14. Analyzing NILM data highlighted this particular day as an area of interest for further study. Data obtained from the accelerometers was overlaid with the power stream data in Figure 4-15. The areas of increased vibration are indicative of hull impact with ice floes. Additionally, the pattern of throttle position changes exhibited by THUNDER BAY is consistent with that of a ship conducting continuous icebreaking operations, which is common based on the time of year and operating area for which this data was recorded. During each section of high vibration THUNDER BAY is actively breaking ice, and due to the prevailing conditions is able to do so continuously. Since no throttle position changes are necessary these areas are seen as flat on the power stream plot. The area where there is minimal vibration and multiple power fluctuations are the instances where the operator is turning the ship around to break through ice on the same track as before. This type of continuous icebreaking is typically referred to as track maintenance, where a specific section will be groomed multiple times in order to create a safe passage for other vessels to transit. Ultimately the NILM is able to successfully identify and properly classify these icebreaking operations of interest, and with the assistance of a minimally invasive vibration sensor this data can be verified without the need for additional insight from the crew.

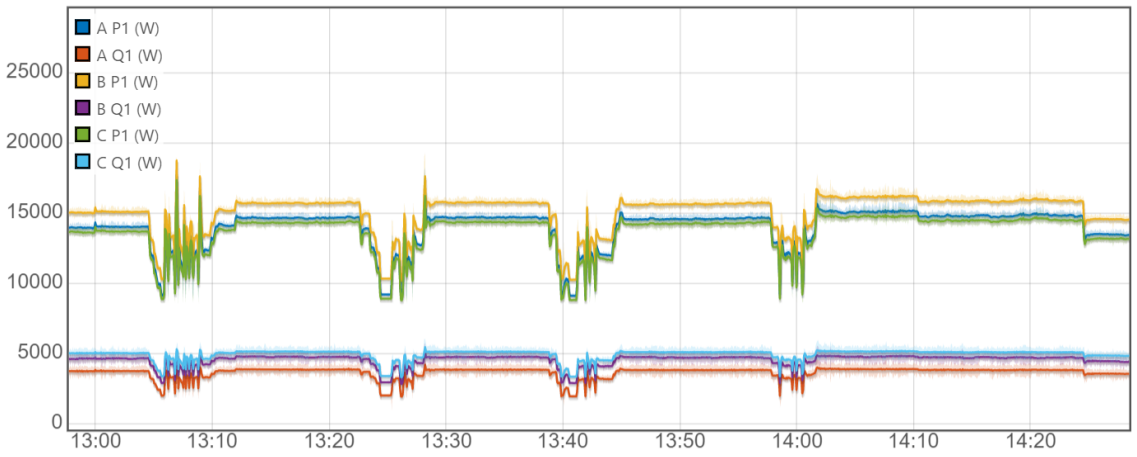

Figure 4-14: Potential icebreaking operations from NILM power stream.

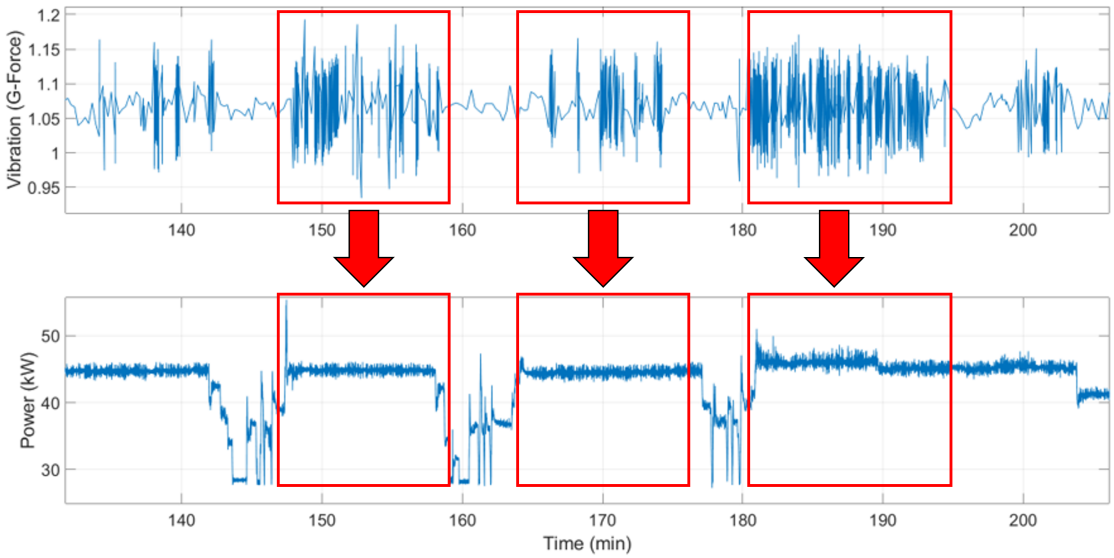

Figure 4-15: Sample of verified continuous icebreaking from USCGC THUNDER BAY.

Chapter 5

Sensor Upgrades

While the NILM is a powerful tool, there are times when additional equipment insights are desired that cannot be derived from the power stream. Some of these include, but are not limited to temperature, acoustic, and vibration signatures. One way to collect this type of information is to request it via a distal node that correlates with a specific electrical transient. If properly configured, a Fault Detection and Diagnostics (FDD) network orchestrated by the NILM can fuse these different data sets for proper synthesis and analysis. This specific FDD network can then be physically secured to provide detailed information and analysis only to trusted operators physically present in a facility or system. After installing the current NILM configuration on THUNDER BAY, several upgrades were made to both hardware and software components of the AIO box, allowing the NILM to be capable of coordinating this type of FDD network of sensors, and will be described in further detail in this section. Portions of this section were written in coordination with LT Devin Quinn, US Coast Guard, as part of a joint thesis presentation.

5.1 Sensing Platforms

This work will focus on discussing two sensing platforms for the proposed FDD network. These include the upgraded NILM with wireless capabilities, and a separate wireless sensing platform that can be easily integrated into the network. It is impor-

tant to note that the upgraded NILM is capable of interacting with and coordinating diagnostics with any other sensing device that has wireless capability.

5.1.1 "All-In-One" Box Modifications

In order to upgrade the NILM with wireless sensing capabilities, software and hardware modifications were made to the original design. These modifications were designed to be modular in nature, in that major components from the original AIO box were able to be recycled and reused in the new and improved iteration of the system. The upgrade modifications include the replacement of the original ACER laptop, which acted as both the computer and touch screen monitor for the AIO box. The ACER was replaced with with a new GK41 computer and WIMAXIT touch screen monitor. Additionally, a wireless router with antennas were installed on the new box design to allow for the desired wireless capabilities, as seen in Figure 5-1. Further details concerning design specifications and assembly instructions for the new AIO box can be found in Appendix B.

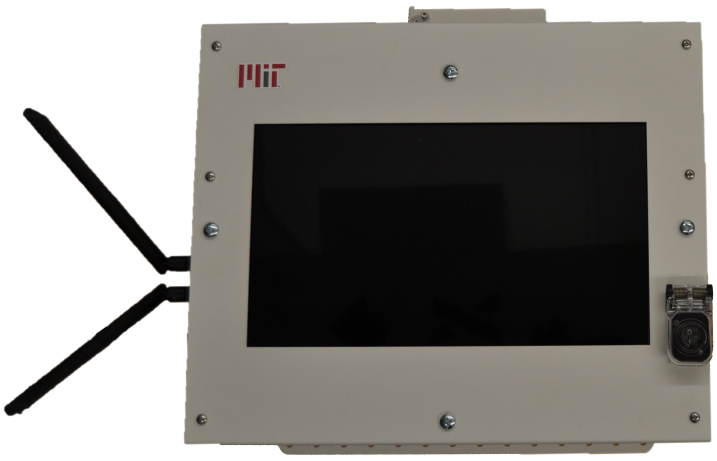

Figure 5-1: Upgraded AIO box with internal wireless capabilities

5.1.2 Wireless Sensing Platform

In order to supplement the relevant diagnostics information that cannot be derived from a power stream, a wireless sensor platform described in [24, 25] serves as an easily-installable sensor node that can measure these desired quantities. A block diagram of this device is shown in Figure 5-2. The sensor platform acquires signals from up to four channels and supports sampling rates up to 128 kHz with 16- or 24-bit resolution. Each acquisition channel can measure arbitrary +/- 5 V signals or signals from Integrated Electronics Piezoelectric (IEPE) sensors. The IEPE standard provides high noise immunity and power and signal delivery on the same two wires. Since the IEPE interface is limited to ac signal transmission, companion hardware proposed in [25] extends IEPE to include dc and slowly varying quantities. The IEPE channels on the sensor platform can interface with any resistive or voltage-based sensor such as thermistors, strain gauges, and pressure sensors, as well as traditional IEPE devices such as microphones and accelerometers. The diverse set of compatible sensing elements provides a unique opportunity for diagnostics that complement electrical data observed by the NILM. Vibration analysis is particularly useful for electromechanical load diagnostics, as changes in mechanical health are often reflected in the vibration signature of the machine [24, 26], and will be the focus of this study.

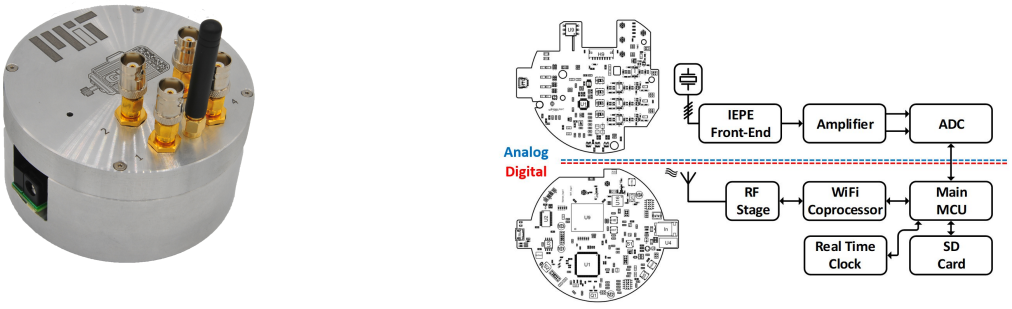

(a) Wireless sensor platform.

(b) Block diagram of the wireless sensor platform.

Figure 5-2: Wireless sensor platform used for integration with the wireless enabled NILM.

5.2 Physically Securable Network

The NILM can use either wired or wireless channels for creating a secured sensor network. However, wireless configurations allow the installation to remain minimally intrusive and allows for the implementation of modular sensing solutions. Wi-Fi provides a link medium that is securable through encryption and can be implemented inexpensively with commercial, off-the-shelf hardware. Industrial and shipboard environments are often assumed to be ill-suited to wireless communication [27, 28, 29, 30]. However, experiments were conducted in multiple shipboard environments to prove Wi-Fi's utility as a viable communication channel for shipboard fault detection and diagnostics with multiple sensors.

5.2.1 Wireless Platform Evaluation

In certain scenarios, commercial off-the-shelf wireless hardware can sufficiently link distributed sensors. The non intrusive sensors described in Section 5.1 were used to evaluate this claim on three US Coast Guard cutters of various sizes and construction types, all of which were previously or are currently monitored by nonintrusive load monitoring equipment. For each connectivity test, the wireless-enabled NILM was placed in the same location as each ship's actual NILM installation, allowing wireless interference to be characterized for realistic installation locations. The wireless IEPE sensing device described in Section 5.1.2 was moved along a grid of positions within each ship. For each sensor position, a set of tests was conducted to determine if there was sufficient wireless connectivity between the sensing device and the NILM, such that equipment diagnostic data could be reliably transmitted.

The four tests for the NILM and sensing device were as follows: (1) maintain a Wi-Fi connection throughout testing, evaluated using the `ping` utility, (2) access the sensing device's memory and list all files in storage using the NILM, (3) direct the sensing device to capture a sample measurement of data using the NILM, and (4) successfully download the sample measurement from the sensing device to the NILM.

If a testing location passed all tests, the location was labeled as "good." If a testing location passed one to three of these tests, the location was labeled as "unreliable." If there was never a stable Wi-Fi connection between the sensing device and NILM, the test location was labeled as "bad". Figure 5-3 through Figure 5-6 show visual representations of the wireless connectivity tests conducted in the three shipboard environments. The "good" tests are represented by blue dots, the "unreliable" tests are represented by yellow triangles, and the "bad" tests are represented by an orange circle with a slash. Both the solid and dashed lines represent the bulkheads (vertical walls in the ship's structure), as well as the ship's hull. Finally, the purple rectangle represents the location of the NILM during testing. Other significant equipment and obstructions are identified throughout the spaces.

The first of the three shipboard environments tested was that of USCGC MARLIN, a 87-foot coastal patrol boat. Testing results on three levels of the ship are shown in Figure 5-3. As can be seen, the wireless connection range was sufficient to link almost all points tested on the second level with the NILM located on the first level. The second environment was that of USCGC THUNDER BAY, a 140-foot icebreaking tug. As can be seen in Figure 5-4, there was a strong wireless connection throughout the entire engine room, where the equipment monitored by the NILM is located. Additionally, the wireless connection was able to reach into the forward transverse bulkhead into the Auxiliary Machinery Room. The final environment was that of USCGC SPENCER, a 270-foot Coast Guard Cutter. Results are shown for the upper and lower engine rooms in Figure 5-5 and Figure 5-6, respectively. Wireless connection was available throughout both the upper and lower engine rooms.

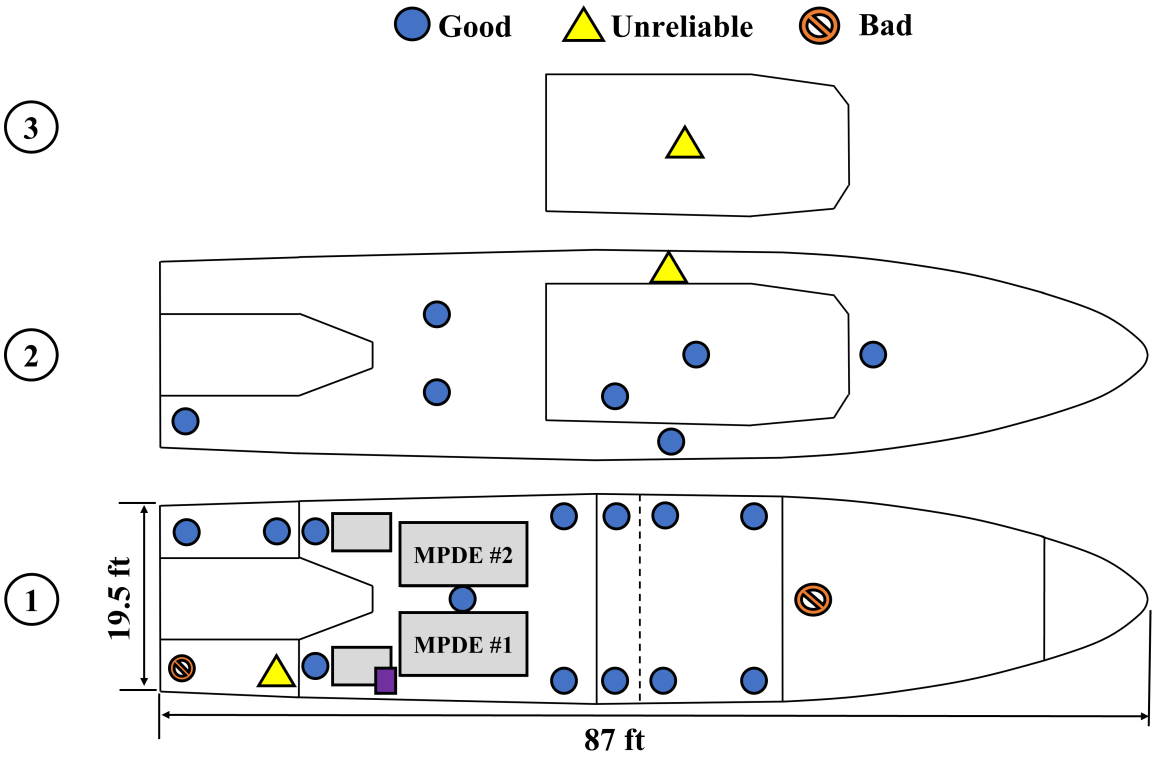

Figure 5-3: USCGC MARLIN Station Mode Testing

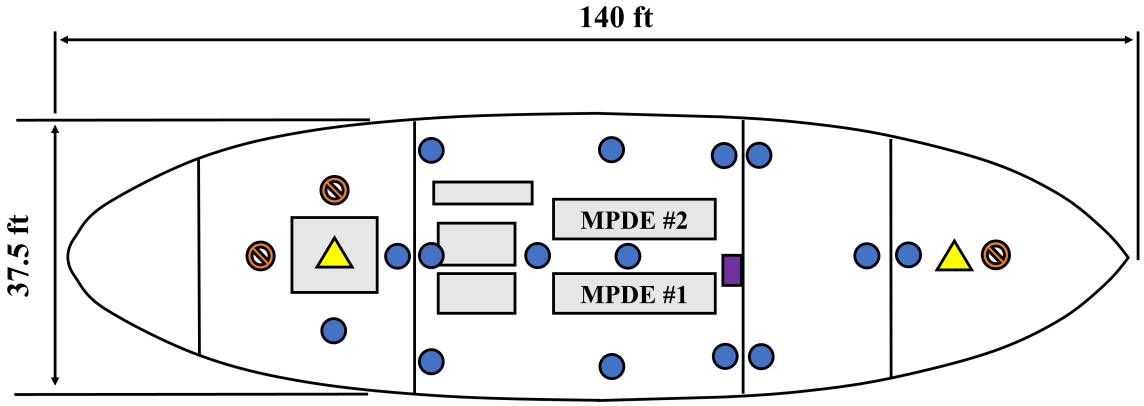

Figure 5-4: USCGC THUNDER BAY Station Mode Testing

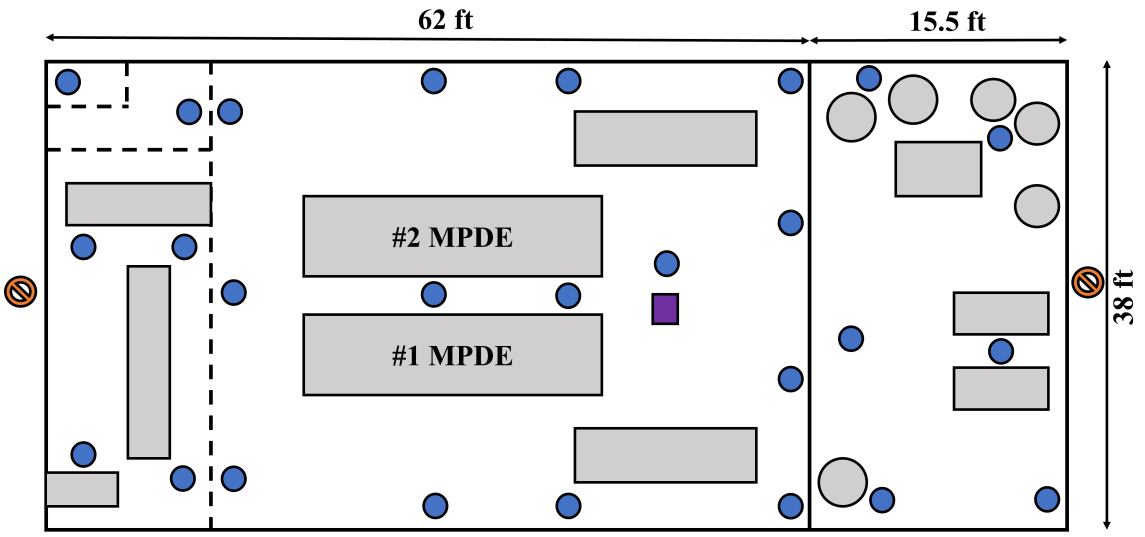

Figure 5-5: USCGC SPENCER Station Mode Testing (Upper Engine Room)

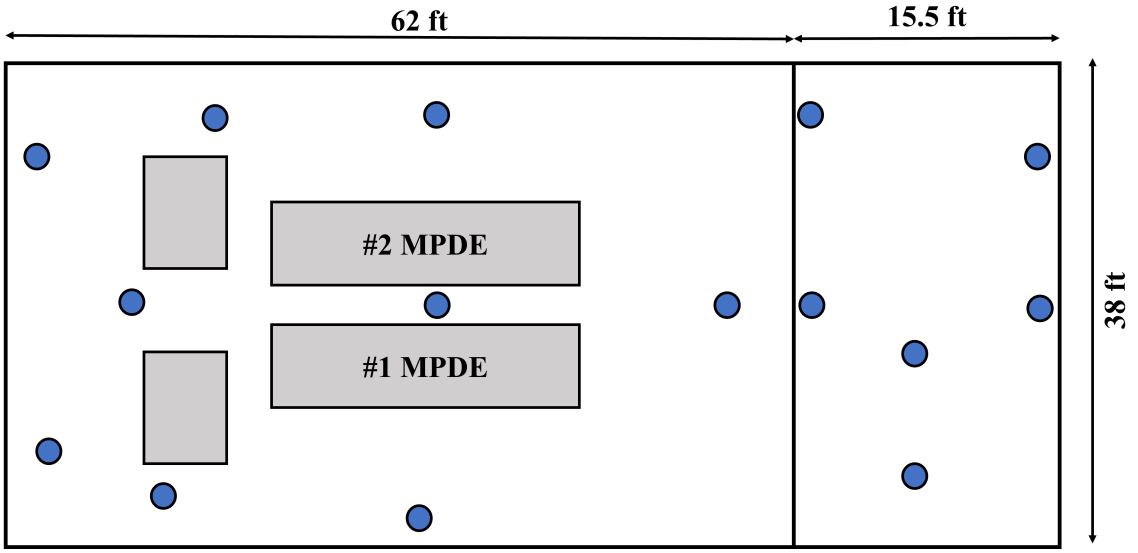

Figure 5-6: USCGC SPENCER Station Mode Testing (Lower Engine Room)

Identical wireless testing procedures described in this section were also conducted on the US Navy's Self Defense Test Ship (Figure 5-7), a retired Spruance Class Destroyer used by the Naval Surface Warfare Center for various forms of experimental shipboard testing. The results obtained from this testing are similar to those of the other ships, however all of the data is classified and not available for public release.

Figure 5-7: US Navy Self Defense Test Ship

In summary, wireless communication proved to be reliable and was surprising given the conventional wisdom that shipboard and industrial environments are not suitable to such communication. Although maintaining a wireless connection throughout the entire ship is not always practical, the areas relevant to nonintrusive monitoring, such as the engine rooms, were well-covered.

5.2.2 Data Transmission and Synthesis

Once a communication channel is acquired via Wi-Fi, either the NILM or the sensor platform can initiate data transmission, depending on the use case. Choice of network protocol is an important design consideration, with the two prominent choices being the transmission control protocol (TCP) and user datagram protocol (UDP). For certain IoT and cyber-physical applications, UDP is attractive, since it prioritizes speed and simplicity in packet transmission, at the expense of reliability [31]. However, TCP is more suitable for the FDD intranet, since it guarantees reliability. The additional power and computation overhead of establishing a connection and verifying data integrity is more than outweighed by the assurance that data is received in order. This is especially significant for automatic fault detection and diagnostics, because a corrupted data transmission may cause a critical sensor measurement to be missed entirely.

Data is processed with Joule [32], which models the data pipelines as a series of

"modules" with streams of information passing between them, allowing for efficient, real-time measurement and signal processing. Joule modules are used to continuously run an event detector, feature extractor, and classifier on the power stream to identify load transient events. Once a load event is found, a separate Joule module establishes a TCP/IP socket with the wireless sensor platform of interest. The sensor takes a measurement for a user-configured duration and then sends the data back through the socket. Since timestamps from the remote sensor nodes are not guaranteed to be available or reliable, the NILM infers them to avoid clock drift and time misalignment. This is done via linear interpolation when data of a known duration is retrieved. Once data is received and timestamped, it is inserted into a time-series database [33] for further analysis.

A case study is shown for a reciprocating A/C compressor. The NILM is configured to direct the sensor platform to capture two minutes of vibration data whenever the NILM detects a transient event in the power stream. Figure 5-8 shows the resulting synchronized and colocated data from both power and vibration sensors, plotted with the Lumen data visualization app on the NILM [34]. Real and reactive fundamental power are plotted for all three phases. Vibration is plotted in red; due to the decimation performed by the data visualizer [33], the solid red line shows the average value (zero) and the lighter red region shows the envelope of the accelerometer measurements. With access to both of these data streams, the NILM can perform online analysis and provide actionable information for load diagnostics in real time.

5.2.3 Security

Strong, unbroken encryption is the keystone of modern network security. As such, the FDD network provides both encryption and authentication of network members using Wi-Fi Protected Access II (WPA2). However, the FDD network provides two additional security layers. First, the network is intentionally isolated from the public internet, in contrast to the IoT strategy. This "air-gapped" scheme denies many attack vectors into the system by simply making it inaccessible to public channels. However, this shifts some of the security burden onto the process of moving data to and from

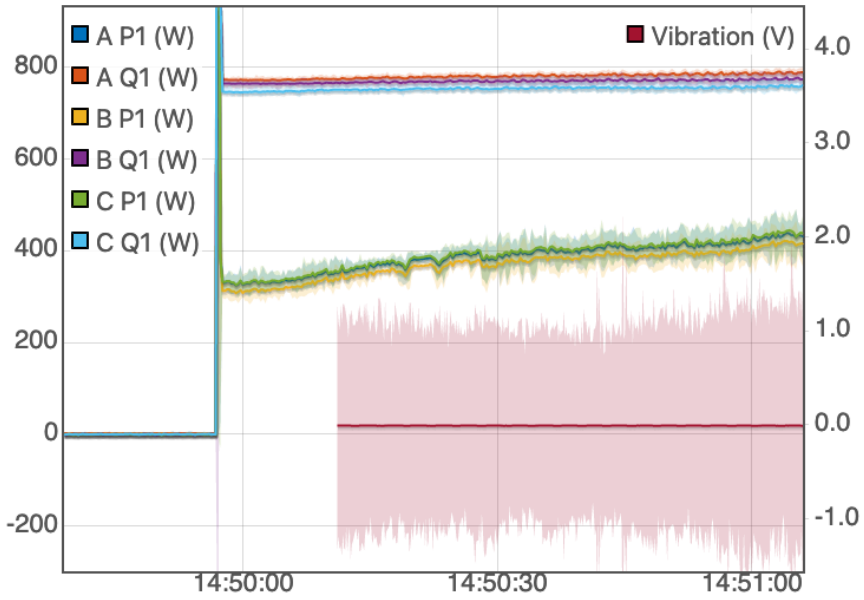

Figure 5-8: Power and vibration data streams, captured synchronously with multiple sensors.

the network. Care must be taken that any interactions with external computers, such as internet connection and removable media, are trusted.

Secondly, many environments relevant to FDD, such as ships, naturally attenuate wireless signal power at their boundaries. Carefully adjusting broadcast power of the NILM's access point to what is only necessary limits the network signals' ability to reach the outside world. In the previously presented shipboard examples, the wireless signals broadcast from the two devices' radios permeate the bulkheads and hull of the ship only minimally, since the ship's steel hull acts as a Faraday cage that blocks electromagnetic fields. For a ship on open water, it would be difficult for an adversary to be in reception range without detection, without immensely powerful radio equipment. Finally, it is worth emphasizing again that these two additional layers do *not* take the place of up-to-date encryption and authentication practices, as a sufficiently determined and powerful adversary may find a way to communicate with the network.

5.3 Sensor Demonstration

This section provides four case studies in which fused nonintrusive sensor data streams from the NILM and wireless sensor platform were used in tandem to shed further light on load operation and diagnostics that power data alone cannot provide. Each of these four scenarios corresponds to a separate FDD network strategy for collating the sensor data. All experimental data was taken from equipment on United States Coast Guard Cutters (USCGC) MARLIN, THUNDER BAY, and SPENCER, or equipment similar to that found on these ships. Vibration data was captured using Wilcoxon's model 728T single-axis 500 mV/g accelerometer [35].

5.3.1 Bilge and Fire Pump

The most straightforward FDD network strategy involves using the NILM to track the operational state of a load outfitted with a remote sensor. When the load is operating, the NILM continuously requests and downloads data from the remote sensor. The bilge and fire pump on USCGC MARLIN serves as an example of a fault for which this strategy is suitable. This centrifugal pump is designed to expel water from the bilge of the ship and supply water to the on-board firefighting system. The pump is driven by a 3-phase induction motor that is rated to operate at 57.4 rps. In the stable and normal region of operation, the slope of the induction motor steady-state torque-speed curve is negative. The torque developed by the motor and consequently the power consumed increase when rotor speed decreases. Power can therefore provide an indicator of shaft speed. Measurement of the shaft speed is also possible from vibration measurements [36]. Under normal operation the pump maintains a discharge pressure of approximately 110 psi. Changes in operating pressure maintained by the pump could be indicative of a variety of faults such as a blockage in the system or pump impeller wear. Both power and vibration measurements reflect changes in operating pressure of this load, as illustrated by the experiments presented in this section. In these experiments, the flow was adjusted with a controllable valve

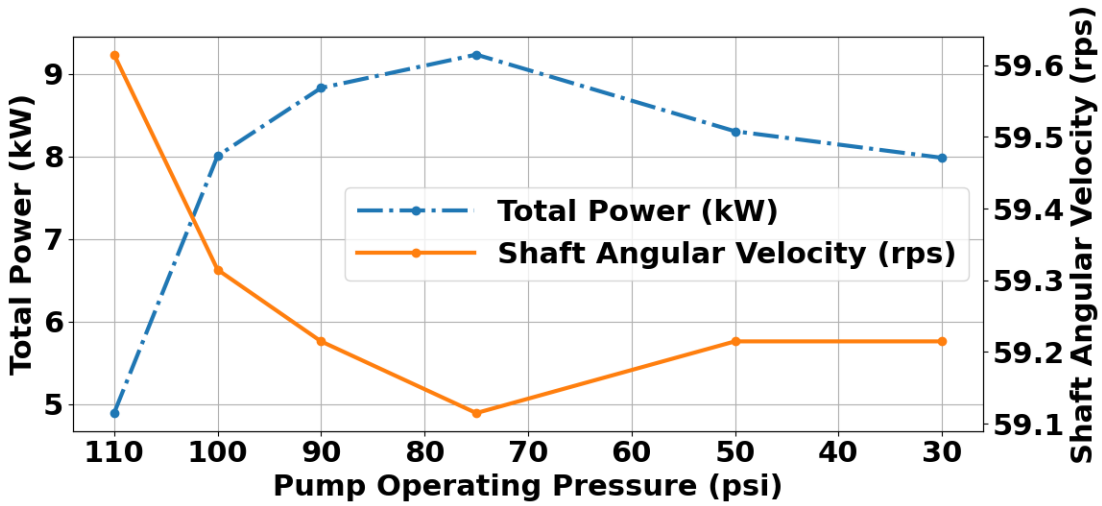

Figure 5-9: Estimated power and shaft angular velocity for different operating pressures of the MARLIN bilge and fire pump.

to simulate an increased demand of the system. As the valve was adjusted, the outlet pressure of the pump varied from 110 to 30 psi. Power consumption and vibration were recorded using the installed NILM and an accelerometer connected to the wireless sensor platform, respectively. The accelerometer was affixed to the pump housing in a perpendicular orientation to the drive shaft.

Figure 5-9 shows a plot of both the steady-state power consumption as measured by the NILM and shaft angular velocity (calculated from the discrete Fourier transform (DFT) of vibration data) across decreasing operating pressures. The steady-state power increases as the pressure changes from 110 to 75 psi, and then begins to slightly decrease as the pressure changes from 75 to 30 psi. The angular velocity of the bilge and fire pump's motor shaft decreases as the operating pressure changes from 110 to 75 psi, and then slightly increases as the pressure changes from 75 to 30 psi. This type of behavior is typical of normal operation of a backwards centrifugal pump [37]. Both curves have an inflection point at an operating pressure of 75 psi. This inflection identifies the point of operation where the pump is imparting the greatest work on the fluid, in terms of flow rate and pressure. Using these relationship curves, a change in operating pressure of the pump could be identified by either power or vibration data. Since this load turns on on infrequently and is critical to shipboard

operation, the proposed FDD network strategy produces two correlated indicators of faulty pump operation. As a result, the NILM has access to a more complete diagnostic picture than power and vibration provide individually.

5.3.2 Air Conditioning Plant

Unlike the previous example, some loads require a minimal amount of remote sensor data to be collected for disaggregation and fault detection. For this FDD network strategy, the NILM requests a small window of data from the remote sensor whenever it detects a transient event of interest related to that load. To illustrate this, consider the air conditioning (A/C) plant on USCGC SPENCER, which consists of two refrigeration skids. Each skid contains two independent refrigeration loops with semi-hermetic compressors; one compressor is shown in Figure 5-10a. The system is charged with R-134A refrigerant and cools a closed-loop chilled water system that circulates throughout the vessel. Each compressor has three piston pairs. A conceptual diagram of the pistons is shown in Figure 5-10b. Solenoid-activated unloaders, referred to as UL1 and UL2, are installed on two of the piston pairs and allow for capacity control. The unloaders activate piston pairs based on cooling demand for efficient system operation [38]. The center piston pair does not have an unloader and is always activated. Activated pistons pull refrigerant through the suction ports and discharge compressed refrigerant to the high-pressure side of the system. In the following discussion, loaded operation refers to six activated pistons, partially loaded refers to four activated pistons, and unloaded refers to two activated pistons.

Figure 5-11 presents a power stream of an A/C skid onboard SPENCER. The power stream depicts the turn-on event of a single compressor and subsequent loading events of the compressor. Upon startup, the compressor operates in an unloaded condition with only the center piston pair (2 and 5) activated. With an increase in loading, the real power consumption increases while reactive power remains nearly constant. As a result, loading the compressor increases the load's power factor. For instance, the step increase at approximately 2.5 minutes in Figure 5-11 is a shift from unloaded to partially loaded operation, with the center and lower piston pairs (1, 2, 4,

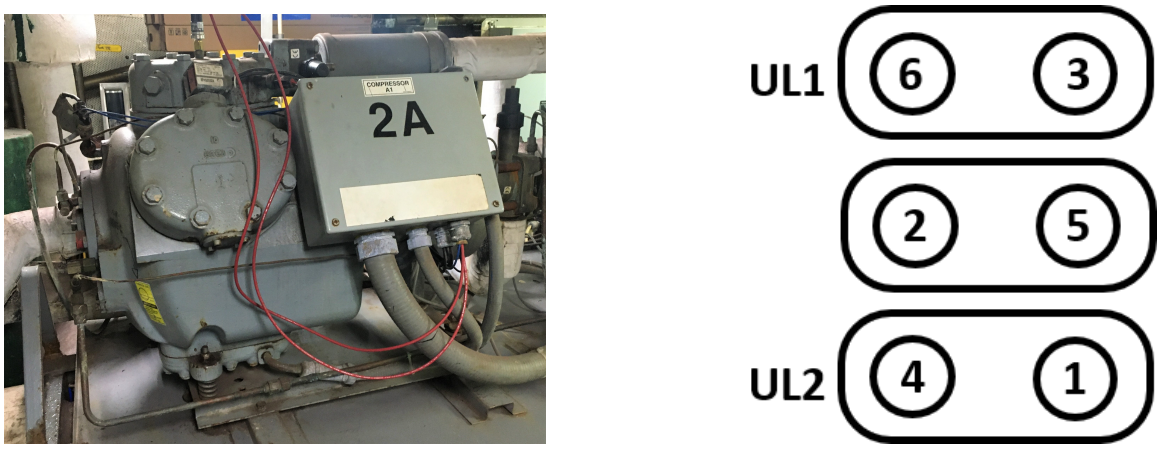

(a) A/C compressor. (b) Piston and unloader arrangement.

Figure 5-10: A/C compressor and unloader arrangement onboard SPENCER.

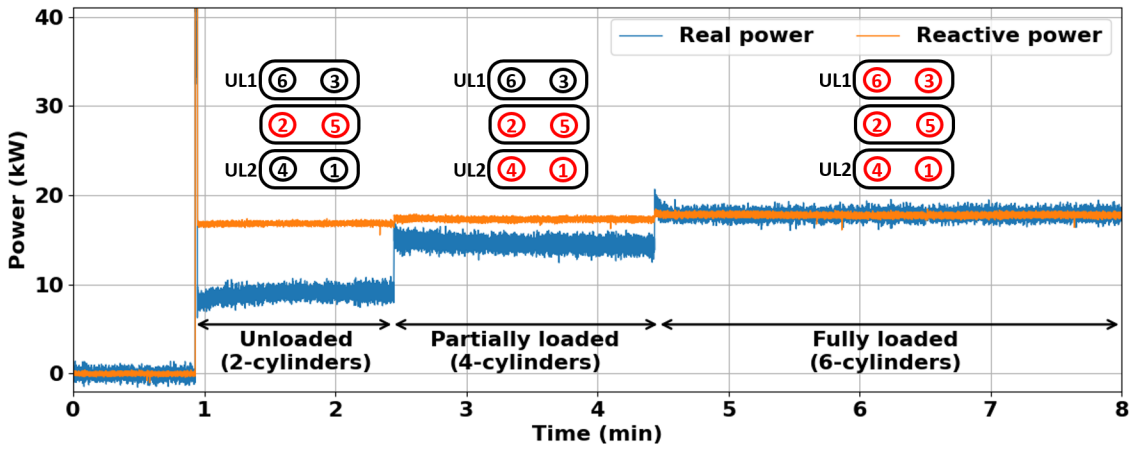

Figure 5-11: SPENCER A/C compressor power stream.

and 5) activated. The final step in real power is a shift from partially loaded to fully loaded operation, with all piston pairs (1 through 6) activated. Table 5.1 presents the observed power factor in each loading state.

The A/C compressors are driven by grid-connected induction motors. The induction motor has 4 poles and a rated torque of 163 N·m while operating at 29.2 rps [39]. Figure 5-12 shows time-domain vibration measurements for each loading condition. Impulsive events due to activated pistons are evident in each case. Low-frequency content in the vibration signature is associated with mechanical events that occur throughout shaft rotation, such as crank and piston movement. Higher-frequency

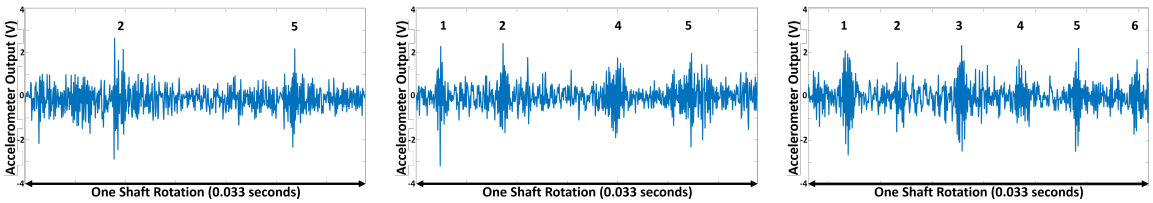

(a) Unloaded operation. (b) Partially loaded operation. (c) Loaded operation.

Figure 5-12: SPENCER A/C compressor accelerometer time-domain plots of varying loading states. Impulsive events due to activated pistons are labeled.

content is likely a result of suction and discharge valve action, turbulent fluid flow, and excitation of natural structural frequencies of the compressor [40]. Vibration data was gathered using an accelerometer mounted to the discharge side of the compressor. At this location, measurements of 40 seconds in duration were taken at various loading conditions from eight compressors of the same model. In total, there were 32 loaded, 19 partially loaded, and 20 unloaded measurements. Based on the expected operating speed of 29.2 rps, the DFT is examined between 28.5 to 30 Hz. The location of the maximum value of the magnitude of the DFT in this range is an estimate of the shaft rotational frequency. The mean and standard deviation of the peak location for each loading condition are shown in Table 5.1. This demonstrates that the compressor shaft rotational frequency is inversely related to loading.

If both compressors on a skid are running, they will likely appear indistinguishable in the power stream. Thus, for healthy machines the NILM is unable to identify which compressor is responsible for a turn-on or loading transient. With access to the FDD network and one remote sensor, however, the NILM can track the loading condition of both compressors. Upon observing a compressor loading event, the NILM requests a small sample of vibration data from the remote sensor deployed to one of the compressors (referred to as the "monitored compressor"). From this measurement, the NILM estimates the shaft rotational frequency, and from that, the loading condition of the monitored compressor. If this compressor's loading condition has not changed from what the NILM last observed, the NILM infers that the loading event occurred in the other compressor, and updates that compressor's tracked state accordingly.

Otherwise, the NILM updates the tracked state of the monitored compressor.

Table 5.1: A/C power factor and shaft frequency for loading conditions.

Loading Condition	**Power Factor**	**Shaft Rotational Freq., Hz (σ_{Freq})**
2 cylinders	0.477	29.74 (0.0229)
4 cylinders	0.642	29.49 (0.0254)
6 cylinders	0.708	29.29 (0.0407)

5.3.3 Crankcase Blower

In the third FDD network strategy, the NILM periodically requests data from the remote sensor at user-configured intervals. This strategy is motivated by imbalance condition faults, which are often invisible in the power stream but are apparent in vibration signatures. A controlled imbalance experiment using a centrifugal fan demonstrates this claim. Tests involved four conditions: a normal (balanced) condition and three imbalance conditions. The imbalance conditions were introduced with weights placed between blades of the fan's squirrel cage wheel. Ten power and vibration measurements of 30 seconds each were captured at each operating condition. The fan was operated at 19.2 rps for all experiments. For each test, average apparent power was computed over the 30-second measurement. Table 5.2 shows the average and standard deviation of these values for each condition. The magnitude of the DFT at the shaft rotational frequency is also shown, relative to the normal condition. The standard deviations of this frequency component were negligible. These results show that operating condition did not change apparent power. However, the magnitude of the DFT component at the shaft frequency and the operating condition are directly correlated. These results align with findings presented in [41] and demonstrate a fault condition that is readily apparent in vibration measurements, but nearly impossible to diagnose in power measurements.

Similar findings were made onboard USCGC THUNDER BAY with its main propulsion diesel engine (MPDE) crankcase blowers previously discussed in Sec-

Table 5.2: Centrifugal fan power and vibration comparison.

Operating Condition	**Eccentric Mass, g**	**Apparent Power, VA (σ_{AP})**	**Norm. Rotational Freq. Magnitude**
Normal	0	838.8 (1.757)	1.000
Imbalance 1	1.085	840.7 (1.858)	1.141
Imbalance 2	2.156	839.5 (1.662)	1.369
Imbalance 3	3.398	839.9 (1.728)	1.500

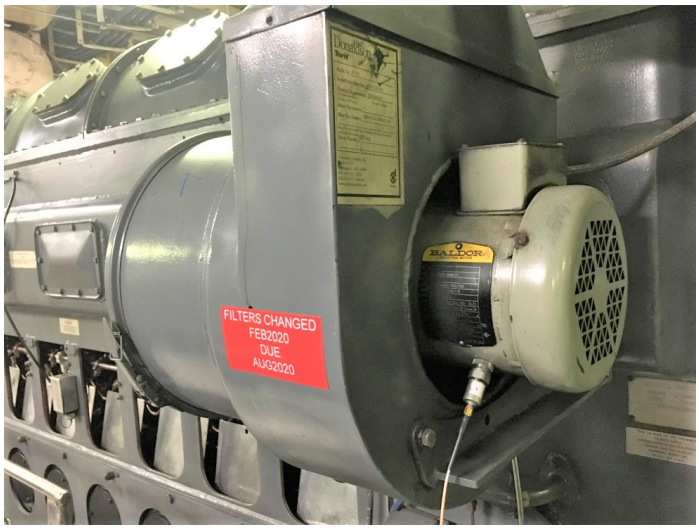

Figure 5-13: THUNDER BAY MPDE crankcase blower.

tion 3.3.1. These centrifugal fans draw air from the engine's crankcase to prevent the buildup of combustible gases. The #1 MPDE blower with a mounted accelerometer for data collection is shown in Figure 5-13. Each blower is driven by an induction motor operating at 57.5 rps and acts to maintain a vacuum in the crankcase. The blowers are fitted with filters to remove atomized oil from the air drawn from the crankcase. The mounting arrangement creates an overhang condition, similar to a cantilever beam, for the induction motor and squirrel cage wheel. With this configuration, minor manufacturing defects, deterioration, or debris buildup on the fan blades can result in imbalance and excessive amounts of vibration. The blower's mounting arrangement is illustrated in Figure 5-14a. The mounting arrangement of the centrifugal fan used during the controlled imbalance experiment is shown in Figure 5-14b. Both create an overhang condition.

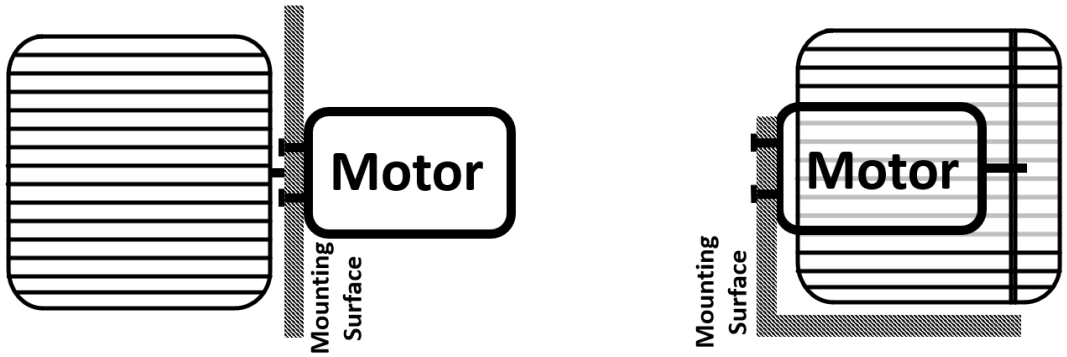

(a) Crankcase blower mounting.

(b) Centrifugal fan mounting.

Figure 5-14: Cantilever mounting arrangements.

The accelerometer measurements were first analyzed in the time domain and are shown in Figure 5-15. It is apparent that there are significant differences in operation between the two blowers. The vibration signal envelope of the #1 blower is relatively uniform; the signal has an rms value of 0.596 V. The #2 blower displays a low-frequency oscillation at approximately 1.4 Hz and has a rms value of 0.278 V. Despite appearing drastically different, drawing firm conclusions from time-domain observations alone is difficult. Variations in mounting, misalignment, bearing faults, and increased looseness of linkages can excite natural frequencies of a machine, affecting its vibration signal envelope [42]. Analysis of the vibration signals in the frequency domain provides more useful insight. The magnitudes of the first six orders in the frequency domain for both blowers are shown in Figure 5-16. The frequency content of the #1 blower is dominated by the first order. As shown during the controlled centrifugal fan experiment, this can indicate an imbalance condition in which an eccentric mass is oscillated once per shaft rotation [42]. The #1 blower is likely imbalanced due to an uneven buildup of soot and coagulated oil within the blower's rotating filter.

The steady-state apparent powers of the #1 and #2 blowers were approximately 646 VA and 786 VA, respectively. Without historical data, it is difficult to attribute the discrepancy in apparent power to a specific fault. Changes in power can be attributed to complex factors particular to the system, such as restrictions and leaks [37]. However large first-order frequency content in vibration is a well-established in-

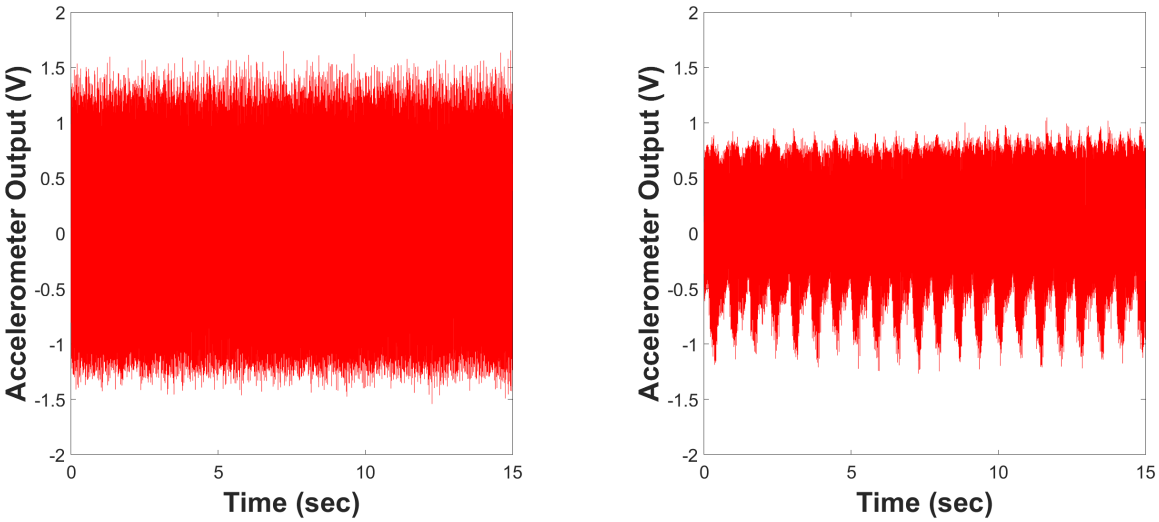

(a) #1 Crankcase blower. (b) #2 Crankcase blower.

Figure 5-15: Crankcase blower time-domain comparison.

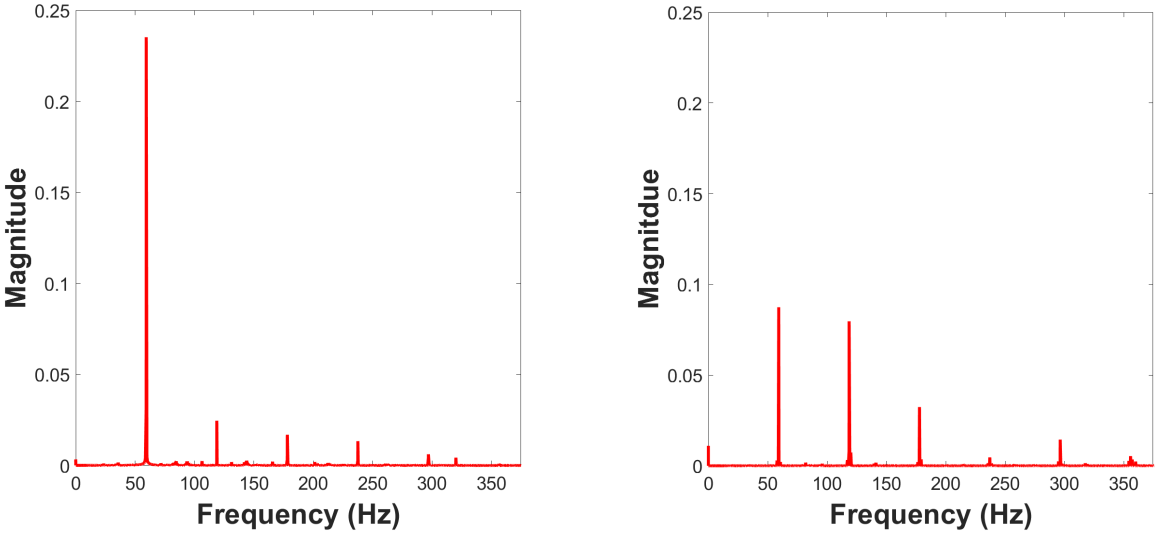

(a) #1 Crankcase blower. (b) #2 Crankcase blower.

Figure 5-16: Crankcase blower frequency-domain comparison.

dicator of imbalance [41], as corroborated by the controlled experiment. In practice, this type of load operates continuously, so turn-on and turn-off events will be sparse. With the proposed FDD network strategy, the NILM continually performs spectrum analysis on the periodically-acquired vibration signals to generate diagnostics of imbalance conditions.

5.3.4 Sewage Vacuum Pumps

The final FDD network strategy presented addresses the case in which a load of interest does not draw power from a panel monitored by the NILM. For this strategy, the remote sensing device sends measurements to the NILM whenever it detects a signal exceeding a user-configured level. A pair of positive displacement vacuum pumps onboard USCGC THUNDER BAY provide a case study. These pumps maintain vacuum in the sewage collection tank and do not draw power from the panel monitored by the NILM on the ship. The vacuum sewage pumps operate in a lead-lag fashion, in which the primary pump turns on when vacuum in the collection tank drops below 12 inHg and the secondary pump turns on when vacuum drops below 10 inHg [43]. Once the collection tank vacuum reaches 18 inHg, both pumps turn off and swap designations as primary and secondary pump, i.e., the primary pump becomes the secondary. These pumps are mounted on top of a small water tank that provides pump cooling and a fluid medium for the pumps to build vacuum via the Venturi effect.

The wireless sensor platform captured vibration data from both vacuum pumps using an accelerometer attached to each pump's motor housing. Figure 5-17 shows the resulting time-domain measurements. The #2 pump exhibits a significantly higher rms value of vibration (1.013V) than the #1 pump (0.306 V). Common fault diagnostic wisdom states that an increase in a machine's vibration level indicates deteriorated operation or a fault. Indeed, pathologies involving imbalances, mounting, or bearings can increase vibration levels [42]. Without baseline measurements, one may be inclined to assume that the #2 pump is operating improperly since its vibration level is clearly larger than the ostensibly identical #1 pump. The following demonstration of sophisticated signal processing techniques yields a surprising result: the #2 pump is healthy and #1 pump is the faulty one. By exploiting the cyclostationary nature of rotating machinery, these techniques offer this conclusion even without historical knowledge of the pump operating conditions.

Vibration measurements from rotating machinery are often modeled as realizations

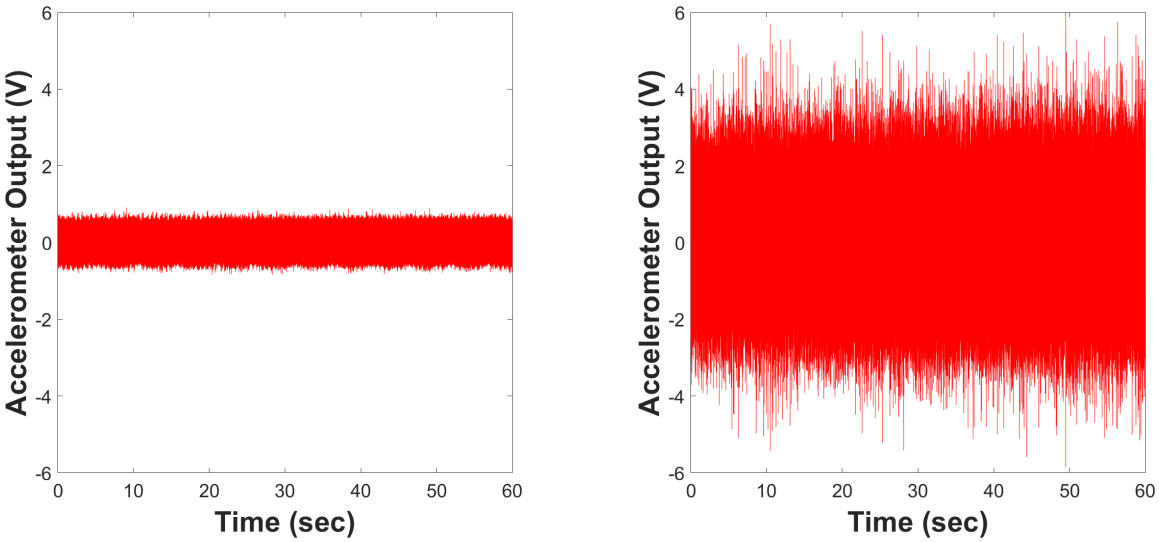

(a) #1 Vacuum pump.

(b) #2 Vacuum pump.

Figure 5-17: Vacuum pump time domain comparison (pre-repair).

of cyclostationary random processes [44, 45, 46]. Cyclostationary random processes are characterized by periodic mean and autocorrelation functions [45]. Periodic vibrations of rotating machinery are due to shaft rotation, piston reciprocation, and other mechanical actions. In many systems, these periodic actions are associated with vibration content that is hard to model analytically such as friction, turbulent flow, and other physical factors. Vibrations from these phenomena are more broadband in frequency and are often modelled as random, with periodic actions modulating the random content. Cyclostationary signal processing tools provide important insights, for example, estimates of the spectral correlation function, or if normalized, the spectral coherence function. These estimates can quantify the frequency of the periodic actions and the nature of the modulation. The mean envelope spectrum (MES) is calculated from the spectral coherence function. Lines in the spectral coherence map at a specific cyclic frequency correspond to relative peaks in the MES and indicate cyclostationarity [47, 24].

Detailed mathematical discussions and intuitive examples of cyclostationary analysis are presented in [47, 24]. Only the necessary definitions for the vacuum pump analysis are presented in this section. The spectral coherence function $\gamma_x^{\alpha}(f)$ is defined

as

$$\gamma_x^{\alpha}(f) = \frac{\hat{S}_x^{\alpha}(f)}{\sqrt{\hat{S}_x^{0}(f - \frac{\alpha}{2})\hat{S}_x^{0}(f + \frac{\alpha}{2})}}, \tag{5.1}$$

where $\hat{S}_x^{\alpha}(f)$ is the spectral correlation function for a signal x, f is the carrier or center frequency, and α is cyclic frequency. For $\alpha = 0$, the spectral correlation function is equal to the traditional power spectral density (PSD). Equation (5.1) shows that the spectral coherence is the spectral correlation function normalized by a function of values from the PSD. The MES $S_x^{<f>}(\alpha)$ over some range of carrier frequencies F is defined as

$$S_x^{<f>}(\alpha) = \frac{1}{|F|}\int_F |\gamma_x^{\alpha}(f)|df, \tag{5.2}$$

where F is chosen by the analyst and the upper bound of F is limited to one half of the sampling frequency (Nyquist frequency) [45]. Equation (5.2) defines the relationship between the spectral coherence and the MES.

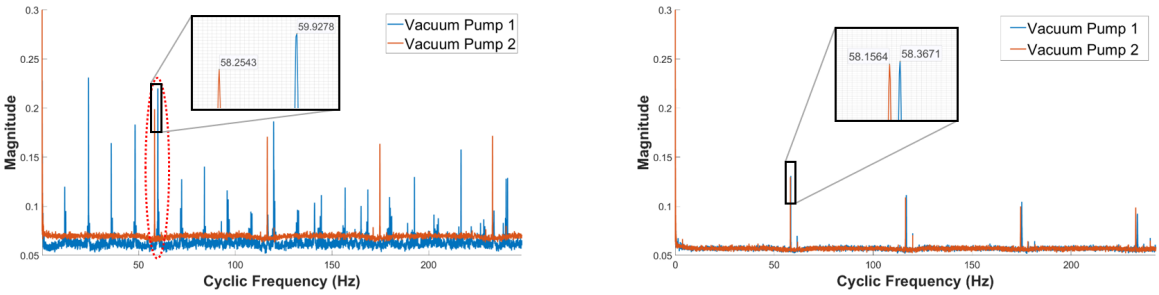

(a) Vacuum pump MES (pre-repair).

(b) Vacuum pump MES (post-repair).

Figure 5-18: Vacuum pump MES comparison.

In the case of the sewage pump, shaft rotation is the main periodic action that modulates broadband content. The vacuum pump motors are rated to operate at 57.5 rps. Thus, relative peaks in the MES at cyclic frequencies around 57.5 Hz and its integer multiples are expected. Figure 5-18a depicts the MES of both vacuum pumps as initially encountered on THUNDER BAY. The MES of the #1 pump has peaks at many cyclic frequencies unrelated to a reasonable shaft rotational frequency. The MES of the #2 pump has expected peaks at multiples of 58.25 Hz. Typically, MES values at cyclic frequencies that correspond to machine physics dominate the

Figure 5-19: Deteriorated vacuum relief valve.

MES. When comparable in size to peaks without direct physical explanation, there is little modulation of broadband content and the system is likely not operating as intended. Additionally, for systems with negligible broadband frequency content, the normalization in Equation (5.1) with small values of the PSD could give rise to artificially large values of the spectral coherence function. Abnormal operation of the #1 pump is further confirmed by investigation of the area around 59 rps circled in Figure 5-18a. The MES peak of the #1 pump is at a noticeably higher cyclic frequency of 59.93 Hz. The shaft rotational frequency is very close to synchronous speed. This indicates the motor operates at very low slip and corresponds to a small load torque.

The differences in the MES prompted further examination of the system. Upon inspection, the #1 pump was not maintaining its water prime from the seal tank. Loss of prime causes the pump housing to become air-bound and deteriorates the pump's ability to build vacuum. The source of the fault was finally identified as the deteriorated sealing surfaces of the vacuum relief valve. Figure 5-19 shows the deteriorated valve and its sealing surfaces.

Figure 5-18b shows the MES profile from measurements taken after cleaning the sealing surfaces and re-installing the valve. After repair, the MES of the two pumps are nearly identical and the additional MES peaks have vanished. The vibration of

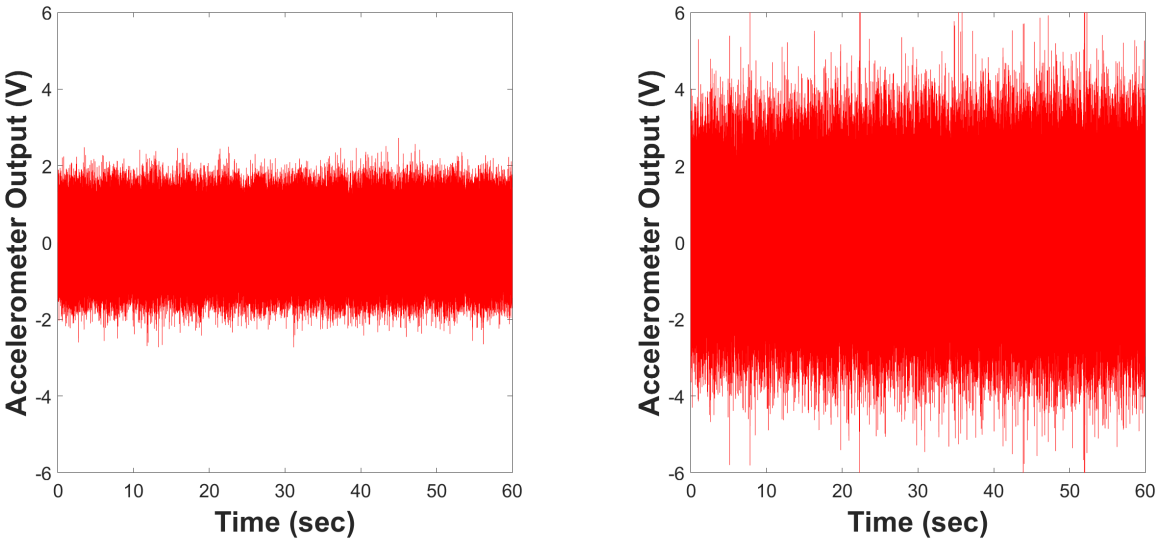

(a) #1 Vacuum pump.

(b) #2 Vacuum pump.

Figure 5-20: Vacuum pump time-domain comparison (post-repair).

the #1 pump, shown in Figure 5-20, increased to an rms value of 0.571 V. Though the #1 pump's vibration level increased, it is still notably less than the #2 pump's rms value of 1.105 V. This may be the result of differences in cumulative run-time, mounting condition, or impeller health, but further inspection is required to confirm these suspicions.

This fault demonstrates that degraded operation can present counterintuitive time-domain vibration signatures. Without the aid of power stream data, cyclostationary vibration analysis successfully diagnosed the faulty relief valve. To integrate this diagnosis into the FDD network, the wireless sensor platform should alert the NILM when there is sufficient vibration to be of interest. Since MES calculation is computationally expensive, the sensor platform sends data either continuously or periodically to the NILM, which uses its higher computing power to perform MES analysis for fault detection.

5.4 Implementation

The previously discussed testing highlights the practical and flexible sensing solution that the proposed Wi-Fi enabled sensor network provides. A sample implementation of this network was employed in a laboratory setting and can be seen in Figure 5-21. Additional AIO boxes and wireless sensor platforms have been manufactured and at the time of this publication are ready for deployment within a shipboard environment.

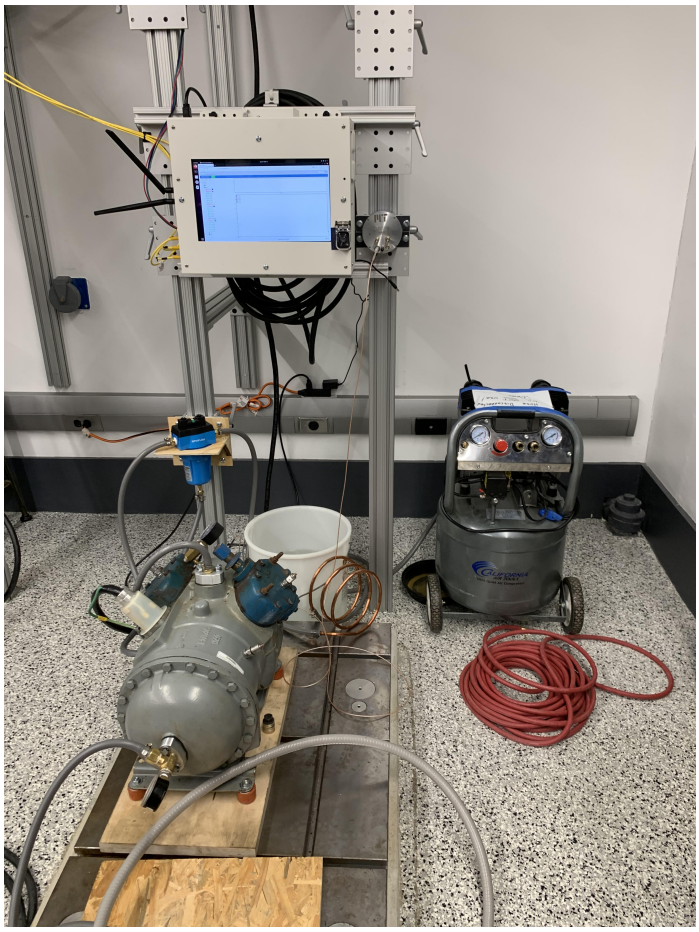

Figure 5-21: Wi-Fi enabled NILM with wireless sensing platform installed in a laboratory setup.

THIS PAGE INTENTIONALLY LEFT BLANK

Chapter 6

Conclusions and Future Work

With new and complex ship designs entering into service, it is of vital importance that the health of the onboard equipment can be properly monitored to prevent potentially catastrophic failures that impact operational availability and capability. While most sensor systems involve complex networks of intrusive sensing equipment, the proposed nonintrusive sensing network provides a low cost and minimally intrusive solution. This work has proven the benefits of fault detection and diagnostics in a shipboard environment, and has also demonstrated the types of insight that are available for crews to observe and record the operational status of their vessel.

For future work, specifically on THUNDER BAY, the insights gained from directly monitoring the electric propulsion system can be further exploited to develop typical underway profiles for the ship. Specifically, if a profile comparing the throttle position input from the operator can be correlated to a specific power measurement from panel 1-66-2 then it will become easier to identify the ship operations without the need for additional verification from the crew.

Additional future work for this project includes the installation of the upgraded AIO box with wireless sensing capabilities in a new shipboard environment. Plans similar to those found in Appendix A have been recently developed and approved by the US Coast Guard for installation on USCGC STURGEON, an 87 ft marine protector class cutter, in the summer of 2022. Once installed the real-time analysis and data collection from multiple nonintrusive sensor nodes can assist with providing

more insightful data for the crew than is currently available. Additionally, if an upgraded wireless capable NILM is able to be installed on THUNDER BAY then the Gulf Coast accelerometers could be replaced with more high-resolution measurements that could be sent over the wireless network for rapid online processing by the NILM.

Overall, the THUNDER BAY has proved itself a useful and insightful platform for obtaining NILM related insights. In addition to the identification of faulty equipment that has been a staple of prior shipboard NILM installations, it has also been able to provide new data on the operation of electric propulsion drives not previously studied. As the research on this vessel continues, it could serve as an exemplar platform for future studies on larger polar icebreakers that the Coast Guard plans to launch and deploy in the near future.

Appendix A

USCGC THUNDER BAY NILM Documentation

This Appendix includes modified documentation created for use by the US Coast Guard Surface Forces Logistics Center (SFLC) Icebreaker, Buoy and Construction Tender Product Line (IBCTPL). The documents were submitted in order to receive appropriate authorization to install all of the aforementioned NILM equipment on USCGC THUNDER BAY (WTGB 108). This documentation was initially provided to the US Coast Guard in October of 2020 and the installation of all equipment was completed in February of 2021. Certain approval documentation was not classified for public release and could not be included in this Appendix.

A.1 MIT NILM Research Proposal for USCGC THUNDER BAY (WTGB 108)

A.1.1 Introduction

The purpose of this proposal is to provide detailed information regarding the request for authorization for the Massachusetts Institute of Technology's (MIT) Research Laboratory of Electronics (RLE) to conduct research onboard United States Coast Guard Cutter (USCGC) THUNDER BAY (WTGB 108). This proposal comes from the listed US Coast Guard Officers in the Electromechanical Systems Group (ESG) under the supervision of Professor Steven Leeb in the MIT Research Laboratory for Electronics.

Since 2004, a strong relationship has existed between United States Coast Guard (USCG) officers pursuing DCMS sponsored graduate level education and USCG assets located in the Boston area including USCGC ESCANABA (WMEC 907), USCGC SENECA (WMEC 906), USCGC SPENCER (WMEC 905), and USCGC MARLIN (WPB 87304). Students have researched vibration and electrical monitoring to improve fault detection, determine machinery health, extrapolate human activity, and provide energy scorekeeping to improve automation and machinery-monitoring technology. These research opportunities allow active duty officers to remain engaged with the fleet while pursuing higher education, simultaneously posing an opportunity for the USCG to remain at the forefront of maritime automation and monitoring research.

A.1.1.1 Research Focus

Current research is focused on Non-Intrusive Load Monitoring. A Non-Intrusive Load Monitor (NILM) takes electrical power readings from a centralized monitoring point, making it a low-cost, durable, and sustainable method of equipment monitoring. Ap-

plications of these readings include energy savings, load factor management, platform energy use optimization, activity monitoring, log generation, and machinery health monitoring. The NILM systems are low-cost and easier to install compared to equivalent systems comprised of individual sensors on each piece of equipment.

MIT RLE requests authorization to install two NILM boxes onboard USCGC THUNDER BAY (WTGB 108) in accordance with the Memorandum of Agreement between MIT-RLE and USCG Surface Forces Logistics Center (SFLC) Engineering Services Division (ESD). Details of the proposed installations will be provided in this document. Installation specifics will be outlined in a separate Installation Plan.

The proposed installation will last for one year, beginning on the installation date. At the end of that year, the MIT RLE will communicate with SFLC ESD to determine if the project will continue or not.

A.1.1.2 Background

Power system microgrids serve mission critical systems for naval platforms. System component degradation can often be observed as changes in demand on the power system. As the performance of a critical component in a system degrades, automatic controllers often compensate to maintain commanded output levels. By design, feedback control works to mask the effect of "soft faults," variations and vagaries in internal component performance in a larger system that do not fully stop the system. Low refrigerant charge, slipping belts, fouled fans, vacuum leaks, and degraded hydraulic fluid are all examples of mechanical insults to a system with insidious effect: the system will continue to operate and provide apparently acceptable service and performance while an automatic controller forces more energy consumption and induced wear. Soft faults may elude even vigilant watchstanders. These situations can persist for expensively long periods before a "hard fault" finally stops the system, alerting operators but also creating a "casualty" that may cripple mission readiness.

The vast implementation of automatic controllers often masks soft faults by automatically altering run times and drawing excess power to maintain system operability. Enhanced vigilance in watchstanding can lead to soft fault detection, but it is at the expense of the watchstander. Further, such enhanced inspection leads to increased monitoring efforts and a greater watchstanding demand, as well as a dependence on a multitude of sensors which could introduce additional fault points in an already complex system. While this introduction of new sensors to a system can provide a more detailed view of individual component operation, it does not simplify system operation or watchstanding practices. Instead, it commonly adds to the burden of system maintenance by producing a raft of raw data that is often not presented in a useful way. The ability to parse useful data and present it in an easily-extractable manner is necessary to successfully identify soft faults and allow operators to address them prior to system failure.

A.1.1.3 NILM Technology

Non-intrusive electrical power monitoring has been applied for condition-based maintenance, energy scorekeeping, and activity tracking in marine environments for several decades. The nonintrusive load monitor can determine the operating schedule of individual loads and components by observing electrical transients in an aggregate electrical power stream. Figure A-1 illustrates a NILM installation at the feeder to an electrical panel that serves a collection of loads. Strictly from measurements made at this aggregate point, a NILM determines the operating schedule of the downstream loads through association of observed waveforms with specific loads. This technology can then develop a physics-based load model and determine the health of the loads. Then, by effectively detecting transient events, a NILM can automatically log operation of system components, producing a computer-generated log that rivals or exceeds human-made logs for accuracy and vastly reduces watchstander effort in documenting equipment operation. A NILM's ability to record the operation time and power consumption for individual loads creates a convenient, one-stop access point

for energy scorekeeping.

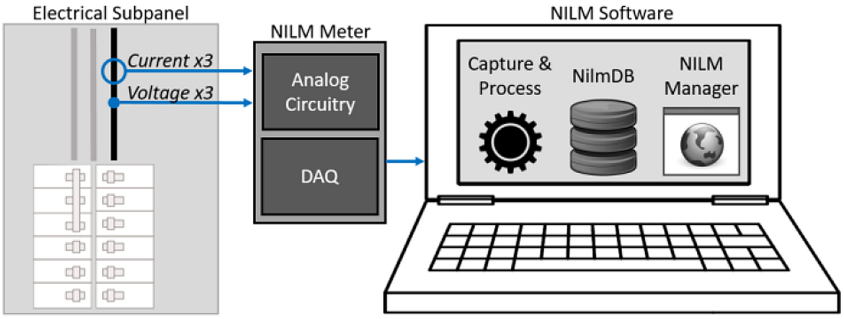

Figure A-1: Schematic overview of a typical installation of a NILM at the feeder to a power panel on a ship. The NILM Meter provides sensing for waveform measurement. The NILM Software runs on a Linux-based personal computer, laptop, or similar platform.

Within a NILM, sensors record current and voltage from the electrical panel and analyze waveforms to compute real power, reactive power, apparent power, and higher harmonic content. This information directly corresponds to the physics that governs load behavior, producing distinct signatures in power data, to which the NILM is "trained" to recognize. Such load transients can be identified by developing fingerprint exemplars in the laboratory through testing of example loads, from previous shipboard equipment observation, or from on-site observations of loads during a training period following installation. The monitor can also observe load behavior for a period of time and classify the loads using guided machine learning and clustering to produce a data set that is likely most useful after a facilities operator has reviewed and corrected the automatic load identifications as needed.

A.1.1.4 Past NILM Installations

Various configurations of nonintrusive monitoring equipment have been installed onboard USS Michael Murphy (DDG-112), USS Independence (LCS-2), USS Champion (MCM-4), the USNA YP (Yard Patrol) Fleet, USS Indianapolis (LCS-17), USCGC MARLIN (WPB-87304), and the Famous-class US Coast Guard Cutters in Boston. The longest installations have provided observations from the three Famous-class

Medium Endurance Cutters (MECs) SENECA, ESCANABA and SPENCER for over 10 years with various hardware setups. These 270 ft. (82 m) length overall vessels have a 440 V electrical power distribution system run by diesel power generation and distribution equipment required to support missions and sustain operations at sea.

On SPENCER, a readout for the crew displays the NILM Dashboard. Figure A-2 shows front and side views of a touch screen installed that displays graphical results from NILM Dashboard. The front view on the left shows the NILM Dashboard displaying a timeline of operation for three different service loads in the main engineering space, extracted from the power monitoring of the electrical panel feeding these loads. The side view on the right shows the screen displaying “meter"-style displays with green (normal), yellow (worrisome), and red (poor) operating zones for the different statistics concerning the monitored load of interest. This display allows the crew to quickly select and interpret visual indicators that draw awareness to unusual or unacceptable operating parameters, including too frequent or infrequent operation, excessive power demand, excessive or inadequate duration of operation, and other unacceptable operating states. With such a tool available to the crew, watchstanders have the ability to identify soft faults in their engineering systems prior to their failure as highlighted by the NILM.

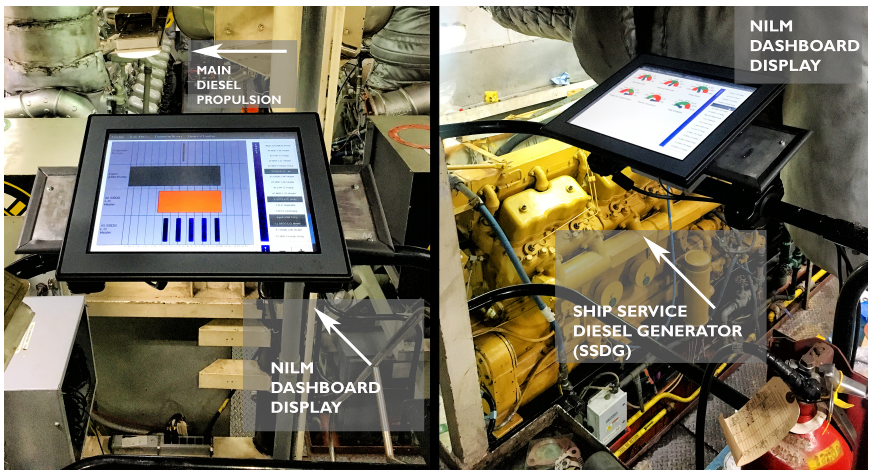

Figure A-2: The NILM Dashboard display on USCGC SPENCER (WMEC 905).

A.1.2 Installation Requirements

This section will denote the details regarding the proposed NILM installation for USCGC THUNDER BAY (WTGB 108). It will begin outlining the equipment required for the installation, then detail the proposed locations for installation onboard the WTGB. Each proposed NILM installation will include the following components:

- All-in-One (AIO) NILM Box (1)
- Current transducers (3, one per phase)
- Conxall cables (3, one per phase)
- Voltage leads (encased in single conduit)
- IEC power cord (1)
- Mechanical mounting hardware

A.1.2.1 All-in-One (AIO) NILM Box

The All-in-One (AIO) NILM Box combines several aspects of NILM technology into a single, robust, easily-installed box designed for shipboard installation. This configuration minimizes space requirements by combining the sensor hardware, computer, and backup power supply necessary to collect data and display it in a useful manner into a single enclosure that is reasonably-sized with respect to the limited space within shipboard engineering spaces. Figure A-3 shows an example of an AIO NILM Box install. As shown, this single box includes a touch-screen computer display on the outside, while also encasing the majority of the NILM sensor hardware. Figure A-3 also showcases much of the additional hardware required for installation, including the IEC power cord, voltage leads encased in conduit, and Conxall cables. The box dimensions are 16 in x 7 in x 13.5 in.

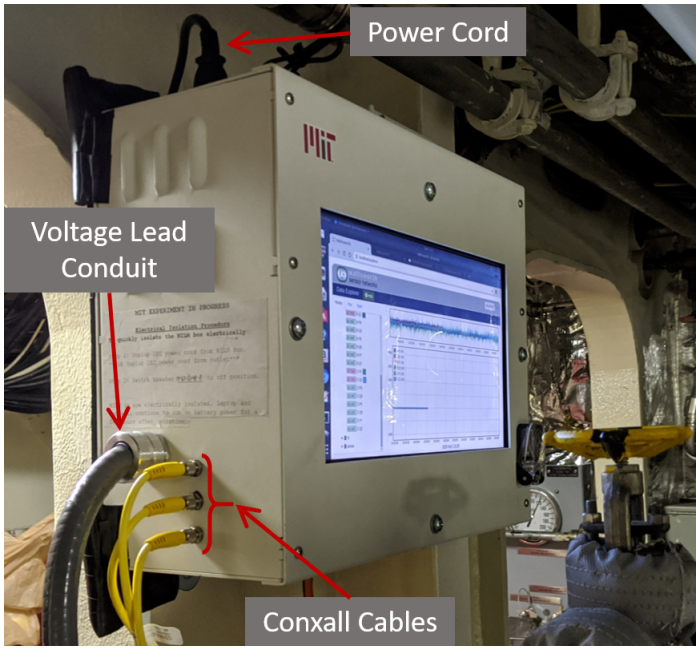

Figure A-3: AIO NILM Box install.

A.1.2.2 Other Installation Hardware

The current transducers, shown in Figures A-4a and A-4b (blue), are installed onto each phase of the power cables feeding the panel. These sensors connect to the yellow Conxall cables, (also depicted in Figure A-4a), which then feed current readings to the All-in-One Box as shown in Figure A-3. Figure A-4b also shows the voltage lead installation onto the spare breaker within the power panel. Once these wires exit the power panel, they are encased in conduit that runs to the AIO box, which is shown in Figure A-3. The final piece of hardware to install is a IEC Power Cord that connects the AIO Box to a 120V power supply. This IEC cord will plug into the nearest power outlet and run through neighboring cable runs to provide power to the AIO Box. All mounting hardware is specific to each ship and each install, and will be addressed in greater detail in the Installation Plan.

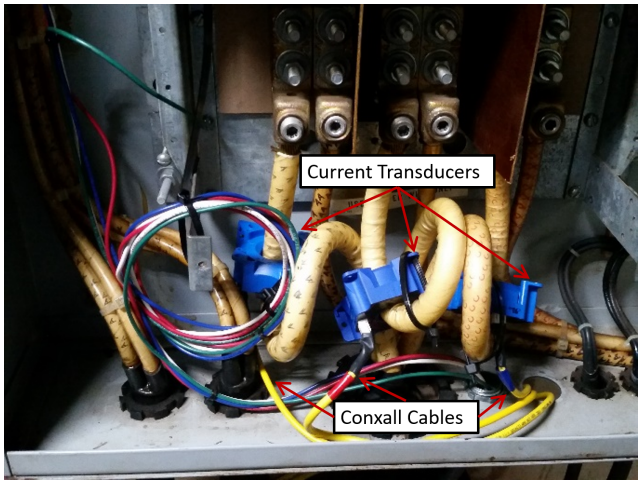

(a) Close-up view of installed current transducers (blue). Conxall cables connect to each current transducer.

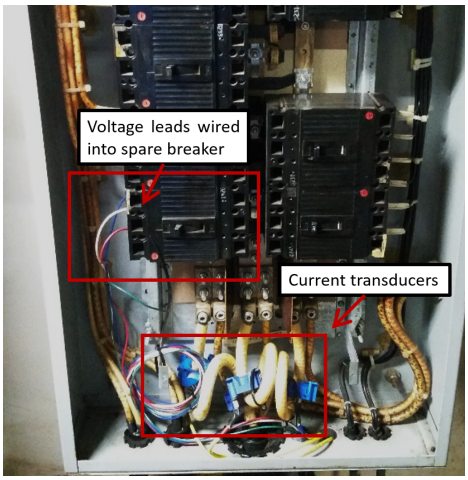

(b) Open power panel with NILM hardware installed. Current transducers are shown at the bottom installed on the 3-Phase power cables leading into the panel. Voltage leads are shown wired into a spare breaker on the panel (red, white, & blue wires leading into breaker.)

Figure A-4: Current and voltage sensor installation on USCGC SPENCER (WMEC 905).

A.1.3 Proposed Installation & Mounting

The MIT NILM team proposes that NILM devices be installed on Power Panels 1S-4P-(1-66-2) and 1S-4P-(2-32-1). Each device will include all the items listed previously (AIO Box, current transducers, Conxall cables, etc.). Each AIO box would monitor one of the designated panels. Figure A-5 shows a modified schematic of the electrical generation and distribution plant onboard USCGC THUNDER BAY (WTGB 108), highlighting the power panels that will be monitored using NILM sensors.

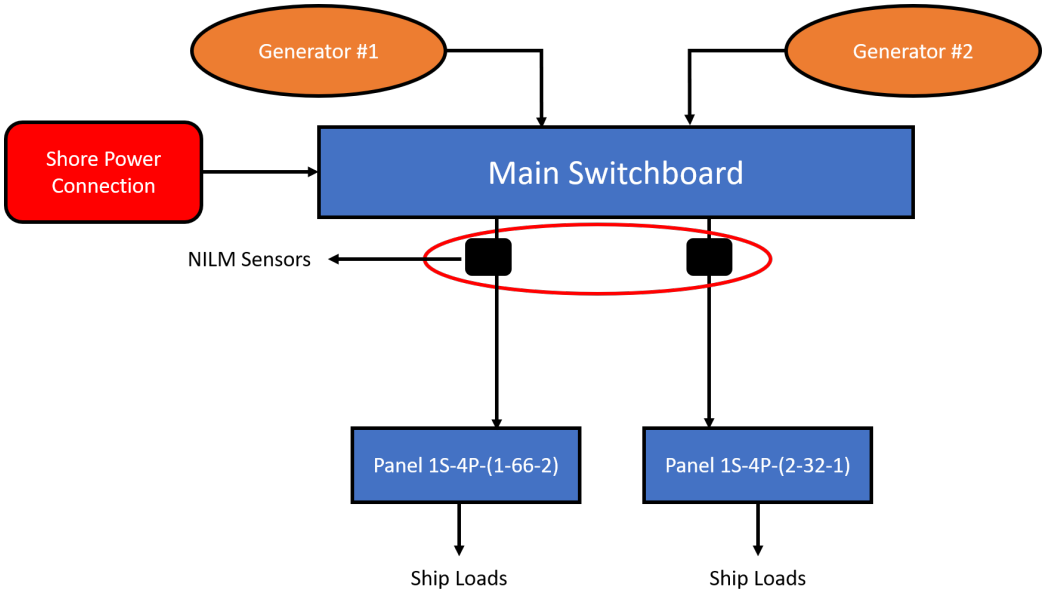

Figure A-5: USCGC THUNDER BAY (WTGB 108) electrical diagram with NILM sensor installation points identified (black boxes).

A.1.3.1 Hardware Mounting Location

The proposed installation locations for the boxes can be found in Figures A-6 and A-7. The AIO boxes for Panels 1S-4P-(1-66-2) and 1S-4P-(2-32-1) will be mounted on the supporting struts for the cable runs directly next to the power panels. These locations provide ample space for the AIO boxes to be mounted on temporary brackets to be installed by the MIT-RLE team. Further, because of the close proximity to the Power Panels, the length required for the Conxall Cables and Voltage Leads will be minimized.

Figure A-6: Proposed installation location for AIO box on Power Panel 1S-4P-(1-66-2) located in the Engineering Control Center (1-58-0-C).

Figure A-7: Proposed installation location for AIO box on Power Panel 1S-4P-(2-32-1) located in the Engine Room.

A.1.4 Conclusion

Further information regarding the nature of this project can be found by contacting the US Coast Guard graduate students at MIT (listed below). The details of the exact installation regarding hardware, bracketry, and procedures for install will be outlined in the Installation Plan. Further details regarding MIT and the Coast Guard's roles with regard to this situation can be found in the Memorandum of Agreement between MIT-RLE and SFLC-ESD.

All questions should be directed to LT Andrew Moeller (amoeller@mit.edu), LT Joseph O'Connell (joeyoc@mit.edu), LT Devin Quinn (dwquinn@mit.edu) and LTJG Brian Mills (millsbt@mit.edu).

A.2 MIT NILM Installation Proposal for USCGC THUNDER BAY (WTGB 108)

A.2.1 Proposed Mounting

A.2.1.1 Mounting Hardware Details

The proposed installation and mounting will be set up to be temporary. That is, no permanent modifications will be made with regard to the mounting hardware for the All-in-One (AIO) boxes. Instead, the majority of all hardware and brackets will be installed using existing holes or brackets on the ship. Additional hardware, provided by the Massachusetts Institute of Technology Research Laboratory of Electronics (MIT RLE), will be custom-built and modified for the AIO boxes to be mounted securely without making permanent alterations to the cutter. AIO boxes will be installed in two separate shipboard locations, including the Engine Room (3-32-0-E) and Engineering Control Center (ECC) (1-58-0-C). The mounting brackets for these two locations will be nearly identical.

Figures A-8 and A-9 show the proposed locations of the mounting brackets to be installed in the port aft section of ECC and the forward starboard section of the Engine Room. The brackets will be bolted to existing structures on the cutter and then the AIO box will mount directly to the installed brackets for a secure fit. Both types of mounts utilised for this installation will be explained in further detail in this section.

A.2.1.2 Mounting Brackets

The mounting system in both ECC and the Engine Room will utilise the existing vertical cableway structures for support. Four horizontal mounting bars will be attached to the struts affixed to the bulkhead using the existing holes. Once these bars are mounted to the struts, angle brackets will be used to attach a vertical mounting

Figure A-8: Proposed mounting location for AIO box in ECC.

Figure A-9: Proposed mounting location for AIO box in the Engine Room.

plate that the AIO boxes will directly mount to. The layout for these brackets are further illustrated in Figure A-10.

In order to affix the AIO box bracketry to the existing struts, the existing horizontal cable run brackets will have to be removed. Since these are attached using bolts, this will allow for easy removal and easy re-installation once the AIO boxes are eventually removed. Although the cable run guides will be removed, the newly affixed mounting plate for the AIO boxes will serve the same purpose and ensure the cables will remain properly secured. Figure A-11 shows the struts and existing holes that will be utilised for the bracket mount in ECC.

The mounting brackets will be identical in both ECC and the Engine Room, however in the Engine Room there will be an additional bar to separate the cables within the cable run (see Figure A-12) and maintain the current layout configuration of the Cutter.

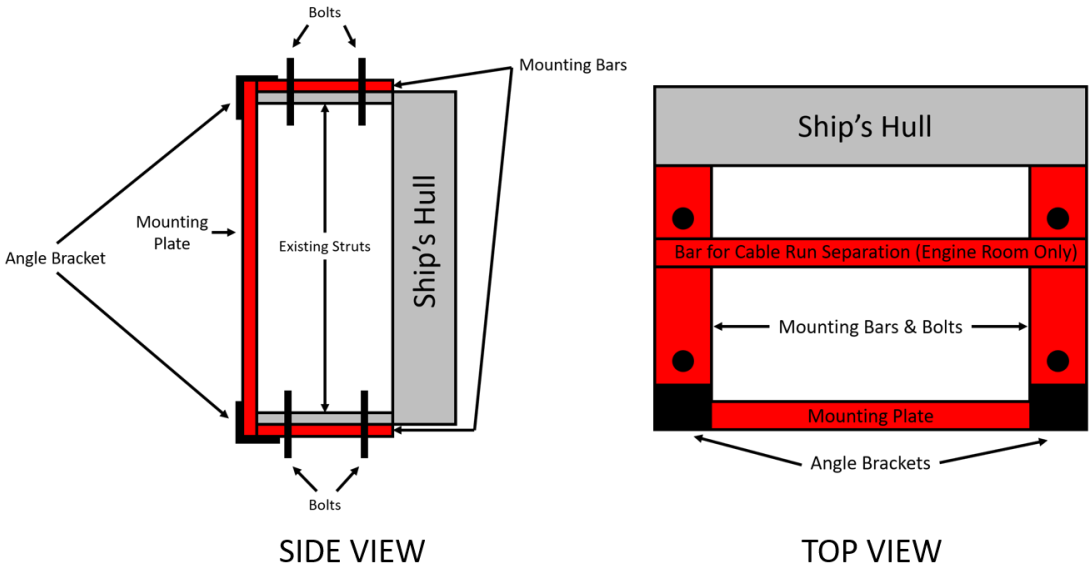

Figure A-10: Layout of bracket mounting configuration for Engine Room and ECC.

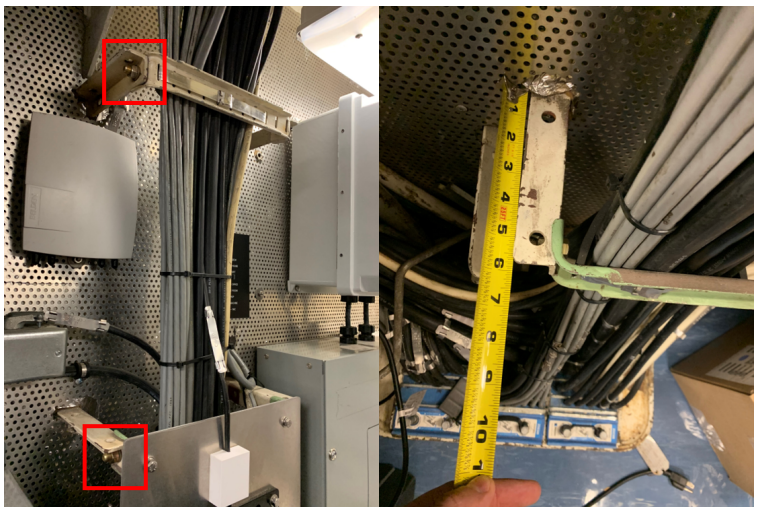

Figure A-11: Struts and holes with bolt inferences.

Figure A-12: View of the double cable run in the vicinity of the mounting location in the Engine Room.

A.2.1.3 Cable Runs

Cables will come out the bottom of the mounted AIO Boxes in both the Engine Room and in ECC. This will allow for easy organization and ensure that all cables can be properly secured to existing cableways.

The IEC Power Cords will be installed at the nearest power receptacle to each panel.

The proposed receptacles for for the IEC Power Cords can be seen in Figures A-13 and A-14. These receptacles will be used to provide power to the Data Acquisition Units (DAQ). In ECC, a marine power strip (IAW NSTM 300-2.7.3.5) will be plugged into the power receptacle in order to keep other power receptacles open for the crew's use in this specific space.

All cables and cords shall be installed in accordance with Mil-STD-2003B. The cables and cords will run along existing cableways and fittings that will allow them to be properly secured and will not impede the movement of personnel or equipment in any area.

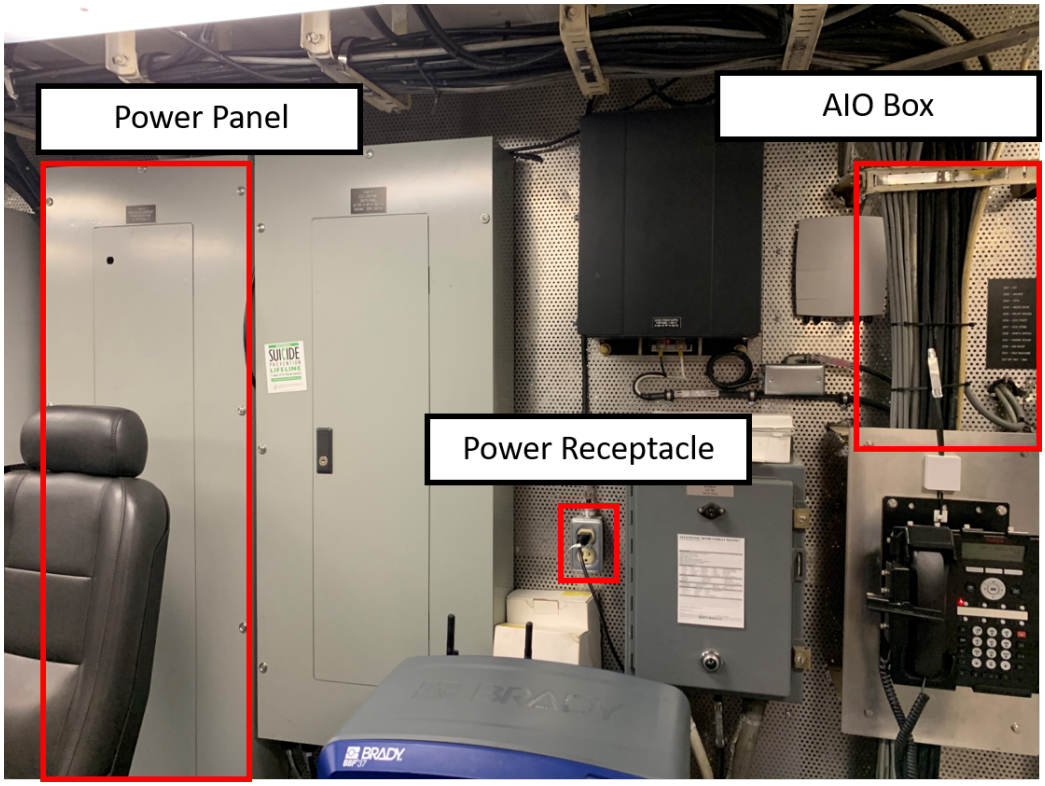

Figure A-13: Location of power receptacle for Panel 1S-4P-(1-66-2)

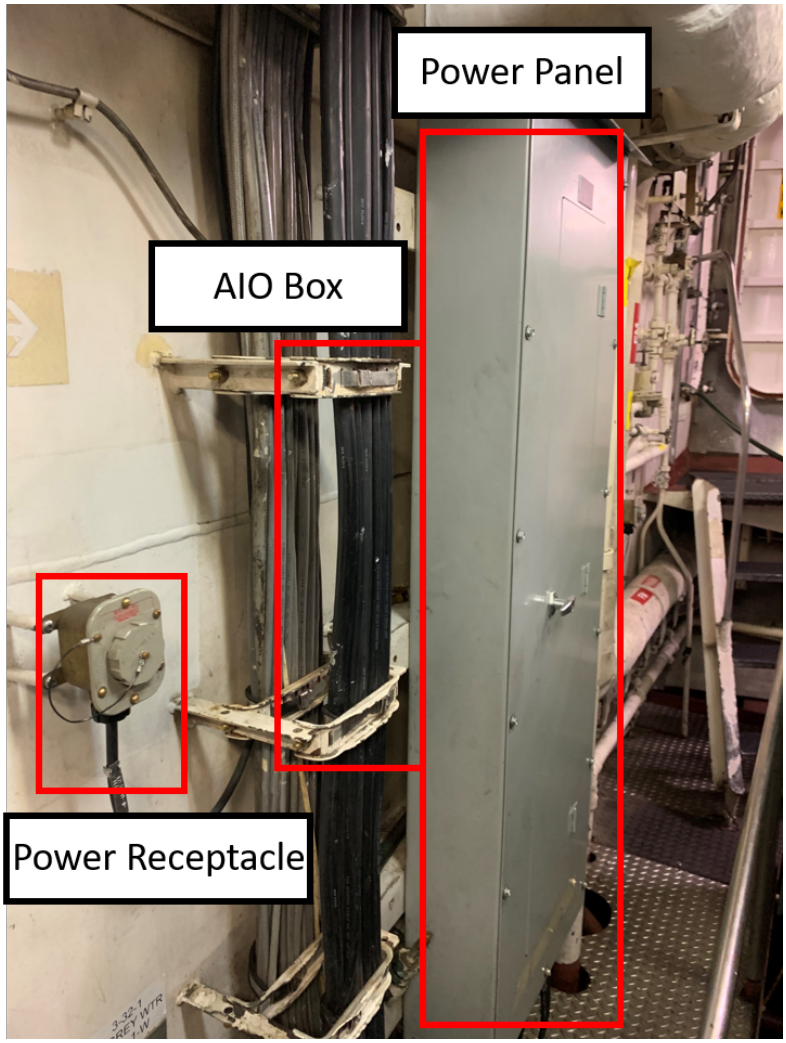

Figure A-14: Location of power receptacle for Panel 1S-4P-(2-32-1)

A.2.2 Installation on Panel

This section will detail the plan for equipment installation on the electrical panel. This will include installation of the current transducers, their connection to the Conxall cables, and the wiring of the voltage leads to the spare breaker. **Prior to conducting any electrical work, equipment shall be tagged out IAW COMDTINST 9077.1 (series)**.

A.2.2.1 Cable Entry into Panel

Cables will enter into the panel via new holes that will be drilled and fitted with boot shrinks that shall maintain watertight integrity. **For the new holes to be drilled, assistance from a Ship's Force (SF) Electrician's Mate (EM) is necessary. The SF EM must Tag Out the panel installation and verify that the power is secured in accordance with (IAW) all electrical tag out and safety procedures. Then, the SF EM may proceed to drill the necessary holes in the panel.** Use of an SF EM in this step is necessary for safety and quality assurance of work. MIT RLE graduate students are not certified electricians, therefore they shall not conduct the work on the electrical panel.

For installation, two groups of cables will enter each panel: the three Conxall cables, and the voltage leads encased in conduit. The conduit used will be abrasion resistant as well as liquid tight to maintain the watertight integrity of the panel. The proposed method for both groups to enter the panel safely is to drill two 1.25" diameter holes in the top of the power panel. Then, the cables can enter into the panel via bootshrink fittings like those pictured in Figure A-15. These fittings are watertight and meet military specifications (MILSPEC) for running cables into power panels onboard ships and in engineering spaces. Later, following removal of equipment, these fittings will be fit with neoprene plugs IAW ASTM F1836M.

Other commonly used fittings include cord grips, which are shown in Figure A-15

as well. Figure 9 shows an example of the voltage leads (in conduit) as well as the Conxall cables exiting a typical power panel.

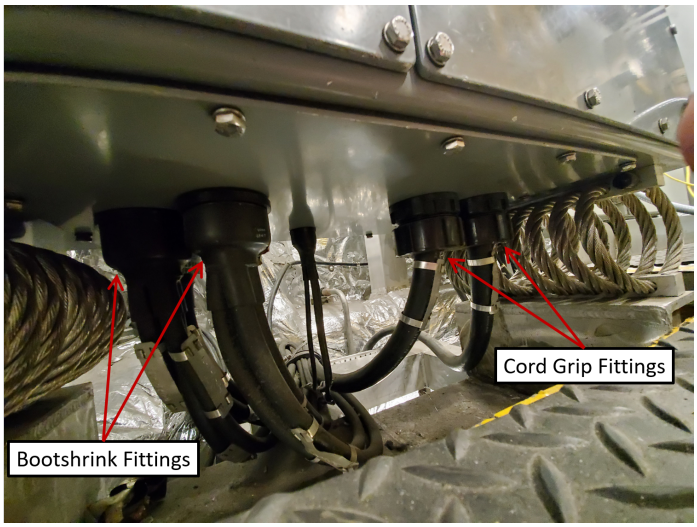

Figure A-15: Example of bootshrink and cord grip fittings feeding into power panel (from US Navy panel).

Figure A-16: Example of voltage leads (in conduit) and Conxall cables exiting from power panel.

A.2.2.2 Panel 1S-4P-(1-66-2) (Engineering Control Center)

Figure A-17 shows the bottom of power panel 1S-4P-(1-66-2). NILM Conxall cables and voltage leads in conduit will enter through two new holes in this section of the

panel. As can be seen, cord grips are used as the watertight fittings for the cables on this panel.

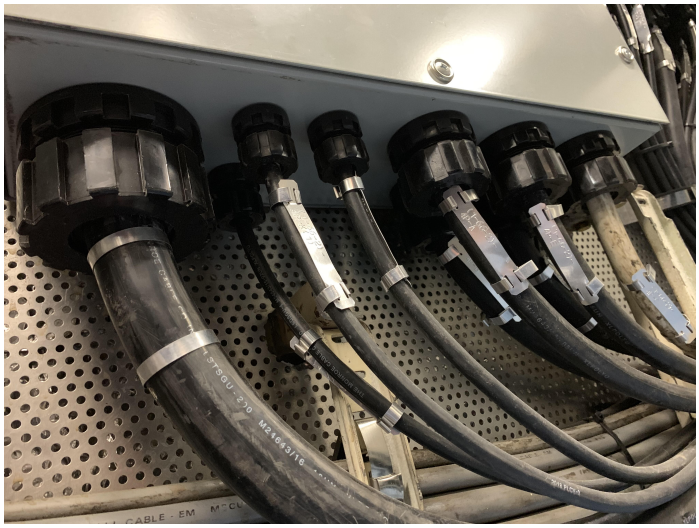

Figure A-17: Cables entries into the bottom of 1S-4P-(1-66-2).

A.2.2.3 Panel 1S-4P-(2-32-1) (Engine Room)

Figure A-18 shows the bottom of power panel 1S-4P-(2-32-1). NILM Conxall cables and voltage leads in conduit will enter through two new holes in this section of the panel. As can be seen, cord grips are used as the watertight fittings for the cables on this panel.

Figure A-18: Cables entries into the bottom of 1S-4P-(2-32-1).

A.2.3 Inside the Panel

This step will also require the assistance of the SF EM. The SF EM will need to open the power panel in order to gain access for installation of the current transducers and voltage leads. **As a reminder, all equipment shall be tagged out IAW COMDTINST 9077.1 (series) prior to performing any electrical work.**

A.2.3.1 Current Transducer Installation

Once confirmed that power has been secured to the panel, the SF EM will remove the lugs on the power cables feeding the panel for each phase. This will allow the current transducers to be installed on each power cable by slipping them over the open lugs. Then, the SF EM will reinstall the power cable lugs.

Next, MIT RLE graduate students will secure the current transducers using zip ties and connect the Conxall cables to the current transducers. Figure A-19 shows the end result of the current transducers and Conxall cables inside the electrical panel on USCGC SPENCER (WMEC 905). As is shown, the current transducers and Conxall cables are neatly organized inside the panel and secured with zip ties.

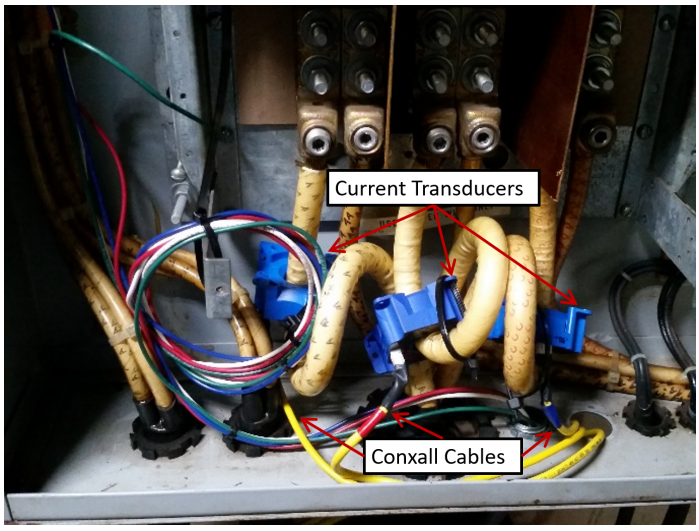

Figure A-19: Current transducers and Conxall cables installed on power cables feeding an electrical panel on USCGC SPENCER (WMEC 905).

A.2.3.2 Voltage Lead Installation

The next step in the internal panel installation is to wire the voltage leads into the spare breaker. As is shown in Figure A-20, there are adequate spare breakers for installation on all three panels. For panel 1S-4P-(1-66-2) in ECC, the MIT RLE team proposes using the (1-66-2)-4P-G breaker seen in the left side of Figure A-20a. For panel 1S-4P-(2-32-1), the MIT RLE team proposes using the (2-32-1)-4P-M breaker seen in the bottom right corner of Figure A-20b.

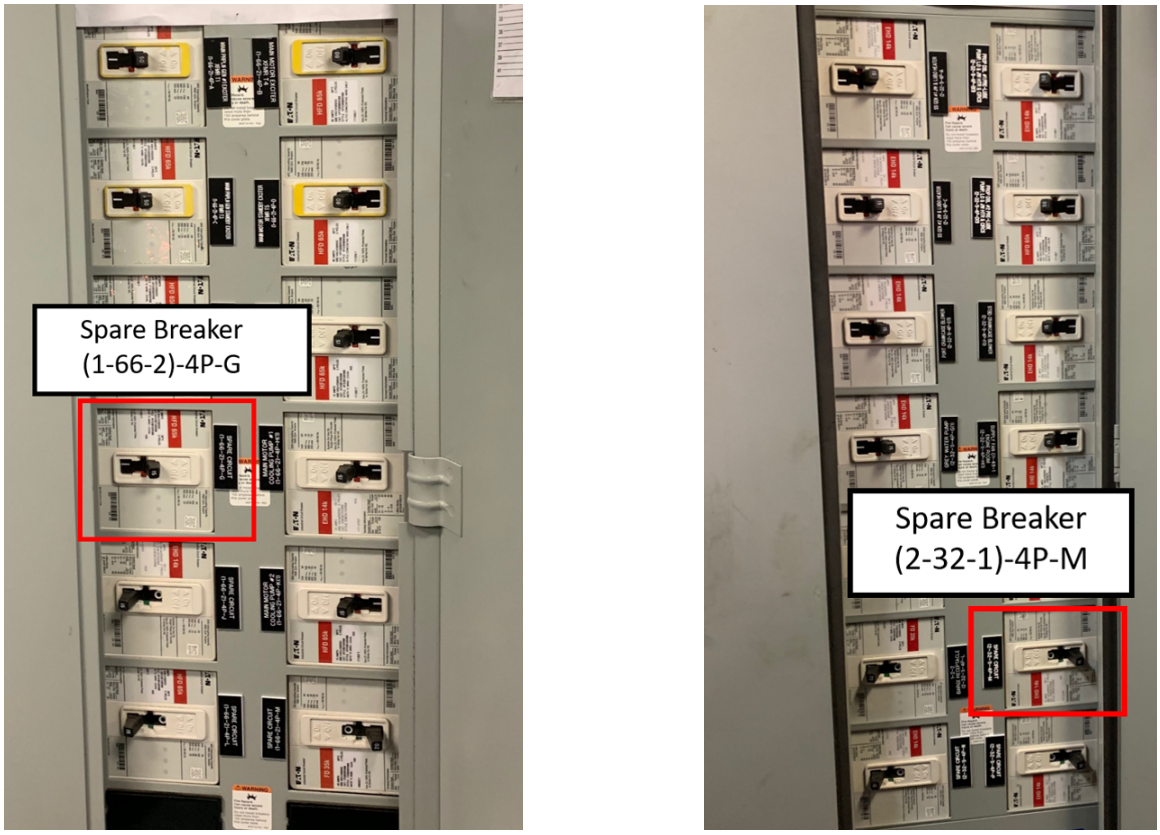

(a) 1S-4P-(1-66-2)

(b) 1S-4P-(2-32-1)

Figure A-20: USCGC THUNDER BAY (WTGB 108) Power Panels

This step requires assistance from the SF EM once again. The SF EM will need to wire the 3 voltage leads into the designated spare breaker. Each lead will wire into one power phase on the breaker. Additionally, there is a ground lead that will need to lead to an appropriate ground location as determined by the SF EM. In previous

installs ground bolts inside the panels have been used. Figure A-21 shows a complete voltage lead install on a spare breaker from USCGC SPENCER (WMEC 905).

Once the voltage leads are connected to the spare breaker, the current transducers are installed on the power cables, the Conxall cables are connected to the current transducers, the cables and wires from the NILM installation are neatly organized within the panel with zip ties, and bootshrink fittings are secured, the SF EM will close the panel and reenergize it IAW all electrical safety and tag out procedures. **No circuit or panel shall be re-energized until final connections and continuity checks have been performed.**

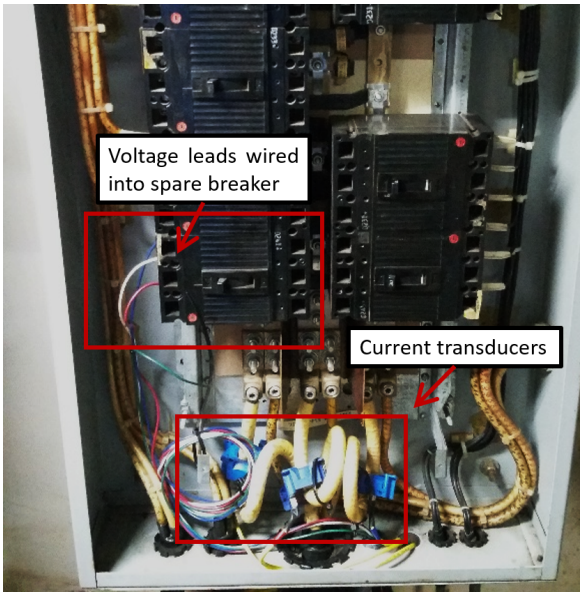

Figure A-21: Interior panel view on USCGC SPENCER (WMEC 905) showing voltage leads wired into a spare breaker as well as current transducers installed on power feed cables.

A.3 Equipment Testing

Following all setup steps on the panels, the MIT RLE team will work to ensure the equipment is working correctly. This will include energizing all MIT equipment, as well as the downstream loads, to ensure proper operation of NILM sensors. In the event of poor or inept readings, the panels will need to be tagged out once again and hardware be adjusted to ensure proper data capture.

Once data is capturing correctly, the MIT RLE would like to energize all downstream loads if possible. This will provide the MIT RLE team with “test data" for each piece of equipment, allowing for it to be classified individually for processing and further understanding. Acquiring this data early allows for NILM Dashboard software to be customized to work for the 140’ Icebreaking Tug class as quickly as possible.

A.4 Equipment Removal

Prior to removing any equipment from the Cutter, all equipment shall be tagged out IAW COMDTINST 9077.1 (series).

A.4.1 Electrical

This step will also require the assistance of the SF EM. **To begin, the SF EM will tag out the entire panel which the NILM is being removed from IAW the shipboard tag out and electrical safety procedures. The SF EM will then remove the front casing on the power panel, and ensure power is secured using a multi-meter IAW all shipboard electrical safety procedures.**

A.4.1.1 Current Transducer Removal

The first step in removing the NILM is securing power to the panels. Once confirmed that power has been secured to the panel, the SF EM will remove the lugs on the

powercables feeding the panel for each phase. This will allow the current transducers to be removed from each powercable by slipping them over the open lugs. Then, the SF EM will reinstall the power cable lugs. MIT RLE Grad Students will take custody of the current transducers and remove conxall leads, zipties and any other equipment from inside the power panel. Next the SF EM will inspect the inside of the power panel to ensure it is clear of debris.

A.4.1.2 Voltage Lead Removal

The second step of the electrical uninstall is the removal of the voltage leads. This step requires assistance from the SF EM once again. The SF EM will need to unwire the 3 voltage leads from the designated spare breaker. Additionally the ground wire will need to be unwired. Once all voltage leads, current conxall cables, current transducers and zip ties are removed both MIT RLE Grad Students and SF EM will inspect the panel ensuring equipment is removed and the panel is in good working order. Upon concurrence that the panel is restored to the original condition the SF EM will close the panel and reenergize it IAW all electrical safety and tag out procedures.

A.4.1.3 Cable Holes

The bootshrink fitted holes into the panels will be sealed with bootshrink caps. This provides adequate watertightness and prevents intrusion into the energized panel. MIT RLE students will provide the caps and install caps under SF supervision. All holes will be sealed prior to re-energizing the electrical circuits IAW COMDTINST 9077.1 (series).

A.4.2 Hardware

Because the mechanical portion of the supporting bracketry is temporary there will be no permanent alterations to the physical structure of the vessel. MIT RLE students will remove all associated bolts, nuts, brackets and hardware mounting under the

supervision of SF. All cable runs will be removed and NILM hardware and cabling will be removed by MIT RLE students after the electrical portion of the system has been removed.

A.5 Cybersecurity

The installation of the AIO box will conform with all applicable US Coast Guard Command, Control, Communications, Computers, Cyber, and Intelligence (C5I) policies and directives. The AIO box is a self-contained data acquisition unit that will not be connected to any external network. All of the power stream data collected by the unit will be stored locally and internally inside the armored AIO box. The only way to retrieve this data will be through a manual download using a manually connected cable connection to the AIO box.

A.5.1 Conclusion

This document summarizes the steps necessary for the MIT RLE NILM installation onboard USCGC THUNDER BAY (WTGB 108). Further information regarding the nature of this project can be found by contacting the US Coast Guard graduate students at MIT (listed below). The details of the project proposal can be found in the Research Proposal. Further details regarding MIT and the Coast Guard's roles with regard to this situation can be found in the Memorandum of Agreement between MIT-RLE and SFLC-ESD. All questions should be directed to LT Andrew Moeller (amoeller@mit.edu), LT Joseph O'Connell (joeyoc@mit.edu), LT Devin Quinn (dwquinn@mit.edu) and LTJG Brian Mills (millsbt@mit.edu).

THIS PAGE INTENTIONALLY LEFT BLANK

Appendix B

AIO Box Version 3.0 Technical Specifications

This Appendix will outline the detailed information necessary for construction of a newly upgraded AIO Box “Version 3.0”. This includes detailed assembly instructions, a bill of materials, and selected technical drawings. The technical drawings included in this Appendix are only for those parts developed and designed for the modifications to convert an original AIO box into the new "Version 3.0".

B.1 Assembly Instructions

Hardware Assembly

1. Verify all materials are on hand for box assembly (see Bill of Materials).

2. Starting with the AIO Box Version 2.0 (Kane Box), remove both side plates from the main chassis. Side plate #1 (one with hard drive holder) will not be needed for this assembly. Keep side plate #2 to the side for step 3.

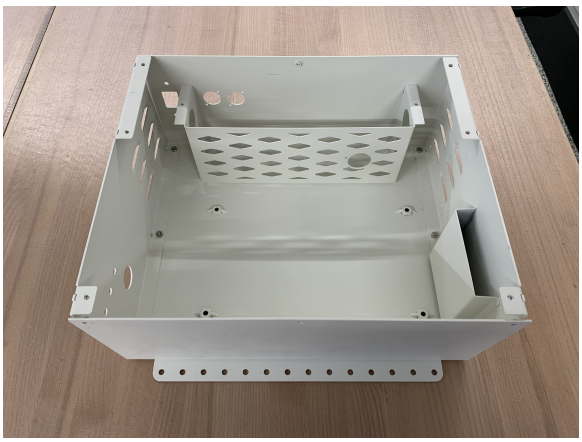

Figure B-1: Original AIO Box (Kane Box).

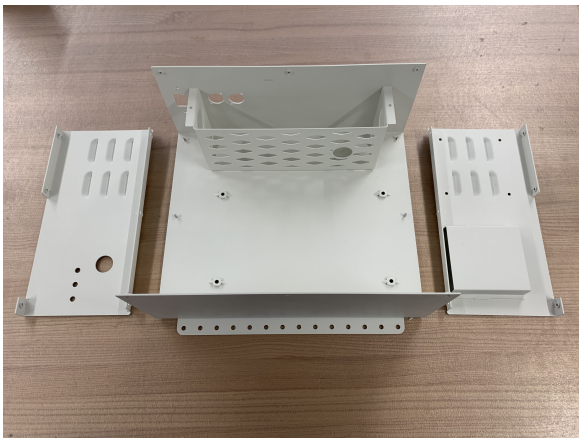

Figure B-2: Original AIO Box (Kane Box) with side plates removed.

3. Drill two $\frac{1}{4}$" holes in side plate #2 in accordance with the appropriate technical drawing.

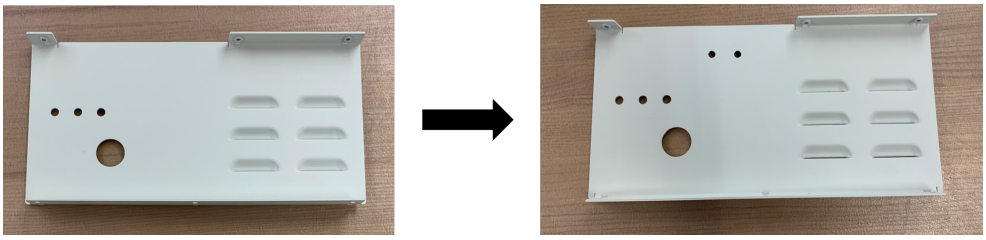

Figure B-3: 1/4" holes drilled into side plate #2

4. Place new side plates (updated side plate #1 from Protocase conversion kit and side plate #2 from Step 3) into the chassis and secure with Protocase provided nuts.

Figure B-4: AIO box with new side plates (expanded view).

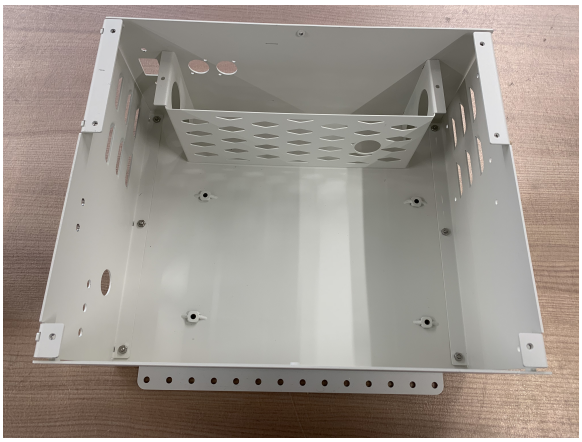

Figure B-5: AIO box with new side plates.

5. Insert grommets on all squirrel cage access holes (4 x 1.5”, 1 x 1”).

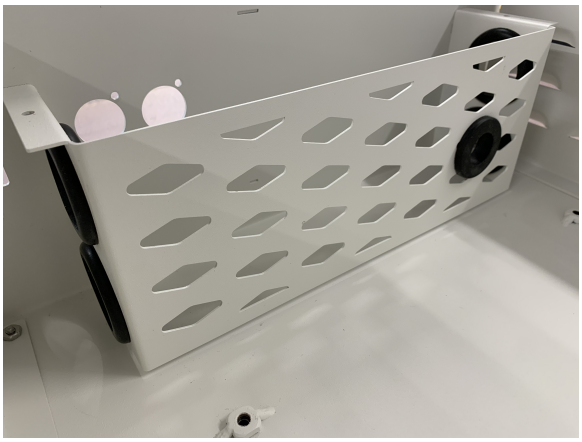

Figure B-6: Grommets installed on squirrel cage.

6. Secure the watertight cord grip to side plate #2 utilizing the provided fastening nut. The preferred method of tightening is with long nose pliers.

7. Attach three Conxall receptacles (614P.3) to side plate #2 above the watertight cord grip, using Loctite to secure the nuts.

Figure B-7: Installation of watertight cord grip and Conxall receptacles.

8. Braid the Conxall cables inside of the box to create a more uniform appearance and reduce the risk of loose wires that will interfere with later steps.

Figure B-8: Braided Conxall receptacle wires.

9. Cut the Conxall Nanomizer cable (604ST2), leaving 5" of wire in addition to the female end. Expose 2-3" of the 4 internal wires, strip these to reveal 1" of the stranded wires. Strip the 4 wires from the Conxall receptacle, revealing 1" of the stranded wires. Slip a heat shrink butt solder tube over one end of each wire, taking care to match colors. Slide heat shrink tube over the exposed wires and heat shrink, ensuring the internal solder melts.

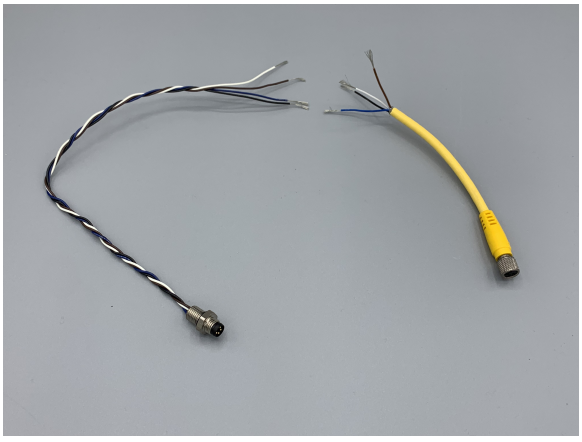

Figure B-9: Conxall cable prior to connection with Nanomizer cable.

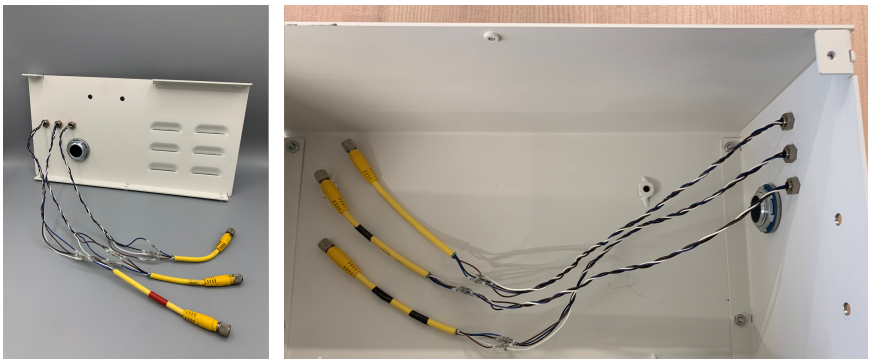

Figure B-10: Conxall cables attached to side plate #2.

10. Insert IEC Panel Mount, securing to box chassis with 1/2" 10-24 screws and locknuts.

11. Attach the USB-A Panel Mounts, with 1/2" 4-40 machine screws and nyloc nuts. Ensure both USB slots are oriented in the same direction.

Figure B-11: Installation of USB-A panel mounts and IEC panel mount.

12. Insert the UPS power cable into IEC mount and snake the cable inside of the squirrel cage.

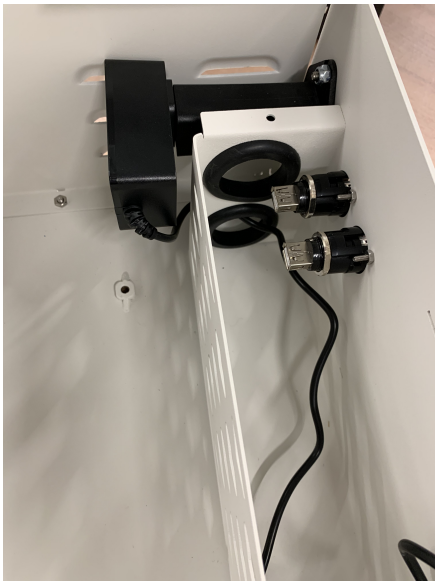

Figure B-12: UPS power cable wiring.

13. Place the UPS inside of the squirrel cage and connect to the power supply cable from Step 12. Attach the output barrel jack power cable and set aside for later steps.

Figure B-13: Example UPS power cable configuration.

14. Take the 12V cooling fan and strip the two wires so there is 1" of exposed internal wiring. Then take a female barrel jack connector and trim the wires so there is 1" of exposed internal wiring. Using the same method as Step 9, connect the wires together using the heat shrink butt solder to form a connection.

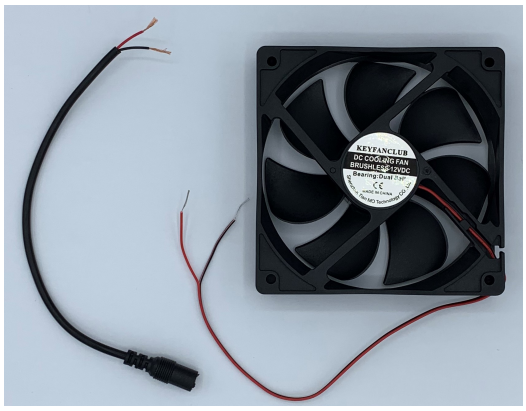

(a) Cooling fan (unconnected wires).

(b) Cooling fan (connected wires).

Figure B-14: Cooling fan wiring configuration.

15. Install cooling fan to side plate #1 with screws provided within the product packaging.

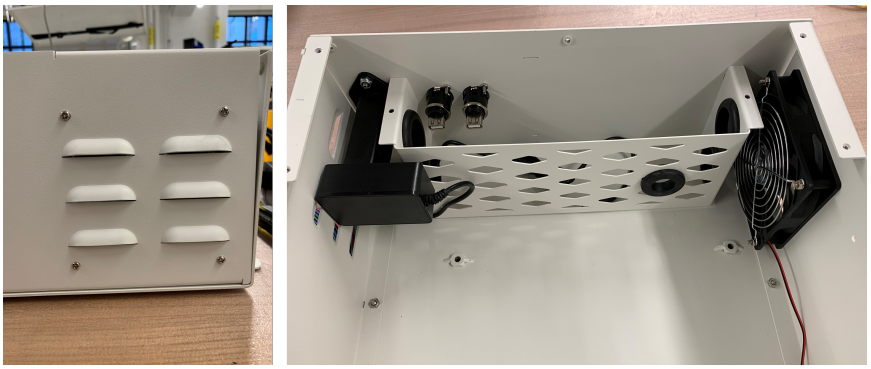

Figure B-15: Cooling fan installation (internal & external views).

16. Using the holes drilled in Step 3, install the Wi-Fi antenna extension cables to side plate #2 and secure with Loctite.

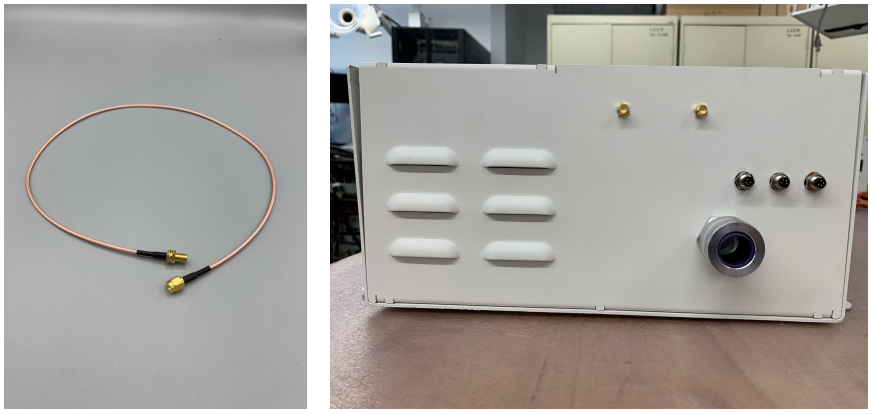

Figure B-16: WiFi antenna cabel installation.

17. Snake the antenna cables inside of the squirrel cage and connect to the mini-Wi-Fi router. Insert the power cable and Ethernet cable into the router and set aside in the squirrel cage. Be sure to insert the Ethernet cable into the **LAN** port.

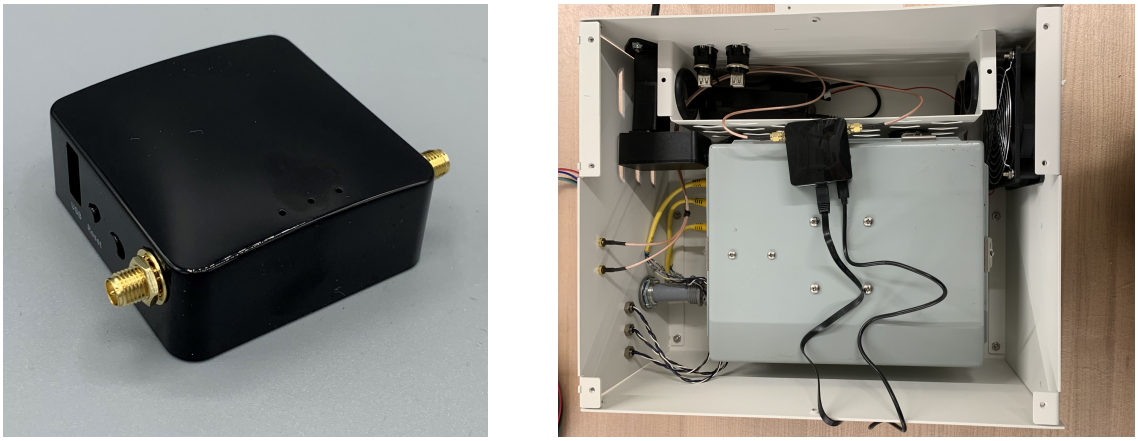

(a) Mini Wi-Fi router.

(b) Wi-Fi router cabling configuration example.

Figure B-17: Wi-Fi router with associated wiring connections.

18. Connect two right angle USB cables to the USB Panel Mounts inside of the squirrel cage.

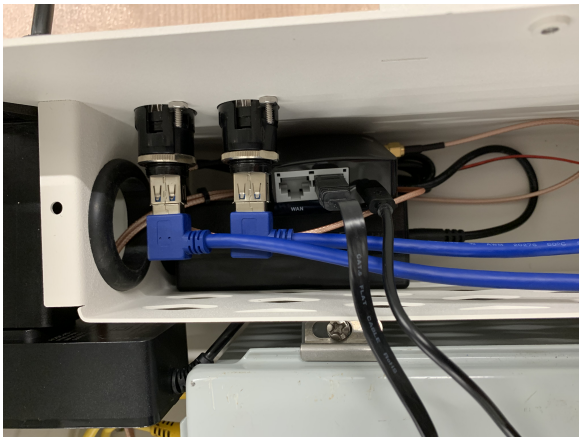

Figure B-18: Right angle USB cables connected to USB-A mounts.

19. Secure the NEMO box with four 1/4" 1/4-20 bolts to the bottom of the AIO box, using Loctite to securely fasten. Verify NEMO NILM is configured in Delta 440-120 transformer configuration with 35 Ohms of resistance.

20. While installing the NEMO NILM box, use 2" of 3/8" abrasion resistant, liquid tight conduit to secure the high voltage wire exit from the NEMO box to the AIO box watertight cord grip. Once this is in place, the Conxal cables from step 9 can be connected to the receptacles on the NEMO box.

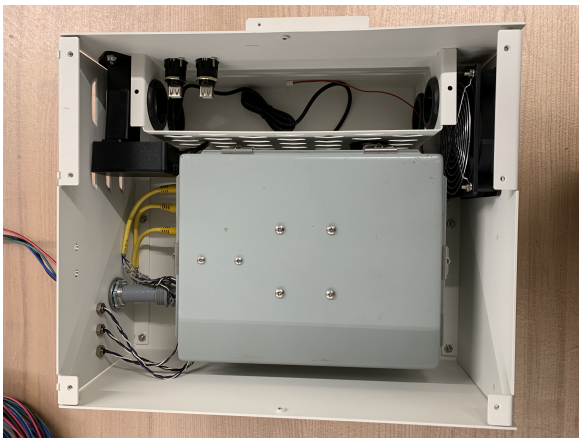

Figure B-19: NEMO box installation.

21. Insert a 12” Ethernet cable into the NEMO box and snake through the squirrel cage. Ensure that the cable exits the squirrel cage next to the cooling fan. The exact size of the Ethernet cable can vary, however a shorter cable is preferred to prevent the excessive buildup of cables.

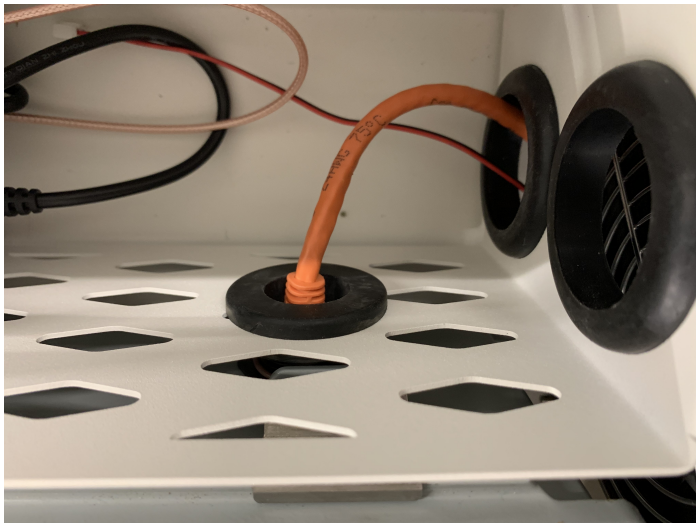

Figure B-20: Ethernet cable connected to NEMO box.

22. Place a 1.5” grommet on squirrel cage cover and secure to the top of the squirrel cage with two 1/8” 4-40 screws/nuts. Be sure to pull the two right angle USB cables, UPS power cable, Wi-Fi router power cable, and Wi-Fi Ethernet cable through the top access hole in the squirrel cage before securing the cover.

Figure B-21: Secured squirrel cage with appropriate cables exiting from the top opening.

23. Insert 4 Up/Down USB adapters, both Ethernet cables (NEMO box & Wi-Fi router), and mini-HDMI cable (from WIMAXIT touch screen monitor packaging) into the GK41 computer.

(a) Isometric view with USB ports.

(b) Isometric view with power and ethernet ports.

Figure B-22: GK41 computer prior to installation.

Figure B-23: GK41 with up/down USB adapters connected.

24. Using a barrel jack splitter power cable, connect the GK41 computer and cooling fan, leaving the single end to the side for later steps. An example arrangement can be seen below for the entire power cabling configuration for the AIO box.

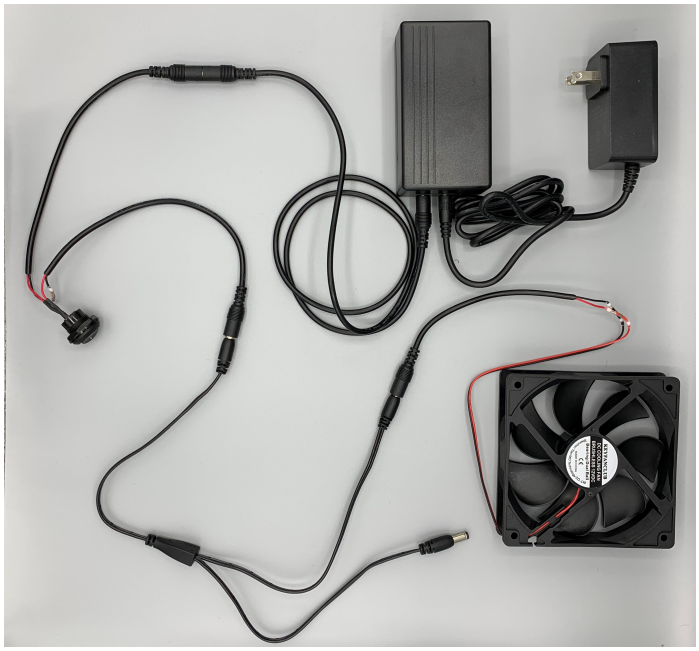

Figure B-24: Power cable configuration for AIO box.

25. Once all applicable cables have been connected to the GK41, slide it into the appropriate place on side plate #1 next to the NEMO box. Ensure that the computer is aligned in the middle of the two holes on the side plate.

Figure B-25: GK41 in place next to the NEMO box.

26. Place three pieces of gasket material on the GK41 holder and secure the GK41 to the side plate using 2 x 1/2" 10-32 screws.

(a) GK41 bracket (front side).

(b) GK41 bracket (back side).

Figure B-26: GK41 bracket with gasket.

Figure B-27: GK41 mounted with bracket.

27. Connect the two right angle USBs to two of the up/down USB connectors attached to the GK41. Connect the Wi-Fi router USB cable and WIMAXIT touch screen USB to Type-C cable to the remaining two up/down USB connectors on the GK41.

Figure B-28: GK41 mounted with holder.

28. Cut a male to female barrel jack connector in half, and expose 1" of the internal wires for each side of the cable. These two cables can be cut down to a shorter/more appropriate size as needed. Connect the black wires using the heat shrink butt solder connectors used in Steps 9 & 14. Solder the red wires to the terminals on the rocker switch, ensuring that heat shrink is used after the solder is complete.

Figure B-29: Rocker switch with soldered wires.

29. Place the rocker switch adaptor piece on the top of the front plate in the same position as the current hole. Secure the rocker switch in this hole.

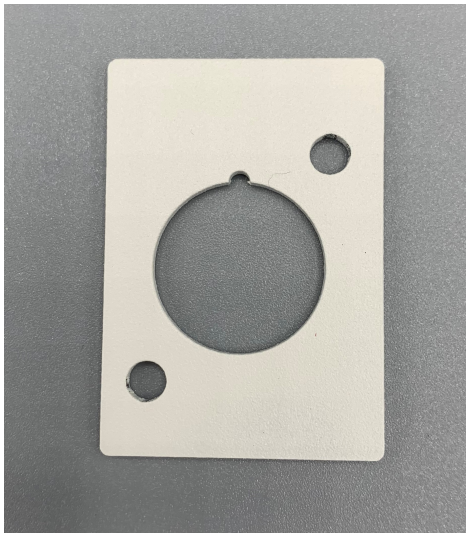

(a) Rocker switch adaptor piece.

(b) Rocker switch inserted in adaptor piece.

Figure B-30: Rocker switch adaptor.

30. Attach the flip cover on top of the rocker switch with 1/2" 4-40 screws and nyloc nuts.

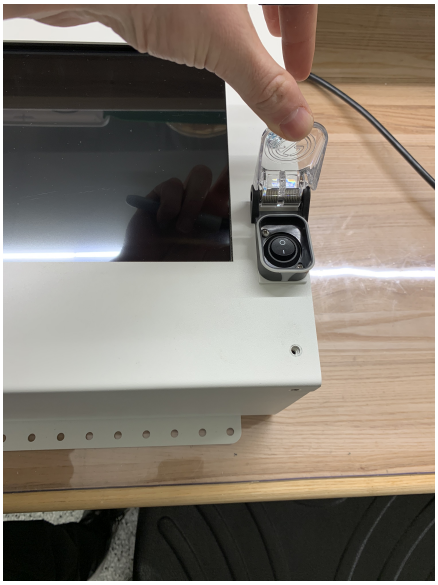

Figure B-31: Rocker switch installed on front plate with flip cover.

31. Place the appropriate gasket provided by Protocase on the back of the face plate.

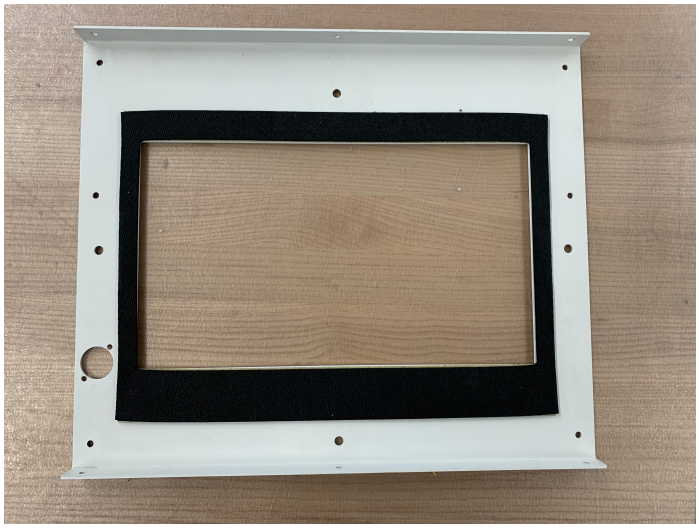

Figure B-32: Faceplate with appropriate gasket.

32. Place the appropriate gasket provided by Protocase on the touch screen support.

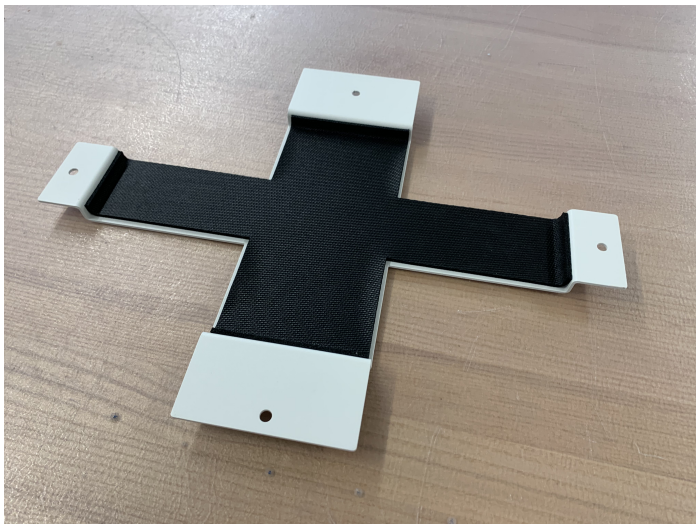

Figure B-33: Touch screen crossbar with appropriate gasket.

33. Place the WIMAXIT touch screen in the support cross bar from step 32. Connect this piece to the face plate using 4 x 3/4” 1/4-20 bolts.

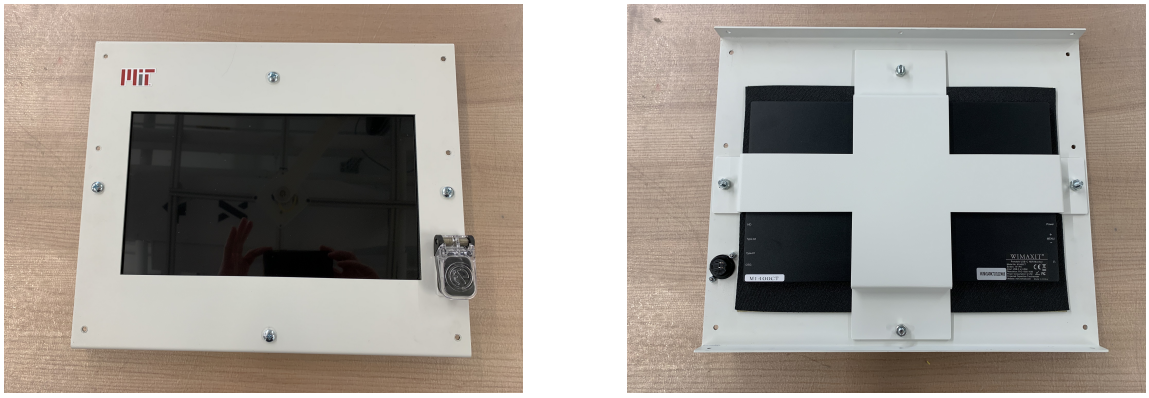

(a) Front view.

(b) Back view.

Figure B-34: WIMAXIT touch screen installed on face plate with cross bar.

34. Install the external hard drive flip cover with 2 x 7/16" 5-40 socket head screws.

Figure B-35: Installed flip cover for external hard drive holder.

35. Connect the HDMI and Type-C USB cables from the GK41 to the WIMAXIT touch screen.

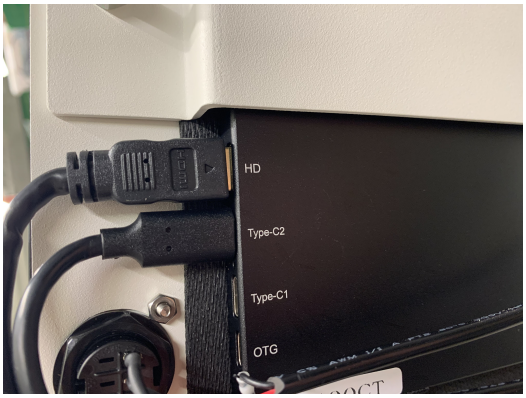

Figure B-36: WIMAXIT touch screen cable connection points.

36. Connect the male end of the rocker switch barrel jack cable to the UPS power cable from Step 14. Connect the female end of the rocker switch barrel jack cable to the barrel jack splitter that supplies the GK41 and the cooling fan. See Figure B-13.

37. Secure the front plate to the rest of the AIO box using 12 x 7/16" 8-32 self-clinching bolts.

38. Attach antennas to the Wi-Fi antenna extension cables on side plate #2 if wireless capability is desired.

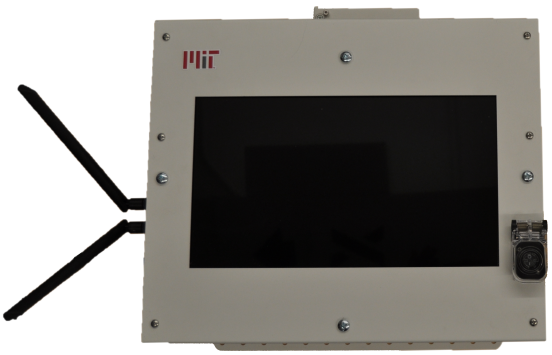

Figure B-37: Final AIO box design.

Software Installation & Setup

1. Plug in power to the AIO box, and make sure that the GK41 is powered off. Insert the bootable NILM Ubuntu USB drive. Plug in an external USB keyboard.

2. Turn on the GK41. While doing so, press ESC while the GK41 is booting to launch the BIOS setup utility.

3. Once in the BIOS setup utility, navigate to the boot page.

4. Change the boot priority of the USB device to 1.

5. Exit the BIOS setup utility, saving changes.

Now, the system should boot from the USB drive and proceed to the Ubuntu installation dialog. Select "Install Ubuntu" and follow the guided setup. Erase any other operating system installed. If the computer for the installation uses UEFI instead of BIOS, it is necessary to connect to the internet during installation and to allow for updates by selecting "Install Updates." After the installation is complete and the computer is able to boot to the installed NILM Ubuntu operating system, the BIOS/UEFI settings can be changed to the previous boot priority order so that the drive with the NILM Ubuntu operating system has first boot priority.

Initial Setup

Once installed, follow the steps outlined in the `NILM_README` file located on the Desktop, which are elaborated on here:

1. Authorize local user access to the Joule server:

   Command Line:

   ```
   $> sudo –E joule admin authorize
   ```

2. Connect Joule to the local Lumen server:

   Command Line:

   ```
   $> joule master add lumen 127.0.0.1
   ```

   Enter the desired credentials information, which will be used for the Wattsworth data viewer app.

3. To configure data capture, edit `meters.yml` on the Desktop and run the following command. This command must be run any time `meters.yml` has been updated. More details about setting up a `meters.yml` file are in the next two subsections, for contact and noncontact meters, respectively.

   Command Line:

   ```
   $> sudo nilm configure
   ```

4. Restart Joule:

   Command Line:

   ```
   $> sudo service joule restart
   ```

5. Check that data capture and process modules are running:

Command Line:

```
$> joule module list -s
```

The output should look similar to the following:

Name	Inputs	Outputs	CPU %	Mem %
meter1 capture		/meter1/sensor	2	1.2
meter1 process	/meter1/sensor	/meter1/IV /meter1/sinefit /meter1/prep	10	1.3

If the entries for CPU % and Mem % have dashes instead of numbers, there is an error with the corresponding module. The logs for a specific module can be viewed by running the following command. This can help with debugging any errors.

Command Line:

```
$> joule module logs "ModuleName"
```

Contact Meter Setup

Connect to the contact meter to the NILM computer using wired Ethernet. Once physically connected, go to the Wired settings in the Network settings. Manually set up an IPv4 connection. Set the Address to an IPv4 address of the form 192.168.X.Y, as long as this address is not the same as the IP address of the LabJack or NerdJack. The default IP address of both the LabJack and NerdJack is 192.168.1.209. Assuming the default IP is used, an example of a valid IP address for the NILM computer is 192.168.1.201. Set the subnet mask ("Netmask") to 255.255.0.0 (or 16). Click Apply. The settings should look similar to the following:

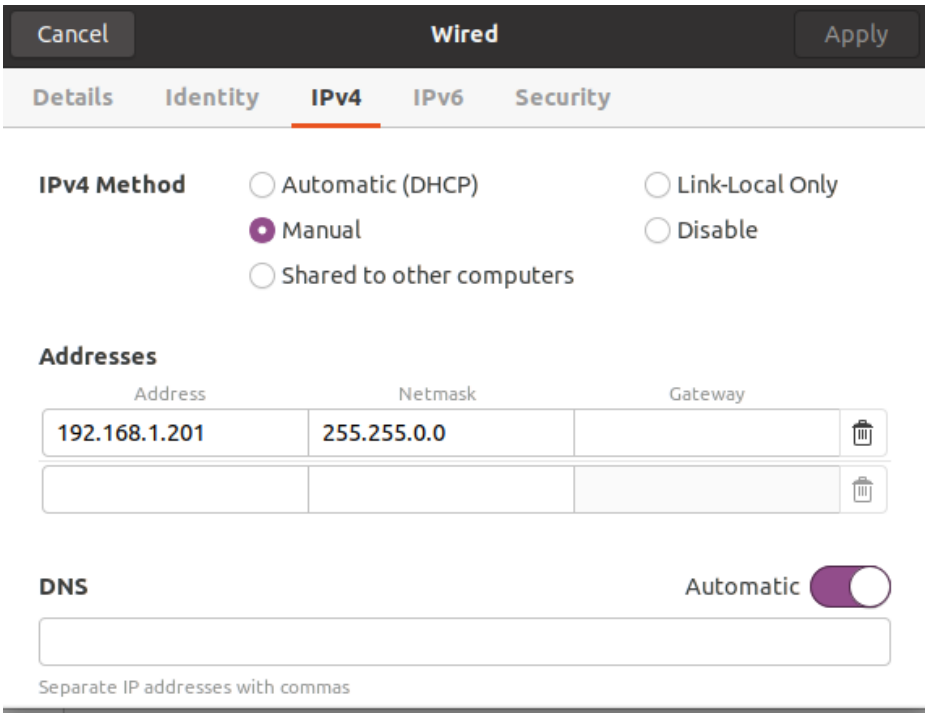

An example `meters.yml` file is shown below for a contact meter:

Listing B.1: meters.yml

```yaml
meter1:
  type: contact
  enabled: true                       # set to false to disable
  daq_type: nerdjack                  # labjack or nerdjack
  ip_address: 192.168.1.209           # default LJ or NJ address
  phases: 3                           # 1 - 3
  sensors:
    voltage:
      sensor_indices: [3,4,5]         # maps to phase A,B,C
      sensor_scales:  0.0919          # built-in constant
      sinefit_phase:  A               # [A,B,C] voltage
      nominal_rms_voltage: 120        # used to scale prep to W
    current:
      sensor_indices: [0,1,2]         # maps to phase A,B,C
      sensor_scales: 0.00156402587    # set by resistors and LEM
      sinefit_rotations: [240,0,120]
    filter:
      enabled: false
      #filter_index: 0                # filter index 0 - 5
  streams:
    sinefit:
      decimate: true
      keep: 1m
    iv:
      decimate: true
      keep: 1w
    prep:
      decimate: true
      keep: 3w
      nshift: 1
      goertzel: true
    sensor:
      decimate: true
      keep: 1w
```

The sensors must be scaled correctly to convert the measurements to volts and amps. The voltage scale factor is set in hardware to 0.0919. The current scale factor depends on the load resistance set by the channel DIP switches and the conversion ratio found on the LEM datasheet. The load resistance, R, should be set according to the DIP switches as below, and the corresponding current conversion factor (`sensor_scales` in the `meters.yml` file) can be calculated, where α_{LEM} is the conversion ratio obtained from the LEM datasheet:

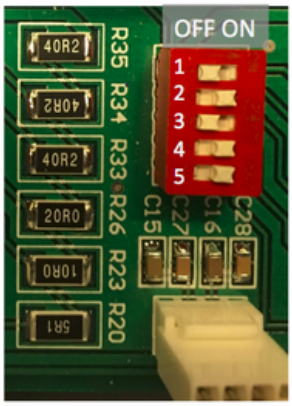

Switch	OFF Value
1	80 Ω
2	40 Ω
3	20 Ω
4	10 Ω
5	5 Ω

ON switches add 0 Ω

Current Conversion Factor

$$\frac{5.07-(-5.18)}{2^{16}} \times \frac{\alpha_{LEM}}{R}$$

α_{LEM}: from LEM datasheet

Voltage Conversion Factor

0.0919 (fixed)

For shipboard installations, R is typically set to 35 Ω. Typically deployed LEMs are the LF 305-S (with maximum measurable current of 300 A) and LF 505-S (with maximum measurable current of 500 A). In the lab, R is typically set to 100 Ω, with the LA-55P LEMs (with maximum measurable current of 50 A). The current conversion ratios for these setups are listed in the table below.

Table B.1: Current conversion factors

	α_{LEM}	R	Current conversion factor
LA 55-P	1000	100 Ω	0.001564026
LF 305-S	2000	35 Ω	0.008937291
LF 505-S	5000	35 Ω	0.02234323

Different LEMs and different R values will yield different current conversion factors. Typically these values should be set such that R is within the allowable maximum load resistance as specified in the LEM datasheet, while also using the full voltage range of the DAQ without clipping (usually ±5 V). For instance, for the LA 55-P setup described, the voltage range is $\pm 50 \cdot \frac{1}{1000} \cdot 100 = \pm 5$ V. The above assumes that a closed loop current transducer with current output is used. An open loop current transducer with voltage output has also been tested, which has a split core for easy mounting. The tested sensor, LEM HTR 300-SB has an output voltage of ±4 V. For this sensor, a resistance greater than 10 kΩ should be used (i.e., one of the resistors set by the DIP switch will need to be replaced).

Additional notes about the `meters.yml` file:

- The `sinefit_rotations` will need to be updated by cycling a known load and viewing the prep streams. For a wye-configured contact box, the sinefit rotations will be some permutation of [0, 120, 240] degrees. For a delta-configured contact box, the sinefit rotations will be either a permutation of [30, 150, 270] degrees or [90, 210, 330] degrees. This comes about because it is possible for there to be a phase shift of 180 degrees in the voltages with respect to the currents.
- For each of the streams, a time duration can be specified for how much data to keep (h for hours, d for days, m for months, or y for years).
- If using the notch filter of the NerdJack, the `filter: enabled` should be set to true. The `filter_index` should be uncommented and the desired filter index specified.

IMPORTANT: Enabling the NerdJack filter results in a sensor stream with seven columns. Using a NerdJack with the filter disabled or using a LabJack results in a sensor stream with six columns. These cannot be combined. A new meter will need to be created (e.g., meter2) if switching between LabJack and NerdJack or disabling and enabling the NerdJack filter.

Table B.2: AIO Box v3.0 bill of materials.

Part	Description	Supplier	Part No.	Quantity	Unit Cost ($)	Total Cost ($)
AIO Box Conversion Kit	Protocase manufactured modification components	Protocase		1	268.02	268.02
Computer	MINISFORUM (DeskMini Series GK41)	Amazon	GK41	1	249.99	249.99
Touch Screen Monitor	WIMAXIT 15.6” 1080p Portable Display	Amazon	M1400CT	1	199.99	199.99
IEC Panel Mount	Power connection for internal components	AC Works	AD1308-FG	1	13.99	13.99
Cooling Fan	KEYFANCLUB 12 V Brushless Cooling Fan (120x120x25mm)	Amazon	0789371779158	1	12.99	12.99
Hard Drive (1 TB)	External Hard Drive	Amazon	B079D359S6	1	48.99	48.99
UPS	12 V 2 A Mini DC UPS (Model: UPS1202B)	Amazon	XD44.4	1	39.00	39.00
Mini Wi-Fi Router	GL.iNet Portable Mini Travel Wireless Pocket Router	Amazon	GL-AR300M16	1	31.90	31.90
Wi-Fi Router Antennas	BrosTrend 1200 Mbps Long Range USB Wi-Fi Adapter	Amazon	Model #AC3	1	33.90	33.90
Wi-Fi Antenna Extension Cables	Bingfu WiFi Antenna Extension Cables (24” - pack of 2)	Amazon	BFN00356	1	8.99	8.99
Rocker Switch	E-Switch RR3130ABLKBLKFS	DigiKey	EG1889-ND	1	2.80	2.80
Flip Cover	Cover for rocker switch protection	Amazon	B00Q3M3DXU	1	11.99	11.99
Liquid-Tight Cord Grip	For conduit passthrough	McMaster-Carr	8302K211	1	19.00	19.00
Fan / Case Cover / IEC Screws		McMaster-Carr	91772A193	8	0.0664	0.53
Fan / Case Cover / IEC Nuts		McMaster-Carr	91841A009	8	0.0365	0.29
USB Panel Mount Screws		McMaster-Carr	91772A126	4	0.0636	0.25
Flip Cover Screws		McMaster-Carr	91864A030	2	0.8300	1.66
Flip Cover / USB Panel Nuts		McMaster-Carr	90730A006	6	0.0566	0.34
1.5” Grommet	Grommet for component case	McMaster-Carr	9600K225	5	0.6250	3.13
Computer Screws	To secure computer to cover	McMaster-Carr	90825A213	4	1.4000	5.60
Computer Nuts		McMaster-Carr	95462A029	4	0.0488	0.20
Self-Clinching Nuts	Provided/assembled by Protocase	Protocase	SP-832-1	12		
Self-Clinching Studs	Provided/assembled by Protocase	Protocase	FH4-832-6	6		
Standoffs	For attaching NILM box to enclosure	Protocase	CSS-0420-6	4		
Gaskets	Made and assembled by Protocase	Protocase	8613K31			
Nano-Mizer Receptacle		Switchcraft	614P.3	3	12.75	38.25
Nano-Mizer Cable		Switchcraft	604ST2	3	24.76	74.28
USB Panel Mount	For connecting keyboard/mouse/etc.	Switchcraft	EHUSBAABX	2	15.64	31.28
USB Cap	For sealing USB ports	Switchcraft	CAPME	2	1.38	2.76
USB-A to USB-A 90 degree	Internal connections from panel mount to hub	zdyCGTime	B01IF3QODU	2	7.99	15.98
USB male-to-female 90 degree	Internal connection to GK41 (Brand: Chadou)	Amazon	B084WPG7QG	4	8.99	35.96
Grand total						1152.06

B.2 Selected Technical Drawings

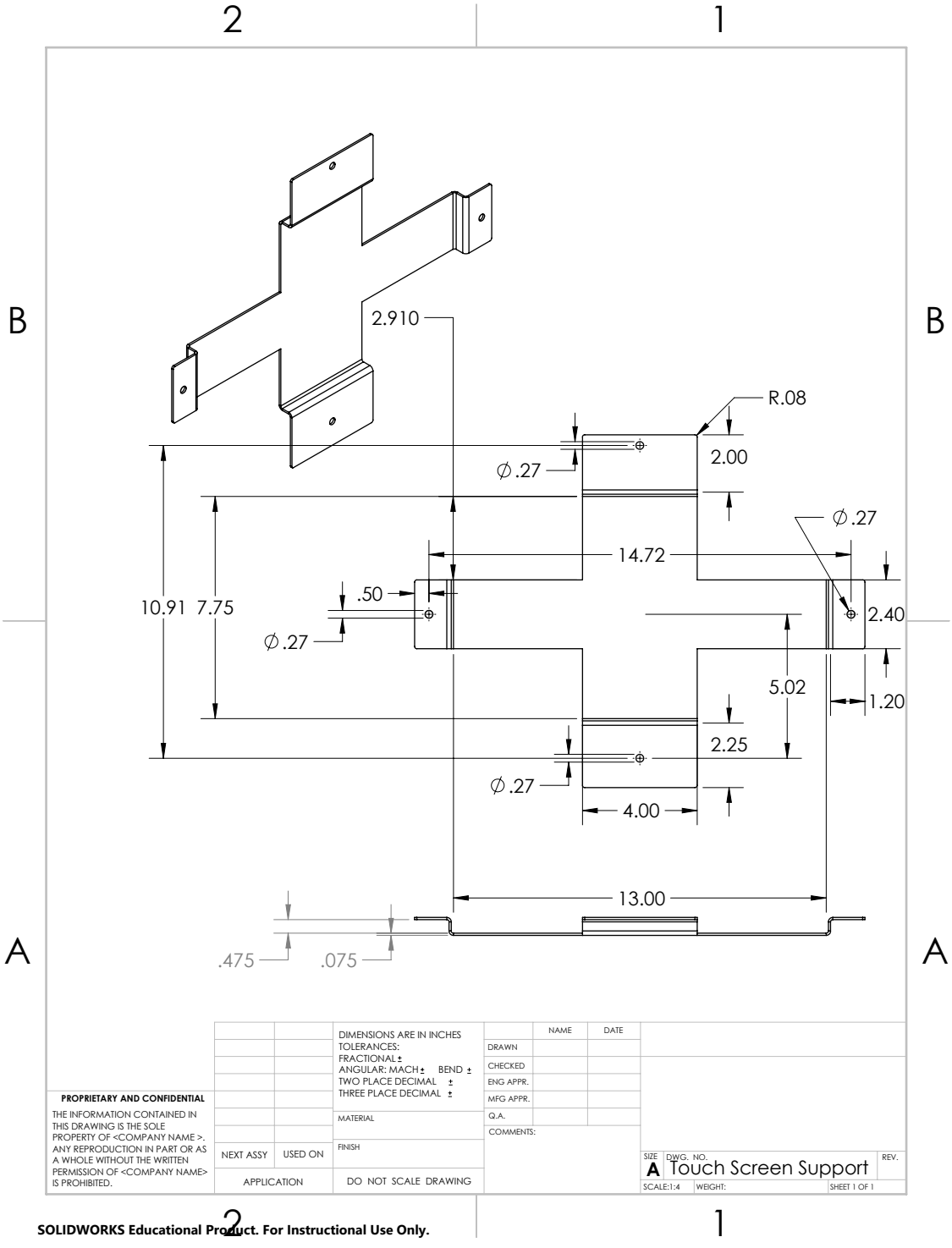

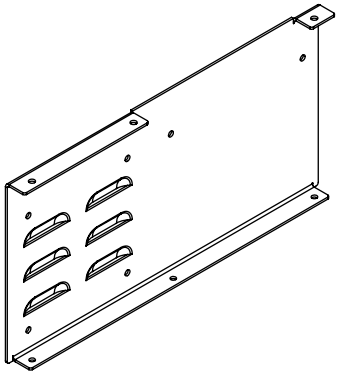

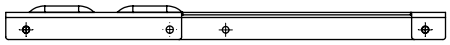

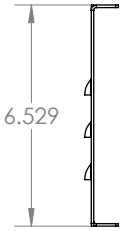

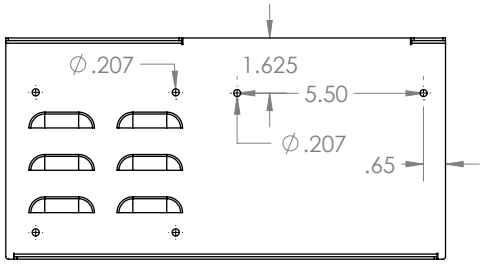

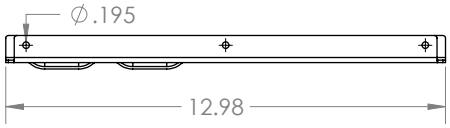

		DIMENSIONS ARE IN INCHES TOLERANCES: FRACTIONAL ± ANGULAR: MACH ± BEND ± TWO PLACE DECIMAL ± THREE PLACE DECIMAL ±		NAME	DATE
			DRAWN		
			CHECKED		
			ENG APPR.		
			MFG APPR.		
		MATERIAL	Q.A.		
			COMMENTS:		
NEXT ASSY	USED ON	FINISH			
APPLICATION		DO NOT SCALE DRAWING			

PROPRIETARY AND CONFIDENTIAL

THE INFORMATION CONTAINED IN THIS DRAWING IS THE SOLE PROPERTY OF <COMPANY NAME >. ANY REPRODUCTION IN PART OR AS A WHOLE WITHOUT THE WRITTEN PERMISSION OF <COMPANY NAME> IS PROHIBITED.

SIZE	DWG. NO.	REV.
A	Side Plate_1	
SCALE:1:4	WEIGHT:	SHEET 1 OF 1

SOLIDWORKS Educational Product. For Instructional Use Only.

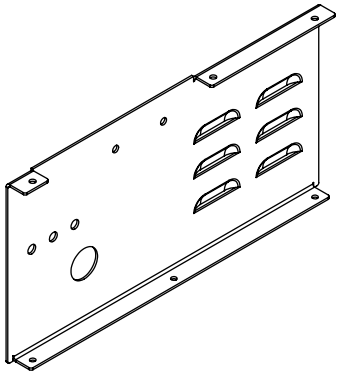

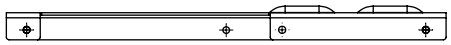

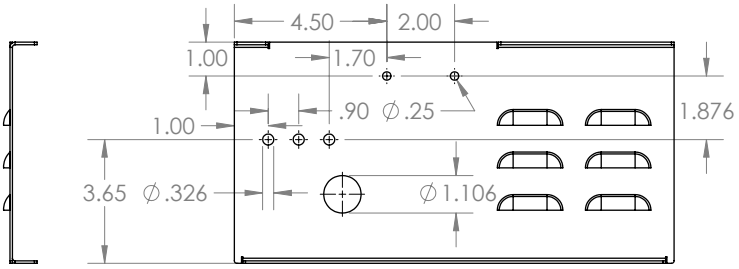

		DIMENSIONS ARE IN INCHES TOLERANCES: FRACTIONAL ± ANGULAR: MACH ± BEND ± TWO PLACE DECIMAL ± THREE PLACE DECIMAL ±		NAME	DATE
			DRAWN		
			CHECKED		
			ENG APPR.		
			MFG APPR.		
		MATERIAL	Q.A.		
			COMMENTS:		
NEXT ASSY	USED ON	FINISH			
APPLICATION		DO NOT SCALE DRAWING			

SIZE A	DWG. NO. Side Plate_2	REV.
SCALE:1:4	WEIGHT:	SHEET 1 OF 1

PROPRIETARY AND CONFIDENTIAL

THE INFORMATION CONTAINED IN THIS DRAWING IS THE SOLE PROPERTY OF <COMPANY NAME >. ANY REPRODUCTION IN PART OR AS A WHOLE WITHOUT THE WRITTEN PERMISSION OF <COMPANY NAME> IS PROHIBITED.

SOLIDWORKS Educational Product. For Instructional Use Only.

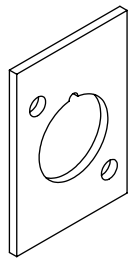

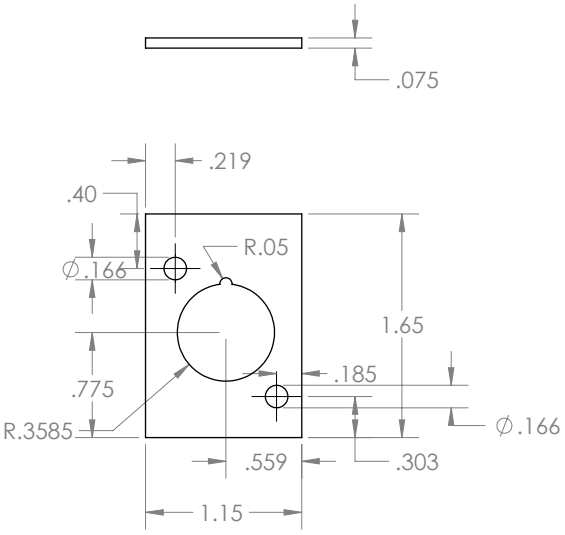

		DIMENSIONS ARE IN INCHES TOLERANCES: FRACTIONAL ± ANGULAR: MACH ± BEND ± TWO PLACE DECIMAL ± THREE PLACE DECIMAL ±		NAME	DATE
			DRAWN		
			CHECKED		
			ENG APPR.		
			MFG APPR.		
		MATERIAL	Q.A.		
			COMMENTS:		
NEXT ASSY	USED ON	FINISH			
APPLICATION		DO NOT SCALE DRAWING			

PROPRIETARY AND CONFIDENTIAL

THE INFORMATION CONTAINED IN THIS DRAWING IS THE SOLE PROPERTY OF <COMPANY NAME >. ANY REPRODUCTION IN PART OR AS A WHOLE WITHOUT THE WRITTEN PERMISSION OF <COMPANY NAME> IS PROHIBITED.

SIZE	DWG. NO.	REV.
A	Switch Piece_UPDATE	
SCALE:1:1	WEIGHT:	SHEET 1 OF 1

SOLIDWORKS Educational Product. For Instructional Use Only.

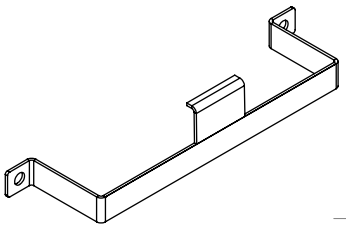

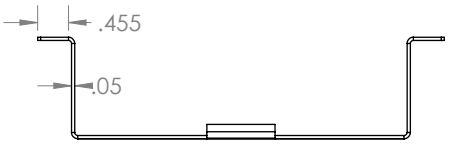

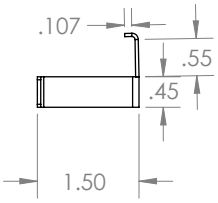

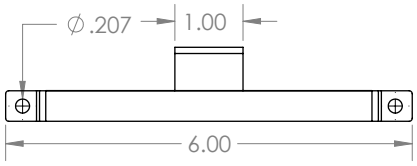

		DIMENSIONS ARE IN INCHES TOLERANCES: FRACTIONAL ± ANGULAR: MACH ± BEND ± TWO PLACE DECIMAL ± THREE PLACE DECIMAL ±		NAME	DATE
			DRAWN		
			CHECKED		
			ENG APPR.		
			MFG APPR.		
		MATERIAL	Q.A.		
			COMMENTS:		
NEXT ASSY	USED ON	FINISH			
APPLICATION		DO NOT SCALE DRAWING			

PROPRIETARY AND CONFIDENTIAL

THE INFORMATION CONTAINED IN THIS DRAWING IS THE SOLE PROPERTY OF <COMPANY NAME >. ANY REPRODUCTION IN PART OR AS A WHOLE WITHOUT THE WRITTEN PERMISSION OF <COMPANY NAME> IS PROHIBITED.

SIZE	DWG. NO.	REV.
A	CPU Brace_UPDATE	
SCALE:1:2	WEIGHT:	SHEET 1 OF 1

SOLIDWORKS Educational Product. For Instructional Use Only.

Bibliography

[1] R. Powers, "Automation as a manpower reduction strategy in navy ships," M.S. thesis, Massachusetts Institute of Technology, Department of Mechanical Engineering, 2016.

[2] A. S. Eruguz, T. Tan, and G. J. van Houtum, "A survey of maintenance and service logistics management: Classification and research agenda from a maritime sector perspective," *Computers & operations research*, vol. 85, pp. 184–205, Sep. 2017.

[3] A. Benigni, G. D'Antona, U. Ghisla, A. Monti, and F. Ponci, "A decentralized observer for ship power system applications: Implementation and experimental validation," *IEEE Transactions on Instrumentation and Measurement*, vol. 59, no. 2, pp. 440–449, 2010.

[4] P. A. Lindahl, D. H. Green, G. Bredariol, A. Aboulian, J. S. Donnal, and S. B. Leeb, "Shipboard fault detection through nonintrusive load monitoring: A case study," *IEEE Sensors Journal*, vol. 18, no. 21, pp. 8986–8995, 2018.

[5] A. Aboulian, D. H. Green, J. F. Switzer, T. J. Kane, G. V. Bredariol, P. Lindahl, J. S. Donnal, and S. B. Leeb, "Nilm dashboard: A power system monitor for electromechanical equipment diagnostics," *IEEE Transactions on Industrial Informatics*, vol. 15, no. 3, pp. 1405–1414, 2019.

[6] U. S. C. Guard, *COMDTINST 16151.1D - Domestic Icebreaking Operations Policy*, Department of Homeland Security, Dec 2011.

[7] T. Lamb, *Ship Design and Construction, Vol. II.* Society of Naval Architects and Marine Engineers, 2003.

[8] J. F. Hansen and F. Wendt, "History and state of the art in commercial electric ship propulsion, integrated power systems, and future trends," *Proceedings of the IEEE*, vol. 103, no. 12, pp. 2229–2242, 2015.

[9] G. D. Ashton, *River and Lake Ice Engineering.* Water Resources Publications, LLC, 1986.

[10] B. Michel, "Winter regime of rivers and lakes," United States Army Corps of Engineers, Cold Regions Research amd Engineering Laboratory, Tech. Rep., 1971.

[11] G. P. Vance, "Analysis of the performance of a 140-foot great lakes icebreaker: Uscgc katmai bay," United States Army Corps of Engineers, Cold Regions Research amd Engineering Laboratory, Tech. Rep., 1980.

[12] "Donaldson torit - centrifugal mist collecters (models e and ea)," Accessed 2022.

[13] Technical Manual 3458-86-A: System Operations, accessed: 2022.

[14] Technical Manual 3474-262-A: Pump and Motor, Main Lube Oil, accessed: 2022.

[15] Technical Manual 3474-262-B: Lube Oil System - MDE Support System, accessed: 2022.

[16] Technical Manual 3474-233-A: Jacket Water System - MDE Support System, accessed: 2022.

[17] Technical Manual 3367-311-A: General Information - Alban Engine Power System, accessed: 2022.

[18] Technical Manual 3474-256-A: Pump and Motor, Main Motor Sea Water Cooling, accessed: 2022.

[19] C. C. Youngren, *Modern Marine Engineer's Manual, Vol. II.* Cornell Maritime Press, 2002, ch. 22.

[20] Technical Manual 3456-86-E: Propulsion and Control Systems, accessed: 2022.

[21] Technical Manual 4982-202-A: MPCMS Drive System Operation Instructions, accessed: 2022.

[22] T. J. Kane, "The nilm dashboard: Shipboard automatic watchstanding and real-time fault detection using non-intrusive load monitoring," M.S. thesis, Massachusetts Institute of Technology, Department of Mechanical Engineering, 2019.

[23] USB Accelerometer Model X16-1C Technical Data Sheet, accessed: 2022.

[24] L. Huchel, T. C. Krause, T. Lugowski, S. B. Leeb, and J. Helsen, "Chasing the cut: A measurement approach for machine tool condition monitoring," *IEEE Transactions on Instrumentation and Measurement*, vol. 70, pp. 1–10, 2021.

[25] L. Huchel, T. C. Krause, S. B. Leeb, and J. Helsen, "Stretched sensing strategies for IEPE," *IEEE Transactions on Instrumentation and Measurement*, vol. 70, pp. 1–10, 2021.

[26] S. Fong, J. Harmouche, S. Narasimhan, and J. Antoni, "Mean shift clustering-based analysis of nonstationary vibration signals for machinery diagnostics," *IEEE Transactions on Instrumentation and Measurement*, vol. 69, no. 7, pp. 4056–4066, 2020.

[27] J. M. Batalla, "On analyzing video transmission over wireless WiFi and 5G c-band in harsh IIoT environments," *IEEE Access*, vol. 8, pp. 118 534–118 541, 2020.

[28] H. Farhat, H. Kdouh, C. Brousseau, G. Zaharia, G. Grunfelder, and G. El Zein, "Radio wave propagation characterization between adjacent decks on board ships," in *2015 IEEE 82nd Vehicular Technology Conference (VTC2015-Fall)*, 2015, pp. 1–4.

[29] X. Zeng, K. Liu, J. Ma, M. Chen, and M. Yu, "Reliability and delay trade-off analysis of unslotted IEEE 802.15.4 sensor network for shipboard environment," *IEEE Sensors Journal*, vol. 21, no. 2, pp. 2400–2411, 2021.

[30] M. Chen, K. Liu, J. Ma, and C. Liu, "Spatio-temporal fingerprint localization for shipboard wireless sensor networks," *IEEE Sensors Journal*, vol. 18, no. 24, pp. 10 125–10 133, 2018.

[31] G. Mois, T. Sanislav, and S. C. Folea, "A cyber-physical system for environmental monitoring," *IEEE Transactions on Instrumentation and Measurement*, vol. 65, no. 6, pp. 1463–1471, 2016.

[32] J. Donnal, "Joule: A real-time framework for decentralized sensor networks," *IEEE Internet of Things Journal*, vol. 5, no. 5, pp. 3615–3623, 2018.

[33] J. Paris, J. S. Donnal, and S. B. Leeb, "NilmDB: The non-intrusive load monitor database," *IEEE Transactions on Smart Grid*, vol. 5, no. 5, pp. 2459–2467, 2014.

[34] J. S. Donnal, "Wattsworth: An open-source platform for decentralized sensor networks," *IEEE Internet of Things Journal*, vol. 7, no. 1, pp. 189–196, 2020.

[35] "Wilcoxon research - model 728t high sensitivity, low noise accelerometers," Accessed 2022. [Online]. Available: https://buy.wilcoxon.com/

[36] C. Peeters, Q. Leclère, J. Antoni, P. Lindahl, J. Donnal, S. Leeb, and J. Helsen, "Review and comparison of tacholess instantaneous speed estimation methods on experimental vibration data," *Mechanical Systems and Signal Processing*, vol. 129, pp. 407–436, 2019.

[37] J. W. O'Connell, D. H. Green, B. T. Mills, A. Moeller, S. Kidwell, K. Lee, L. Huchel, and S. B. Leeb, "Nonintrusive ventilation system diagnostics," *IEEE Sensors Journal*, vol. 21, no. 17, pp. 19 268–19 278, 2021.

[38] Technical Manual 3910A-514-A: Air Conditioning System, accessed: 2021.

[39] "Application data - 06d and 06e semi-hermetic reciprocating compressors," Accessed 2022. [Online]. Available: https://www.shareddocs.com/hvac/docs/2002/Public/09/574-069.pdf

[40] J. N. Trout and J. R. Kolodzie, "Reciprocating compressor valve condition monitoring using image-based pattern recognition," *Annual Conference of the Prognostics and Health Management Society*, 2016.

[41] G. Genta, *Dynamics of Rotating Systems*, 1st ed. Springer, 2005.

[42] R. B. Randall, *Condition Based Monitoring - Industrial, Automotive, and Aerospace Applications*, 2nd ed. John Wiley & Sons Ltd, 2021.

[43] Technical Drawing 101-WTGB-528-001: Sanitary and Deck Drains System Diagram, accessed: 2021.

[44] W. A. Gardner, *Statistical Spectral Analysis: a Nonprobabilistic Theory.* Englewood Cliffs, NJ: Prentice-Hall, 1988.

[45] ——, *Introduction to Random Processes with Applications to Signals and Systems.* New York: Macmillan, 1986.

[46] J. Antoni, "Cyclostationarity by examples," *Mechanical Systems and Signal Processing*, vol. 23, no. 4, pp. 987 – 1036, 2009.

[47] L. Huchel, J. Helsen, P. A. Lindahl, and S. B. Leeb, "Diagnostics for periodically excited actuators," *IEEE Transactions on Instrumentation and Measurement*, vol. 69, no. 7, pp. 4145–4153, 2020.